Current Applied Physics xxx (2009) xxx–xxx

Contents lists available at ScienceDirect

Current Applied Physics

journal homepage: www.elsevier.com/locate/cap

Dielectric and ferroelectric properties of 0.8PZT–0.2PCN ceramics under sintering conditions variation

Anurak Prasatkhetragarn [a,*], Muangjai Unruan [b], Athipong Ngamjarurojana [b], Yongyut Laosiritaworn [b], Supon Ananta [b], Rattikorn Yimnirun [b], David P. Cann [c]

[a] Department of Materials Science, School of Science and Technology, Naresuan University at Phayao, Phayao 56000, Thailand
[b] Department of Physics, Faculty of Science, Chiang Mai University, Chiang Mai 50200, Thailand
[c] Materials Science, School of Mechanical, Industrial and Manufacturing Engineering, Oregon State University, Corvallis, OR 97331, USA

ARTICLE INFO

Article history:
Received 10 August 2008
Accepted 12 January 2009
Available online xxxx

PACS:
77.84.-s
77.84.Dy

Keywords:
PZT–PCN
Sintering conditions
Dielectric properties
Ferroelectric properties

ABSTRACT

The influences of sintering conditions on electrical properties of the $0.8Pb(Zr_{1/2}Ti_{1/2})O_3$–$0.2Pb(Co_{1/3}Nb_{2/3})O_3$ ceramics have been investigated with sintering temperatures of 1175, 1200, 1225, and 1250 °C and dwell times for 2, 6, and 10 h. The crystal structure of dense specimens showed coexistence between tetragonal, rhombohedral and pseudo cubic phases in all sintering temperatures, while tetragonal-rich phase appeared with increasing dwell times. A maximum dielectric constant was observed at sintering condition of 1200 °C for 2 h, while the transition temperature slightly increased with increasing dwell time. All ceramics also showed diffused phase transition behaviors with a minimum diffusivity at sintering condition of 1200 °C for 2 h. In addition, the polarization–electric field (P–E) hysteresis loops of the ceramic systems also changed significantly with sintering conditions. Interestingly, the ferroelectric parameters; remnant polarization (P_r) and loop squareness (R_{sq}) tended to increase with increasing sintering temperatures and dwell times.

1. Introduction

Ferroelectric and related materials continue to be exploited for numerous applications, including recent concepts of "smart" or "intelligent" systems, whereby multifunctional components are required [1]. Nowadays, substantial research and development has been devoted to ferroelectric materials consisting of relaxor and normal ferroelectrics have attracted great interest at the compositions close to the morphotropic phase boundary (MPB) because of their excellent dielectric, piezoelectric, and electrostrictive properties, which are useful in actuating and sensing applications [1,2]. Lead zirconate titanate, $Pb(Zr_xTi_{1-x})O_3$ or PZT ceramics have been investigated from both fundamental and applied viewpoints [2,3]. The MPB of PZT is located at a $PbTiO_3$:$PbZrO_3$ of 0.52:0.48 and separates the Ti-rich tetragonal phase from the Zr-rich rhombohedral phase [4]. Furthermore, the MPB composition has a high T_c of 390 °C, which allows piezoelectric devices to be operated at relatively high temperatures. Most commercial PZT ceramics are designed in the vicinity of the MPB with various doping methods in order to achieve high properties [3,5–8]. Recently, many piezoelectric ceramic materials have been developed from binary systems containing a combination of relaxor and normal ferroelectric materials [3] that yield high dielectric permittivities {e.g., $Pb(Zr_{1/2}Ti_{1/2})O_3$–$Pb(Ni_{1/3}Nb_{2/3})O_3$ (PZT–PNN), and $Pb(Zr_{1/2}Ti_{1/2})O_3$–$Pb(Mg_{1/3}Nb_{2/3})O_3$ (PZT–PMN)} [5,6], excellent piezoelectric coefficients {e.g., $Pb(Zr_{1/2}Ti_{1/2})O_3$–$Pb(Zn_{1/3}Nb_{2/3})O_3$ (PZT–PZN)} [7], and high pyroelectric coefficients {e.g., $Pb(Ni_{1/3}Nb_{2/3})O_3$–$PbTiO_3$–$PbZrO_3$ (PNN–PT–PZ)} [8].

Lead cobalt niobate, $Pb(Co_{1/3}Nb_{2/3})O_3$ or PCN, which exhibits a perovskite structure and a Curie temperature of ≈−30 °C, is a relaxor ferroelectric material with a high dielectric constant [9,10]. On the basis of the above mentioned approach, solid solutions of PZT and PCN are expected to synergistically combine the properties of both the normal ferroelectric PZT and relaxor ferroelectric PCN, which could exhibit electrical properties that are better than those of the single-phase PZT and PCN [9–12]. Our previous investigation on $(1-x)$PZT–(x)PCN ceramic systems has already shown excellent electrical properties with the MPB at $x = 0.2$ [13]. Previously, the influences of sintering conditions on electrical properties have been extensively investigated in PZT [14], PZT–PMN [15,16], PZT–PZN [17], PMS–PZT [18], PMN–PNN–PZT [19], PCW–PMN–PZT [20], PZT–PMN–PZN [21], PFW–PT [22], KNN–ST [23], and BNT–BT [24]. However, there have been no systematic studies on the relationship between sintering temperature and dwell time variation on physical and electrical properties of ceramics within specific morphotropic phase boundary compositions of PZT and PCN. Therefore, the overall purpose of this

* Corresponding author. Tel.: +66 53 943367; fax: +66 53 943445.
E-mail address: Prasatkhetragarn@yahoo.com (A. Prasatkhetragarn).

1567-1739/$ - see front matter © 2009 Elsevier B.V. All rights reserved.
doi:10.1016/j.cap.2009.01.005

study is to examine the influence of sintering conditions on phase formation, microstructure, dielectric and ferroelectric properties of $0.8Pb(Zr_{1/2}Ti_{1/2})O_3$–$0.2Pb(Co_{1/3}Nb_{2/3})O_3$ ceramic systems.

2. Experimental procedure

The specimens studied were fabricated according to the formula: $0.8Pb(Zr_{1/2}Ti_{1/2})O_3$–$0.2Pb(Co_{1/3}Nb_{2/3})O_3$. Raw materials of PbO, ZrO_2, TiO_2, CoO, and Nb_2O_5 with >99% purity were used to prepare samples. The columbite $CoNb_2O_6$ and wolframite $ZrTiO_4$ precursors were weighed and introduced into the batch calculations. $CoNb_2O_6$ and $ZrTiO_4$ powders were prepared at calcination temperatures of 1100 and 1450 °C for 2 h, respectively [25,26]. In this work, the $0.8Pb(Zr_{1/2}Ti_{1/2})O_3$–$0.2Pb(Co_{1/3}Nb_{2/3})O_3$ samples were prepared from PbO, $ZrTiO_4$, and $CoNb_2O_6$ powders using the solid-state reaction of these raw materials. The powders were mixed by a vibratory–milling technique in ethanol for 6 h. After drying, the product was calcined in an alumina crucible at a temperature of 950 °C [25]. The calcined powders were uniaxially cold-pressed at 5000 psi into disc-shaped pellets with a diameter of 12.7 mm and a thickness of 1 mm, with 3 wt% poly (vinyl alcohol) (PVA) added as a binder. Following binder burnout at 500 °C, the pellets were sintered at various sintering temperatures of 1175, 1200, 1225, and 1250 °C for 2, 6, and 10 h with fixed heating/cooling rate of 5 °C/min.

The phase structure of the powders was analyzed via X-ray diffraction (XRD; Bruker-AXS D8). The microstructures of the sintered samples were examined using scanning electron microscopy (SEM; JEOL JSM-840A). The dielectric properties of the samples were measured using Agilent 4284A LCR meter over a wide temperature range using a NorECS ProboStat high temperature measurement cell. The room temperature ferroelectric properties were examined using a simple Sawyer–Tower circuit at fixed measuring frequency of 50 Hz.

3. Results and discussions

Perovskite phase formation and crystal structure were determined by XRD at room temperature. The XRD patterns of $0.8Pb(Zr_{1/2}Ti_{1/2})O_3$–$0.2Pb(Co_{1/3}Nb_{2/3})O_3$ ceramics with various sintering temperatures and dwell times are shown in Figs. 1 and 2, respectively, showing perovskite structure for all compositions. The pyrochlore phase is not observed in this system. For sintering temperature variation, sintered ceramics with various sintering temperature of 1175, 1200, 1225 and 1250 °C are correlated with JCPDS file number 70-4057, as displayed in Fig. 1a. In the XRD patterns, the crystal structure of all specimens appears coexistence between tetragonal and pseudo cubic phases in 0.8PZT–0.2PCN system. As shown in Fig. 1b, XRD peak profiles of the (002)/(200) peaks of tetragonal phase and (200) peak of pseudo cubic phase appeared around 2θ of ≈44°–45°. However, a separate peak at (111) peak, as shown in Fig. 1a, confirmed that the rhombohe-

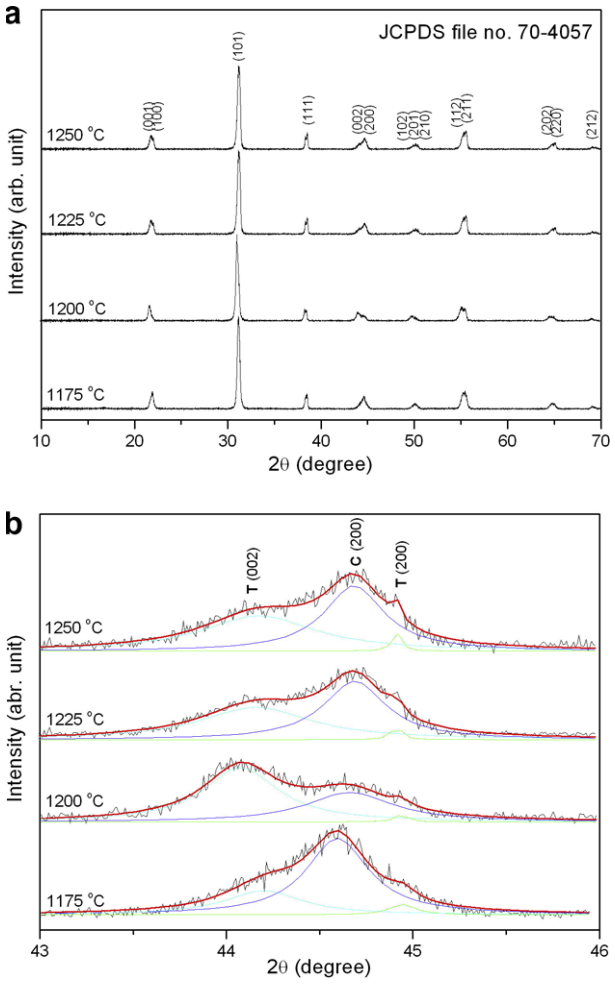

Fig. 1. XRD patterns of $0.8Pb(Zr_{1/2}Ti_{1/2})O_3$–$0.2Pb(Co_1/3Nb_{2/3})O_3$ ceramics with; (a) sintering temperature of 1175, 1200, 1225 and 1250 °C and (b) coexistence of T(002), T(200) and C(200) peaks profile.

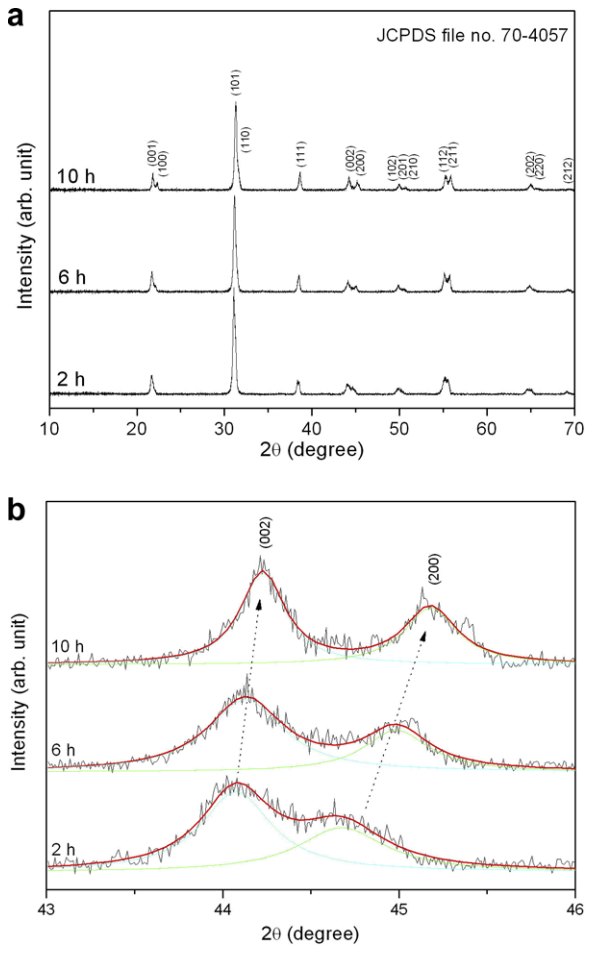

Fig. 2. XRD patterns of $0.8Pb(Zr_{1/2}Ti_{1/2})O_3$–$0.2Pb(Co_{1/3}Nb_{2/3})O_3$ ceramics with; (a) dwell times for 2, 6, and 10 h and (b) the (002)/(200) peaks profile with various dwell times.

Please cite this article in press as: A. Prasatkhetragarn et al., Dielectric and ferroelectric properties of 0.8PZT–0.2PCN ceramics under ..., Curr. Appl. Phys. (2009), doi:10.1016/j.cap.2009.01.005

dral phase is also observed in this system with increasing sintering temperature. It should be noticed that this ceramic system shows coexistence of tetragonal, rhombohedral, and pseudo cubic phases. For samples with fixed sintering temperature of 1200 °C and dwell times variations for 2, 6 and 10 h, the XRD patterns also show single-phase without pyrochlore phase, as shown in Fig. 2a. The tetragonal-rich phase is observed with increasing dwell time for 6 and 10 h, indicating the structural change in 0.8PZT–0.2PCN system, as shown in Fig. 2b. Clearly, these observations show that the sintering conditions have affected the crystal structure of 0.8PZT–0.2PCN ceramics. Previously, a similar behavior was also observed with increasing sintering temperatures in PZT, PZT–PMN, PZT–PZN, PZT–PNN, PMS–PZT, PMN–PNN–PZT, PZT–PMN–PZN, PCW–PMN–PZT, PZT–PMWSN, and PFW–PT [14–22,27].

Effects of sintering conditions on the microstructure of the $0.8Pb(Zr_{1/2}Ti_{1/2})O_3$–$0.2Pb(Co_{1/3}Nb_{2/3})O_3$ ceramics are displayed in Fig. 3. The grain size of the ceramics varies considerably from 0.57 to 13.76 μm, as listed in Table 1. The average grain size and density of this ceramics tend to increases with increasing sintering temperatures and dwell times probably due to the grain growth is

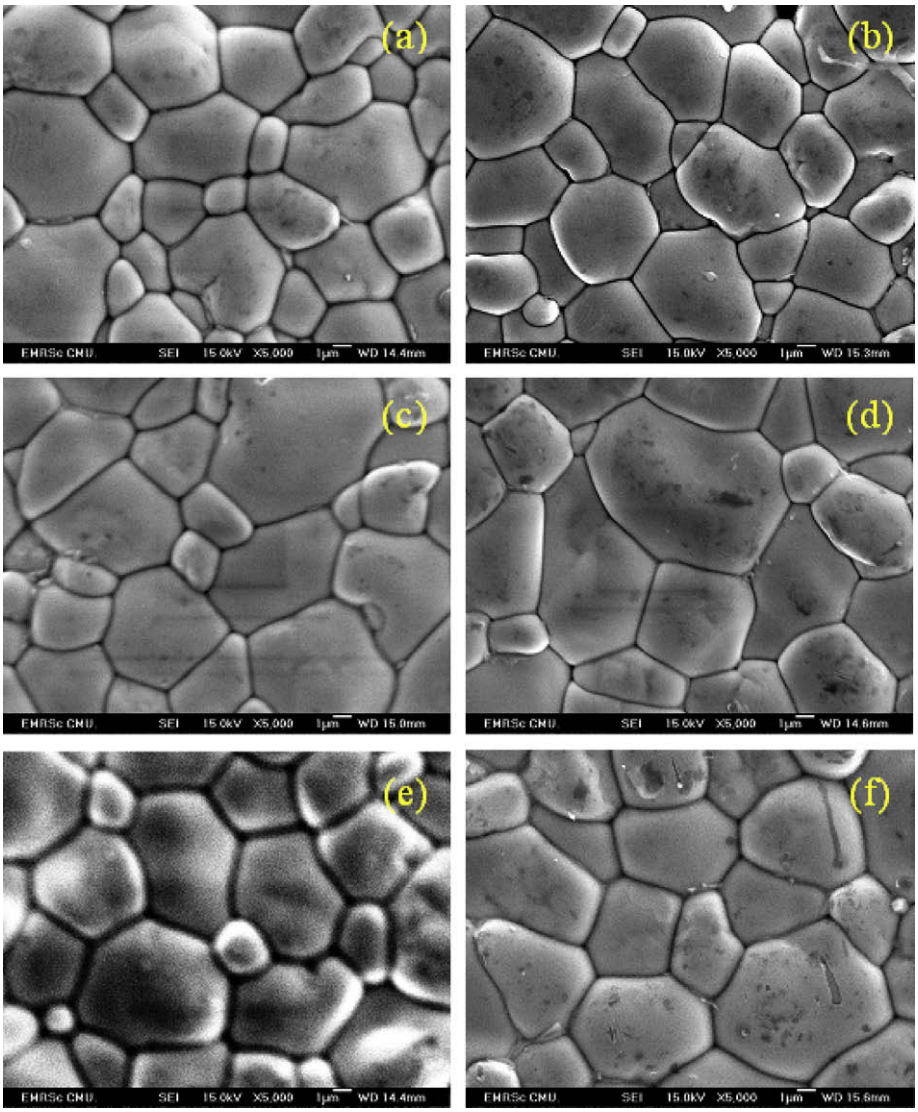

Fig. 3. SEM micrographs of $0.8Pb(Zr_{1/2}Ti_{1/2})O_3$–$0.2Pb(Co_{1/3}Nb_{2/3})O_3$ with various sintering temperatures of (a) 1175, (b) 1200, (c) 1225, (d) 1250, and various dwell times for (e) 6 h and (f) 10 h.

Table 1
Physical properties of 0.8PZT–0.2PCN ceramics at various sintering condition.

Sintering conditions		Density (g/cm^3)	Grain size range (μm)	Average grain size (μm)
Temperature (°C)	Dwell time (h)			
1175	2	7.89 ± 0.05	0.57–10.31	4.19
1200	2	7.91 ± 0.05	0.81–9.67	4.55
1225	2	7.93 ± 0.05	1.29–12.24	5.95
1250	2	7.94 ± 0.05	1.71–13.76	7.94
1200	6	7.92 ± 0.05	1.95–10.43	5.05
1200	10	7.94 ± 0.05	0.81–12.00	5.97

Please cite this article in press as: A. Prasatkhetragarn et al., Dielectric and ferroelectric properties of 0.8PZT–0.2PCN ceramics under ..., Curr. Appl. Phys. (2009), doi:10.1016/j.cap.2009.01.005

controlled by boundary diffusion [28]. This indicates that the sintering process can enhance the diffusion mechanism and promote the densification of the sample with higher relative density [28]. Therefore, the grain size and density of PZT–PCN ceramics strongly depend on the sintering conditions. This trend is similar to those reported in the literature [14–24,27].

Temperature dependences of the dielectric constant (ε_r) and dielectric loss tangent (tan δ) of the $0.8Pb(Zr_{1/2}Ti_{1/2})O_3$–$0.2Pb(Co_{1/3}Nb_{2/3})O_3$ ceramics at various sintering temperatures of 1175, 1200, 1225, and 1250 °C and dwell times for 2, 6,and 10 h are displayed in Figs. 4 and 5, respectively. The maximum dielectric constant ($\square_{max}$) at 1 kHz is also listed in Table 2. For sintering temperature variation, the $\square_{max}$ tends to increase from 28300 at 1175 °C up to 64500 at 1200 °C and then decrease to 39200 at 1250 °C, while tan δ tends to increase with increasing sintering temperature, clearly indicating that the sintering temperature has strong influence on the optimum dielectric properties of 0.8PZT–0.2PCN system. In addition, a clear transition in T_{max} (defined as the temperature at which $\square_r$ is maximum at 1 kHz) is observed. It is noticed that an increased sintering temperature does not significantly change T_{max} of the ceramics, as shown in Table 2. At fixed sintering temperature of 1200 °C, and various dwell times for 2, 6, and 10 h, the dielectric constant shows maxima at 2 h dwell time, and then decreases with increasing dwell times. While board peaks at $\square_{max}$ have been observed, T_{max} shows slightly

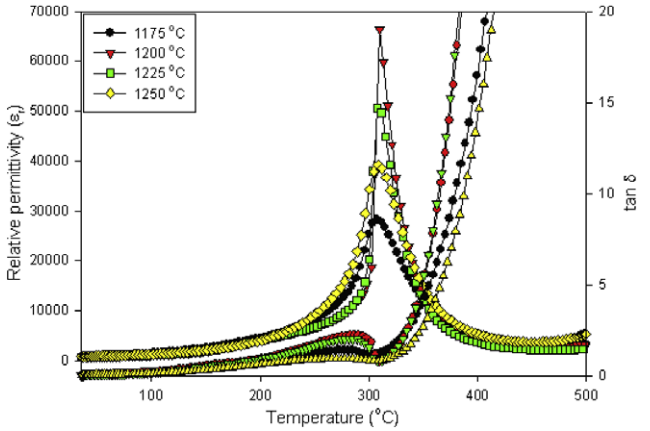

Fig. 4. Temperature dependences of dielectric properties of $0.8Pb(Zr_{1/2}Ti_{1/2})O_3$–$0.2Pb(Co_{1/3}Nb_{2/3})O_3$ at various sintering temperature with fixed dwell time for 2 h and heating/cooling rates of 5 °C/min.

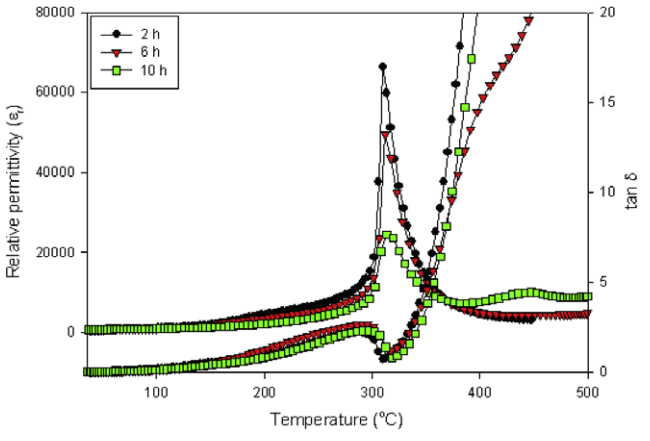

Fig. 5. Temperature dependences of dielectric properties of $0.8Pb(Zr_{1/2}Ti_{1/2})O_3$–$0.2Pb(Co_{1/3}Nb_{2/3})O_3$ with various dwell times (sintered at 1200 °C and heating/cooling rates of 5 °C/min).

Table 2
Dielectric properties of 0.8PZT–0.2PCN ceramics at various sintering conditions.

Sintering conditions		Dielectric properties (at 1 kHz)						
Temperature (°C)	Dwell time (h)	T_{max} (°C)	ε_{RT}	tan δ	ε_{max}	tan δ	γ	δ
1175	2	308	983	0.0552	28300	0.419	1.73	16.52
1200	2	309	929	0.0467	64500	0.73	1.49	15.28
1225	2	309	880	0.042	51000	1.11	1.73	16.08
1250	2	309	716	0.0418	39200	1.089	1.81	16.81
1200	6	312	778	0.0382	49500	1.26	1.55	15.4
1200	10	315	736	0.0432	24600	0.808	1.62	15.71

increase with increasing dwell time, probably caused by a shift to a tetragonal-rich phase composition as shown in Fig. 2. Similar behavior is also reported in previous works [15,17,21,22,24,28].

To further understand the dielectric behavior of the 0.8PZT–0.2PCN ceramic with various sintering conditions, the permittivity of a first-order normal ferroelectric can be described by the Curie–Weiss law and a second-order relaxor ferroelectric can be described by a simple quadratic law [29]. The relative permittivity can then be derived via using

$$\frac{\varepsilon_m}{\varepsilon(f,T)} = 1 + \frac{(T - T_m(f))^{\gamma}}{2\delta^2} \quad (1)$$

where ε_m is the maximum value of the permittivity at $T = T_m(f)$. The value of γ is the expression of the degree of dielectric relaxation, while δ is used to measure the degree of diffuseness of the phase transition. In a material with a "pure" diffuse phase transition, γ is expected to be 2 [30]. As listed in Table 2, the values of γ vary with sintering conditions between 1.49 and 1.81, which confirms that diffuse phase transition occurs in the 0.8PZT–0.2PCN ceramics. It is important to note that in perovskite ferroelectrics it has been established that γ and δ can be affected by sintering conditions and structure of the materials. The values of γ and δ decrease with increasing sintering temperature from 1175 to 1200 °C, and then increase when sintering temperature increases further, as shown in Table 2. For dwell time variation, the values of γ and δ tend to increase with increasing dwell time as also shown in Table 2. However, the results show minimum γ and δ values at sintering temperature of 1200 °C and dwell times for 2 h. It is interesting to observe that the phase transition is least diffused at this optimized sintering condition, possibly due to a sharp increase of dielectric permittivity at MPB. A similar behavior has also been observed in PZT–PNN and PZT–PMN systems [5,6].

The polarization–electric field (P–E) hysteresis loops of $0.8Pb(Zr_{1/2}Ti_{1/2})O_3$–$0.2Pb(Co_{1/3}Nb_{2/3})O_3$ ceramics measured at 15 kV/cm are presented in Figs. 6 and 7. To assess effect of sintering conditions on ferroelectric characteristics of 0.8PZT–0.2PCN ceramics, the ferroelectric parameters have been extracted from the experimental data, as summarized in Table 3. For sintering temperature variation, the remnant polarization (P_r) increases with increasing sintering temperature. However, the largest remnant polarization at sintering temperature of 1250 °C could be caused by effects of grain size, which reaches maximum in this condition [23], as listed in Table 1. However, with fixed sintering temperature at 1200 °C and various dwell times, the P_r also increases with increasing dwell times, while E_c shows the same behavior as in sintering temperature variation case. Furthermore, the ferroelectric characteristics can be assessed with the hysteresis loop squareness (R_{sq}) [25], which can be calculated from the empirical expression $R_{sq} = (P_r/P_s) + (P_{1.1Ec}/P_s)$, where P_s is the saturated polarization obtained at some finite field strength below the dielectric breakdown and $P_{1.1Ec}$ is the polarization at the field equal to $1.1E_c$. For the ideal square loop, R_{sq} is equal to 2.00 [31]. As listed in Table 3, the loop squareness parameter R_{sq} increases to 1.47 at sintering tempera-

Please cite this article in press as: A. Prasatkhetragarn et al., Dielectric and ferroelectric properties of 0.8PZT–0.2PCN ceramics under ..., Curr. Appl. Phys. (2009), doi:10.1016/j.cap.2009.01.005

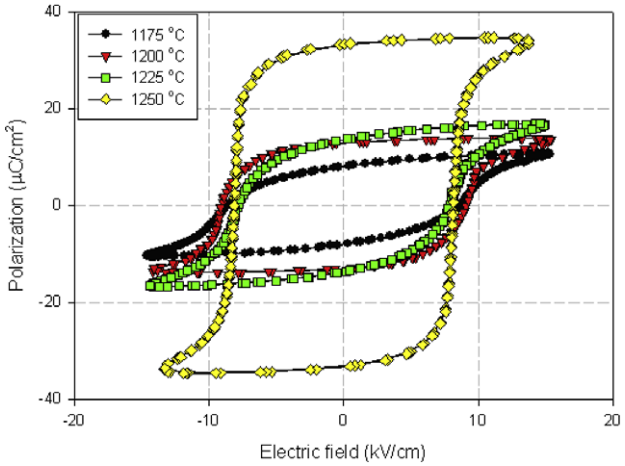

Fig. 6. *P–E* loops of $0.8Pb(Zr_{1/2}Ti_{1/2})O_3$–$0.2Pb(Co_{1/3}Nb_{2/3})O_3$ at various sintering temperatures with fixed dwell time for 2 h and heating/cooling rates of 5 °C/min.

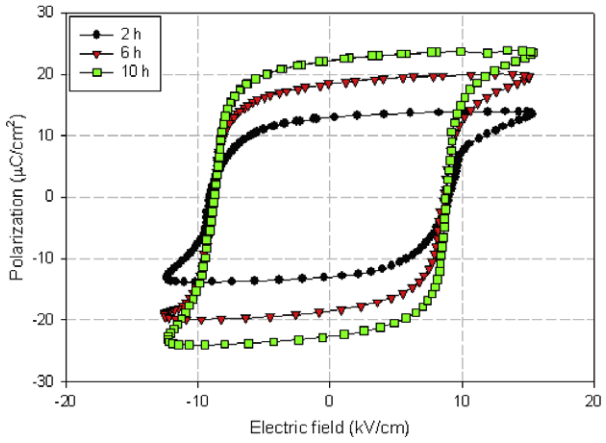

Fig. 7. *P–E* loops of $0.8Pb(Zr_{1/2}Ti_{1/2})O_3$–$0.2Pb(Co_{1/3}Nb_{2/3})O_3$ with various dwell times (sintered at 1200 °C and heating/cooling rates of 5 °C/min).

Table 3
Ferroelectric properties of 0.8PZT–0.2PCN ceramics at various sintering conditions.

Sintering conditions		Ferroelectric Properties					
Temperature (°C)	Dwell time (h)	P_r (μC/cm²)	P_s (μC/cm)	E_c (kV/cm)	P_r/P_{max}	E_c/E_{max}	Loop squareness (R_{sq})
1175	2	8.06	10.73	8.7	0.75	0.58	1.06
1200	2	12.91	13.88	9.13	0.93	0.61	1.47
1225	2	13.61	16.79	7.84	0.81	0.53	1.16
1250	2	33.29	34.43	8.14	0.97	0.59	1.58
1200	6	18.46	19.99	8.76	0.92	0.58	1.48
1200	10	22.33	23.91	8.85	0.93	0.58	1.53

ture of 1200 °C and dwell time for 2 h. However, larger R_{sq} value at 1250 °C could be due to easy polarization rotation in the MPB region with coexistence of the tetragonal and pseudo cubic phase and/or effects of maximum grain size in this sintering condition. Similar behavior is also reported in PZT–PMN and PZT–PZN [32,33].

4. Conclusions

In this study, the influence of sintering conditions on phase formation and electrical properties of the $0.8Pb(Zr_{1/2}Ti_{1/2})O_3$–$0.2Pb(Co_{1/3}Nb_{2/3})O_3$ ceramics with various sintering temperature of 1175, 1200, 1225, and 1250 °C and dwell times for 2, 6, and 10 h have been investigated. The XRD analysis indicates that the tetragonal, pseudo cubic and rhombohedral phases coexist for all compositions sintered at various temperatures, while the tetragonal-rich phase appears with increasing dwell time. The surface micrographs show that average grain size increases with increasing sintering temperature and dwell time. At 1 kHz, the maximum dielectric constant (ε_{max}) of 64500 is observed in ceramics sintered at 1200 °C for 2 h, while the diffusivity (γ) and diffuseness parameter (δ) reach minima. Moreover, the ferroelectric parameters; remnant polarization (P_r) and loop squareness (R_{sq}) increase with increasing sintering temperatures and dwell times, while coercive field (E_c) does not show specific trend. Finally, this study shows that the sintering conditions play critical role on physical and electrical properties of the PZT–PCN ceramics.

Acknowledgements

The authors wish to express profound gratitude to Materials Science Groups, Oregon State University for ceramics preparation and measurement. This work was supported by the Commission on Higher Education (CHE), the Thailand Research Fund (TRF), the Faculty of Science, the Graduate School of Chiang Mai University, and Naresuan University Phayao.

References

[1] G.H. Haertling, J. Am. Ceram. Soc. 82 (1999) 797.
[2] A.J. Moulson, J.M. Herbert, Electroceramics: Materials Properties Applications, Wiley, Chichester, UK, 2003.
[3] L.E. Cross, Mater. Chem. Phys. 43 (1996) 108.
[4] S.-E. Park, T.R. Shrout, IEEE Trans. Ultrason. Ferroelectr. Freq. Control. 44 (1997) 1140.
[5] N. Vittayakorn, G. Rujijanagul, X. Tan, M.A. Marquardt, D.P. Cann, J. Appl. Phys. 96 (2004) 5103.
[6] R. Yimnirun, S. Ananta, P. Laoratanakul, J. Eur. Ceram. Soc. 25 (2005) 3235.
[7] H. Fan, G.T. Park, J.J. Choi, J. Ryu, H.E. Kim, J. Mater. Res. 17 (2002) 180.
[8] D. Luff, R. Lane, K.R. Brown, H.J. Marshallsay, Trans. J. Br. Ceram. Soc. 73 (1974) 251.
[9] M. Unruan, N. Vittayakorn, R. Wongmaneeruang, A. Prasatkhetragarn, S. Ananta, R. Yimnirun, J. Alloy Compd., in press.
[10] T. Hachiga, S. Fujimoto, N. Yasuda, J. Phys. D 20 (1987) 1291.
[11] T. Kudo, T. Yazaki, F. Naito, S. Sugaya, J. Am. Ceram. Soc. 53 (1970) 326.
[12] Z. Brankovic, G. Brankovic, J.A. Varela, J. Mater. Sci. 14 (2003) 37.
[13] A. Prasatkhetragarn, P. Ketsuwan, M. Unruan, A. Ngamjarurojana, S. Ananta, R. Yimnirun, D.P. Cann, Mater. Lett., submitted for publication.
[14] H. Maiwa, O. Kimura, K. Shoji, H. Ochiai, J. Eur. Ceram. Soc. 25 (2005) 2383.
[15] J. Yue, M. Leung, E. Haemmerle, M. Hodgson, G. Li, W. Gao, J. Alloy Compd., in press.
[16] J. Yoo, C. Lee, Y. Jeong, K. Chung, D. Lee, D. Paik, Mater. Chem. Phys. 90 (2005) 386.
[17] Y.D. Hou, M.K. Zhu, H. Wang, B. Wang, H. Yan, C.S. Tian, Mater. Lett. 58 (2004) 1508.
[18] Z.G. Zhu, B.S. Li, G.R. Li, W.Z. Zhang, Q.R. Yin, Mater. Sci. Eng. B 117 (2005) 216.
[19] Y. Jeong, J. Yoo, S. Lee, J. Hong, Sensor Actuator A 135 (2007) 215.
[20] K. Chung, J. Yoo, C. Lee, D. Lee, Y. Jeong, H. Lee, Sensor Actuator A 125 (2006) 340.
[21] C.H. Wang, S.J. Chang, P.C. Chang, Mater. Sci. Eng. B 111 (2004) 124.
[22] C.S. Hong, S.Y. Chu, W.C. Su, R.C. Chang, H.H. Nien, Y.D. Juang, J. Alloy Compd. 459 (2008) 1.
[23] R.C. Chang, S.Y. Chu, Y.P. Wong, C.S. Hong, H.H. Huang, J. Alloy Compd. 456 (2008) 308.
[24] L. Liu, H. Fan, S. Ke, X. Chen, J. Alloy Compd. 458 (2008) 504.
[25] A. Prasatkhetragarn, N. Vittayakorn, S. Ananta, R. Yimnirun, D.P. Cann, Jpn. J. Appl. Phys. 47 (2008) 998.
[26] A. Prasatkhetragarn, R. Yimnirun, S. Ananta, Ferroelectrics 356 (2007) 203.
[27] J.H. Cho, I.K. Park, H.G. Kim, H.T. Chung, J. Am. Ceram. Soc. 80 (1997) 1523.
[28] C.Y. Chen, Y. Hu, H.L. Lin, Mater. Chem. Phys. 99 (2006) 26.
[29] A.A. Bokov, Z.G. Ye, Solid State Commun. 116 (2000) 105.
[30] Y.-M. Chiang, D.P. Birnie, W.D. Kingery, Physical Ceramics, Wiley, Chichester, UK, 1997. p. 522.
[31] G.H. Haertling, W.J. Zimmer, Am. Ceram. Soc. Bull. 45 (1966) 1084.
[32] S. Wongsaenmai, Y. Laosiritaworn, S. Ananta, R. Yimnirun, Mater. Sci. Eng. B (2005).
[33] N. Vittayakorn, G. Rujijanagul, D.P. Cann, J. Alloy. Compd. 440 (2007) 259.

Dielectric Properties of Complex Perovskite PZBT-PMNT Ceramic Under Compressive Stress

Rattikorn Yimnirun*, Muangjai Unruan, Rewadee Wongmaneerung, Orawan Khamman, Wanwilai Chaisan, and Supon Ananta

Department of Physics, Faculty of Science, Chiang Mai University,

Chiang Mai 50200, Thailand

*Author for Correspondence, E-mail: rattikornyimnirun@yahoo.com

ABSTRACT

Effects of compressive stress on the dielectric properties of complex perovskite PZBT-PMNT ceramic were investigated. The dielectric properties measured under stress-free condition showed a composite nature with two distinct temperatures of dielectric maximum associated with PZBT and PMNT. The dielectric properties under the compressive stress were observed at stress levels up to 230 MPa using a homebuilt compressometer. The results clearly showed that the superimposed compression load significantly reduced both the dielectric constant and the dielectric loss tangent in every measuring frequency. The change of the dielectric constant with stress was attributed to competing influences of the intrinsic contribution of non-polar matrix and the extrinsic contribution of re-polarization and growth of micro-polar regions, while the clamping of the domain walls contributed to the change in dielectric loss tangent with stress. Finally, the stress induced decrease in switchable part of spontaneous polarization was seen as a cause for a large drop of the dielectric constant after a stress cycle.

Keywords: Dielectric Properties, PZBT-PMNT, Stress

1. INTRODUCTION

Complex perovskite ferroelectric ceramics have been studied extensively because they can be applied in several micro- and nano-electronic devices such as multilayer capacitors, microactuators and miniaturized transducers [1-5]. Among them, barium titanate ($BaTiO_3$ or BT), lead titanate ($PbTiO_3$ or PT), lead zirconate titanate ($Pb(Zr_{1-x}Ti_x)O_3$ or PZT), lead magnesium niobate ($Pb(Mg_{1/3}Nb_{2/3})O_3$ or PMN) ceramics and a variety of their solid solutions have been investigated extensively and continuously since the late 1940s [1,3,4]. Two of the most studied ferroelectric compounds, PZT and BT ceramics are representative perovskite piezoelectric and ferroelectric prototypes, respectively, because of their excellent electrical properties. While BT has a high dielectric constant with a relatively low Curie temperature (T_C) (~120 ºC), PZT has a higher T_C of 390 ºC which allows PZT-based piezoelectric devices to be operated at relatively higher temperatures [2,4]. Although BT ceramic has better mechanical properties than PZT, the sintering temperature is also higher [1,3,6]. Thus, mixing PZT with BT is expected to decrease the sintering temperature of BT-based ceramics while maintaining excellent dielectric properties. Our earlier studies have already revealed the optimized electrical properties in 0.5PZT-0.5BT ceramic with $\varepsilon_r \sim 4000$ at T_C of 160 ºC [7,8].

Another family of ferroelectric materials which are of great interest due to their high polarizabilities is lead-based relaxor ferroelectrics. PMN has very good dielectric properties [2,3,5]. However, the temperature related to the maximum dielectric constant (T_{max}) of PMN is very low (~ -10°C) [5]. Therefore, PT is systematically added to PMN to enhance the dielectric properties of PMN (as well as increasing T_{max}). In particular, 0.9PMN-0.1PT ceramics, which have $T_{max} \sim 40$ °C and $\varepsilon_{r,max} > 20000$, have been a subject of many investigations and, more importantly, have been widely

applied for capacitor, actuator and transducer applications [9-12]. However, since there have always been a need to obtain ceramic with board dielectric peak and maximum dielectric constant for various applications, especially in capacitive components [2-5], and with the complimentary characteristics between 0.5PZT-0.5BT and 0.9PMN-0.1PT ceramics, it is expected that excellent dielectric properties can be obtained from a mixture composition of the two ceramics. It is, therefore, one of the aims of this study to explore the dielectric properties of the mixture composition of 0.5PZT-0.5BT and 0.9PMN-0.1PT.

In most applications, however, ceramics are often subjected to mechanical loading, either deliberately in the design of the device itself or because the device is used to change shapes as in many smart structure applications or the device is used under environmental stresses [13-15]. A prior knowledge of how the materials behave under different load conditions is therefore very crucial for proper design of a device and for suitable selection of materials for a specific application. Therefore, it is very important to determine the properties of the materials as a function of applied stress. Previous investigations on the stress-dependence dielectric and electrical properties of many ceramic systems, such as PZT, PMN-PZT, and PMN-PT have clearly emphasized the importance of the subject [15-22]. Therefore, the major aim of this study is to investigate the influences of the compressive stress on the dielectric properties of complex perovskite PZBT-PMNT ceramic.

2. EXPERIMENTAL DETAILS

The ceramic composition with a formula $[0.5Pb(Zr_{0.52}Ti_{0.48})O_3–0.5BaTiO_3]$-$[0.9Pb(Mg_{1/3}Nb_{2/3})O_3\text{-}0.1PbTiO_3]$ (abbreviated as PZBT-PMNT hereafter) was selected for this study as outlined above. The PZBT-PMNT powders were prepared

from $0.5Pb(Zr_{0.52}Ti_{0.48})O_3–0.5BaTiO_3$ (abbreviated as PZBT hereafter) and $0.9Pb(Mg_{1/3}Nb_{2/3})O_3$-$0.1PbTiO_3$ (abbreviated as PMNT hereafter) starting powders via a simple mixed-oxide method [7,23]. The detailed descriptions of the PZBT and PMNT powders processing and characterization were presented elsewhere and will not be discussed here [7,8,23]. The PZBT-PMNT ceramics were then fabricated via the same mixed-oxide method. After mixing the powders by ball-milling method and drying process, the mixed powders were pressed hydraulically to form disc-shaped pellets 10 mm in diameter and 2 mm thick, with 3 wt.% polyvinyl alcohol as a binder. The pellets were placed on the alumina powder-bed inside alumina crucible and surrounded with atmosphere powders of the same composition. Finally, the pellets were sintered at 1250 °C for 2 h.

For dielectric property characterizations, the sintered samples were lapped to obtain parallel faces disc-shaped specimens with diameter of 8 mm and thickness of 1 mm, and the faces were then coated with silver paint as electrodes. The samples were then heat-treated at 750 °C for 12 min to ensure the contact between the electrodes and the ceramic surfaces. The samples were subsequently poled in a silicone oil bath at a temperature of 120 °C by applying a dc field of 20 kV/cm for 30 min and then field-cooled to room temperature. The dielectric properties of the sintered ceramics were studied under stress-free condition as functions of both temperature and frequency with an automated dielectric measurement system. The capacitance and the dielectric loss tangent were determined over the temperature range of 25 and 400 °C with the frequency ranging from 1 kHz to 5 MHz. The measurements were carried out on cooling continuously at the rate of 3 °C/min. To study the effects of the compressive stress on the dielectric properties, the compressometer was constructed [20,24]. The dielectric properties were measured by LCR-meter (Instrek LCR-821). The room

temperature (25 °C) capacitance and the dielectric loss tangent were obtained at frequency range 10 to 200 kHz under the compressive stress levels up to 230 MPa. The dielectric constant was then calculated from a parallel-plate capacitor equation, e.g. $\varepsilon_r = Cd/\varepsilon_0 A$, where C is the capacitance of the specimens, d and A are, respectively, the thickness and the area of the electrode, and ε_0 is the dielectric permittivity of vacuum (8.854×10^{-12} F/m).

3. RESULTS AND DISCUSSION

The stress-free dielectric properties, e.g. dielectric constant (ε_r) and tan δ, as functions of both temperature and frequency are plotted in Fig. 1. It is clearly seen that there are two distinct dielectric anomalies. The first dielectric peak at lower temperature region with higher dielectric constant is associated with the PMNT component, which has T_{max} near 40 ºC [12]. A strong dielectric dispersion below T_{max} also indicates a relaxor ferroelectric behavior. In this case, the temperatures of maximum dielectric constant and dielectric loss tangent are shifted to higher temperature with increasing frequency. The maximum value of the dielectric constant decreases with increasing frequency, while that of the dielectric loss tangent increases. The dielectric properties then become frequency independence above the transition temperature [25,26]. Even though these descriptions are not clearly seen on the first dielectric peak because of the appearance of the second dielectric peak, it could still be said that the relaxor behavior exists. The second dielectric peak occurs over temperature range 150-200 ºC, which should be associated with the PZBT component with T_C near 162 ºC [7,8]. A diffuse phase transition with small frequency dispersion of the dielectric maxima is also observed within this second dielectric peak, similar to earlier reported observation for the PZBT component [8]. These observations of the two distinct dielectric peaks

should indicate the composite nature of the PZBT-PMNT ceramic. Moreover, it should also be noted that significant increase in the dielectric constant dielectric loss at high temperatures is a result of thermally activated space charge conduction [25,26].

The fractional changes of the dielectric properties of the PZBT-PMNT ceramic under the compressive stress during loading and unloading are shown in Figs. 2 and 3. There is a significant change of the dielectric properties of the ceramic with increasing stress from 0 to 230 MPa and returning to stress-free condition. As seen in Fig. 2, the dielectric constant decreases monotonically with increasing the compressive stress, then increases only slightly when the compressive stress is gradually removed. The changing of the dielectric constant with increasing and decreasing the applied stress does not follow the same path. In every frequency, the dielectric constant with increasing the compressive stress is larger in value than that with decreasing stress. It is also of interest to see that the stress-free dielectric constant value decreases significantly after a stress cycle. It can be seen very clearly that the dielectric constant decreases as much as 25% at the maximum applied stress and only returns to slightly less than 85% of its original value when the stress is removed. As displayed in Fig. 3, though following a similar trend, the change in the dielectric loss tangent value is less significant, as it only decreases about 10-20% at the maximum stress and almost returns to its original value after a stress cycle. Similar observations have been reported for other ceramic systems, such as BT, PZT, PMN, PMN-PT and PMN-PZT [17,20,22,27-28]. It should also be noted that since the dielectric constant of the sample was measured through the capacitance, there is a change of sample capacitance due to the geometrical deformation under stress. The variation of the sample dielectric constant ($\Delta\varepsilon_r$) can be expressed as $\varepsilon_r * X * ((1+2\upsilon)/E)$, where X is the applied stress, υ is the Poisson's ratio, and E is the Young's modulus [29,30]. By applying the estimated

values of $\upsilon \sim 0.3$ and $E \sim 100$ GPa for the ceramic [15,16,18,22,31] and $\varepsilon_r \sim 4000$, it can be estimated that at the maximum stress of 230 MPa, the variation of the sample dielectric constant due to the geometrical deformation is < 0.5%. Therefore, this variation should not be an important factor in the variation of the dielectric constant under stress observed in Fig. 2.

To understand these experimental results, at least qualitatively, various effects have to be considered. Normally, the properties of ferroelectric materials are derived from both the intrinsic contribution of domains and extrinsic contributions of re-polarization and growth of micro-polar regions [16,17,20,22,27,28]. When a compressive stress is applied to the ferroelectric materials, the domain structure in the materials will change to maintain the domain energy at a minimum; during this process some of the domains engulf other domains or change shape irreversibly. Under the applied stress, the domain structure of ferroelectric ceramics may undergo domain switching through non-180° domain walls, de-aging, clamping of domain walls, and stress induced decrease in switchable part of spontaneous polarization [21,27,31,32,33].

The situation for the PZBT-PMNT system is quite complex because this system is a mixing between the relaxor ferroelectric PMNT and the normal ferroelectric PZBT. Therefore, there is a competing mechanism between the two types of materials, depending upon temperature. Since the stress experiment was carried out at room temperature (~25 °C) which is just below the T_{max} of PMNT (~40 °C) [12], the dielectric properties of the PZBT-PMNT ceramic undet stress should be dominated by the PMNT contribution. Therefore, the experimental observations, which show decreases in both dielectric constant and dielectric loss tangent with increasing stress, can be attributed to competing influences of the intrinsic contribution of non-polar

matrix and the extrinsic contribution of re-polarization and growth of micro-polar regions. Since the dielectric response of both contributions is affected by the applied stress in an opposite way, the behavior of the PZBT-PMNT ceramic depends on the ratio between the micro-polar region and the non-polar matrix, in this case the non-polar matrix still dominates [27,28]. Hence, the dielectric responses of the PZBT-PMNT ceramic are observed to decrease significantly with increasing the compressive stress, as seen in Figs. 2 and 3. More interestingly, it is worth noting that our earlier investigations on the stress-dependent dielectric properties of the two members, i.e. PZBT [32] and PMNT [22], revealed that under a similar loading condition the dielectric constant of the PMNT ceramic decreased nearly 70%, whereas the PZBT ceramic showed approximately 5-10% increase in the dielectric constant. Clearly, the apparent suppression of the dielectric constant change with stress observed in this current study supports the composite nature of the PZBT-PMNT ceramic, as also revealed by the free-stress dielectric properties measurements shown in Fig. 1.

The cause of the stress dependence of the dielectric loss tangent is a little more straightforward than that of the dielectric constant. As depicted in Fig. 3, the clamping of the domain walls under the compressive stress results in a decrease of domain wall mobility and reduces the dielectric loss tangent [22,27]. This is a reversible effect with the domain wall mobility returning to near the original values when the applied stress is removed, as seen in Fig. 3 that the dielectric loss tangents return to near their original values after a stress cycle. In addition, a significant decrease in the dielectric constant after a full cycle of stress application has been observed, and attributed to the stress induced decrease in switchable part of spontaneous polarization at high stress [21,31].

4. CONCLUSIONS

The dielectric properties of complex perovskite PZBT-PMNT ceramic were investigated in this study. The dielectric properties measured under stress-free condition showed two distinct dielectric peaks associated with PZBT and PMNT. The dielectric properties under the compressive stress were observed using a homebuilt compressometer. The results clearly showed that the superimposed compression load significantly reduced both the dielectric constant and the dielectric loss tangent in every measuring frequency. The change of the dielectric properties with stress was attributed to competing influences of the intrinsic contribution of non-polar matrix and the extrinsic contribution of re-polarization and growth of micro-polar regions. Other contributions include the clamping of the domain walls and the stress induced decrease in switchable part of spontaneous polarization. This study clearly indicated that the complex perovskite PZBT-PMNT ceramic possessed a composite nature, as confirmed by the dielectric measurements.

ACKNOWLEDGMENTS

Financial supports from the Thailand Research Fund (TRF), Faculty of Science and Graduate School of Chiang Mai University are gratefully acknowledged.

REFERENCES

[1] B. Jaffe, W.R. Cook. Piezoelectric Ceramics, R.A.N. Inc., New York, 1971.

[2] L.E. Cross, Mater. Chem. Phys. 43 (1996) 108.

[3] G.H. Haertling, J. Am. Ceram. Soc. 82(4) (1999) 797.

[4] N. Setter, J. Euro. Ceram. Soc. 21 (2001) 1279.

[5] A.J. Moulson, J.M. Herbert. Electroceramics: Materials, Properties, Applications, 2nd Ed., John Wiley & Sons Ltd, New York, 2003.

[6] W. Chaisan, S. Ananta, T. Tunkasiri, Cur. Appl. Phys. 4 (2004) 182.

[7] W. Chaisan, R. Yimnirun, S. Ananta, D.P. Cann, Mater. Lett. 59 (2005) 3737.

[8] W. Chaisan, R. Yimnirun, S. Ananta, D.P. Cann, Mater. Sci. Eng. B. (2006) *in press*

[9] S. Jiang, D. Zhou, S. Gong, W. Lu, Sensors Actuat. A69 (1998) 1.

[10] Y.C. Liou, J. Mater. Sci. 103 (2003) 281.

[11] A. Safari, R.K. Panda, V.F. Janas, Appl. Ferro. Ceram. Mater. 1 (2000) 1.

[12] S. Huang, C. Feng, L. Chen, X. Wen, Integrated Ferroelectrics 74 (2005) 45.

[13] L.E. Cross, Ferroelectrics. 76 (1987) 241.

[14] Y.H. Xu, Ferroelectric Materials and Their Applications, North Holland, Los Angeles, 1991.

[15] D. Viehland, J. Powers, J. Appl. Phys. 89(3) (2001) 1820.

[16] J. Zhao, A.E. Glazounov, Q.M. Zhang, Appl. Phys. Lett. 74 (1999) 436.

[17] Q.M. Zhang, J. Zhao, K. Uchino, J. Zheng, J. Mater. Res. 12 (1997) 226.

[18] D. Viehland, J.F. Li, E. McLaughlin, J. Powers, R. Janus, H. Robinson, J. Appl. Phys. 95 (2004) 1969.

[19] D.Zhou, M. Kamlah, D. Munz, J. Euro. Ceram. Soc. 25 (2005) 425.

[20] R. Yimnirun, S. Ananta, E. Meechoowas, S. Wongsaenmai, J. Phys. D: Appl. Phys. 36 (2003) 1615.

[21] R. Yimnirun, Y. Loasiritaworn, S. Wongsaenmai, J. Phys. D: Appl. Phys. 39 (2006) 759.

[22] R. Yimnirun, M. Unruan, Y. Loasiritaworn, S. Ananta, J. Phys. D: Appl. Phys. 39 (2006) 3097.

[23] A. Udomporn, PhD Thesis, Chiang Mai University, 2004.

[24] R. Yimnirun, S. Ananta, A. Ngnamjarurojana, S. Wongsaenmai, Appl. Phys. A: Mater. 81(6) (2005) 1227.

[25] R. Yimnirun, S. Ananta, P. Laoratanakul, Mater. Sci. Eng. B. 112 (2004) 79.

[26] R. Yimnirun, S. Ananta, P. Laoratanakul, J. Euro. Ceram. Soc. 25(13) (2005) 3225

[27] G. Yang, W. Ren, S.F. Liu, A.J. Masys, B.K. Mukherjee, Proc. IEEE Ultra. Symp. 1 (2000) 1005.

[28] O. Steiner, A.K. Tagantsev, E.L. Colla, N. Setter, J. Euro. Ceram. Soc. 19 (1999) 1243.

[29] P. Preu, S. Haussuhl, Solid State Commun., 45(7) (1983) 619.

[30] R. Yimnirun, P.J. Moses, R.J. Meyer, R.E. Newnham, Rev. Sci. Instrum. 74 (2003) 3429

[31] J. Zhao, Q.M. Zhang, Proc. IEEE ISAF. 2 (1996) 971.

[32] R. Yimnirun, Ferroelectrics 331 (2006) 9.

[33] R. Yimnirun, S. Ananta, A. Ngnamjarurojana, S. Wongsaenmai, Curr. Appl. Phys. 6(3) (2006) 520.

List of Figure Captions

Fig. 1. Temperature and frequency dependences of dielectric properties of PZBT-PMNT ceramic under stress-free condition (solid circle indicates dielectric peak associated with PMNT, and dotted circle indicates dielectric peak associated with PZBT).

Fig. 2. Relative changes of dielectric constant (ε_r) as a function of compressive stress for PZBT-PMNT ceramic.

Fig. 3. Relative changes of dielectric loss tangent (tan δ) as a function of compressive stress for PZBT-PMNT ceramic.

.

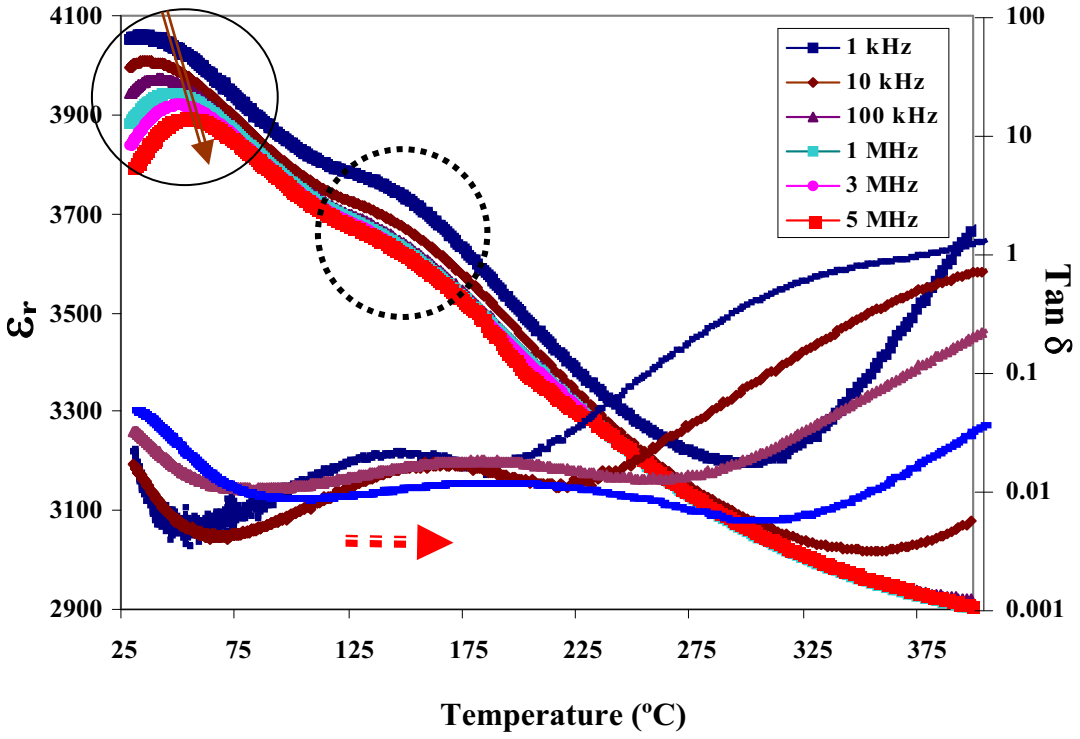

Fig. 1. Temperature and frequency dependences of dielectric properties of PZBT-PMNT ceramic under stress-free condition (solid circle indicates dielectric peak associated with PMNT, and dotted circle indicates dielectric peak associated with PZBT).

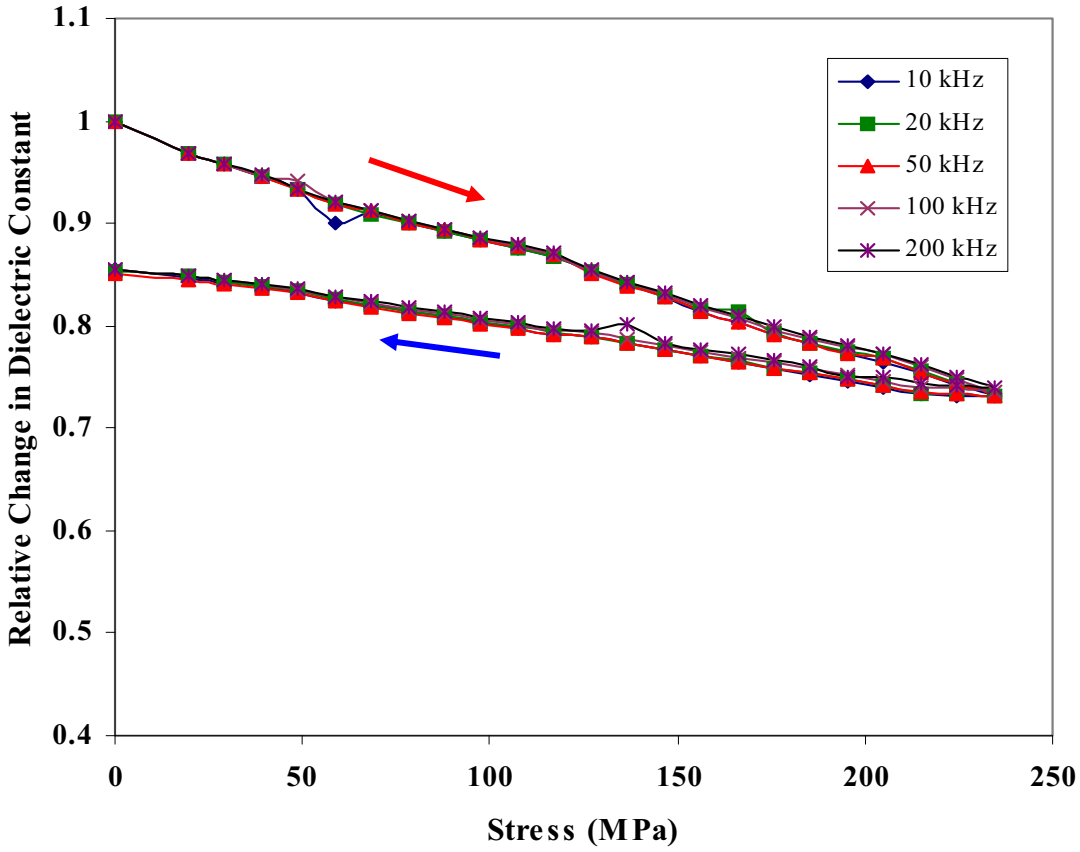

Fig. 2. Relative changes of dielectric constant (ε_r) as a function of compressive stress for PZBT-PMNT ceramic.

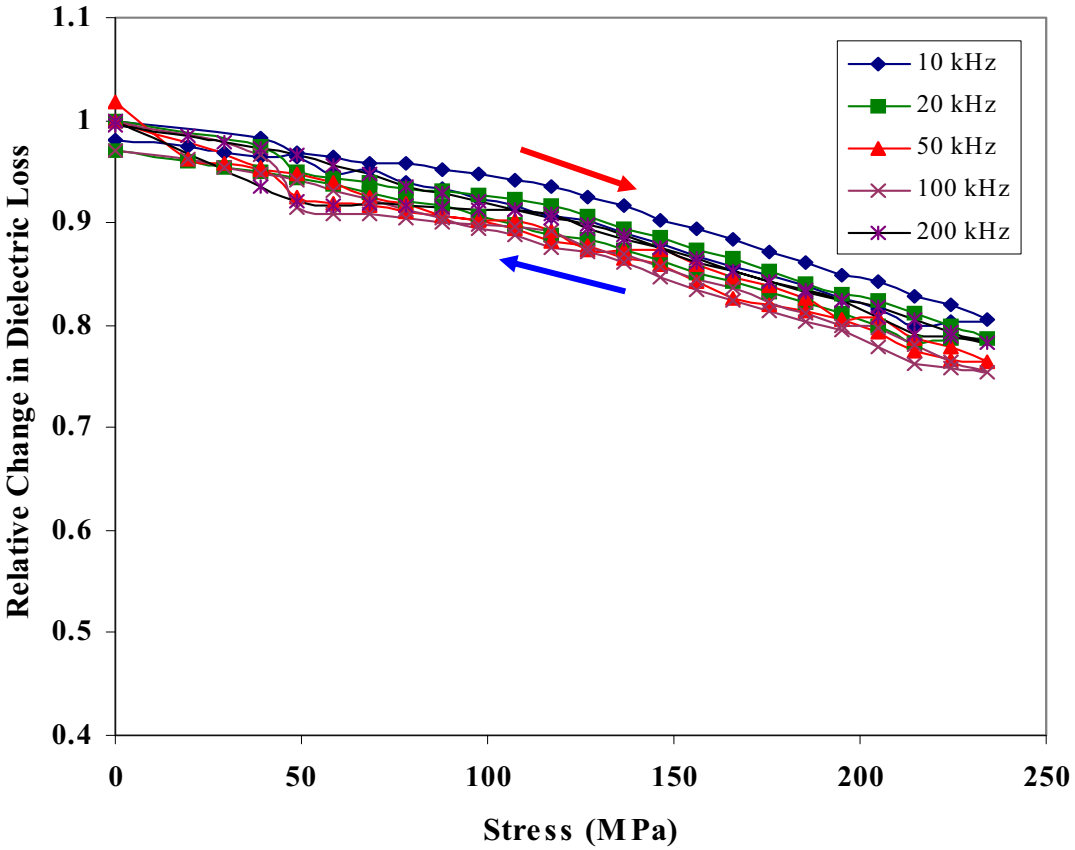

Fig. 3. Relative changes of dielectric loss tangent (tan δ) as a function of compressive stress for PZBT-PMNT ceramic.

Ferroelectric Hysteresis Behavior in 0-3 PZT-Cement Composites: Effects of Frequency and Electric Field

A. Chaipanich*, N. Jaitanong and R. Yimnirun

Department of Physics, Faculty of Science, Chiang Mai University,

Chiang Mai 50200, Thailand

Lead zirconate titanate (PZT) -cement composites of 0-3 connectivity were produced and the effects of the frequency and electric field on the ferroelectric polarization-electric field (*P-E*) hysteresis of the composites were investigated. It was found that there was an increase in both the *instantaneous* remnant polarization (P_{ir}) and coercive field (E_{ic}) when the applied field increased. The *instantaneous* remnant polarization (P_{ir}) was found to reduce when the frequency was increased. The ferroelectric hysteresis loops only existed when the composites were subjected to lower frequency; i.e. at 20 and 40 Hz. At higher frequency, the loops tended to stretch out, showing more of a lossy characteristic.

Keywords: PZT, cement, composite, polarization, ferroelectric hysteresis

* Corresponding author

E-mail address: arnon@chiangmai.ac.th Fax: 66 53 357512

Piezoelectric-cement based composites have recently been developed for civil engineering applications [1-12]. The benefit from the use of such piezoelectric-cement based composite is that these composites possess better matching to the host structure, concrete than normal piezoelectric ceramic or other type of piezoelectric composites. Li *et al.* [1] showed that cement-based piezoelectric composites of 0-3 white Portland cement-lead zirconate titanate (PZT) composite can overcome the matching problem and that ≈40%-50% PZT by volume, the acoustic impedance is close to that of concrete (8.95 $x10^6$ $kg{\cdot}m^{-2}{\cdot}s^{-1}$) as compared to that of PZT at 21.2 $x10^6$ $kg{\cdot}m^{-2}{\cdot}s^{-1}$. However, the study on the ferroelectric hysteresis, which is an important behavior for materials with ferroelectric properties [13] that can be used to give indication of the difficulty of the poling process involved, of piezoleclectric-cement composites is limited. It is thus the aim of this current work to investigate the ferroelectric hysteresis behavior of the piezoleclectric-cement composites. Effects of the frequency and the amplitude of the applied electric field on the hysteresis behavior will be examined to provide the basis for the poling process of the piezoleclectric-cement composites.

In this work a 0-3 of PZT ceramic particles were mixed with normal Portland cement (PC) to form PZT-PC composites [7]. Lead zirconate titanate (PZT) ceramic particles having median size 450μm of composition $Pb(Zr_{0.52}Ti_{0.48})O_3$ were produced from PZT pellet sintered at 1250ºC for 3 h. PZT ceramic particles were then mixed with Portland cement (PC) to produce 0-3 connectivity PZT-PC composites of 50:50 by volume. Thereafter, the composites were placed for curing at 60ºC and 98% relative humidity for 3 days before measurements [7]. Phase characterizations of the composites were carried out by room temperature X-ray diffraction (XRD; Philips PW 1729 diffractometer) using Ni-filtered CuK radiation. The room temperature ferroelectric

hysteresis (*P–E*) loops were characterized using a computer controlled modified Sawyer-Tower circuit [14]. The electric field was applied to a sample by a high-voltage ac amplifier with the input sinusoidal signal with a frequency of 20-100 Hz from a signal generator.

X-ray diffraction pattern of 0-3 PZT–PC composite, as shown in Fig. 1, was found to show diffraction pattern mostly as attributed to that of PZT showing the perovskite phase at 2θ of 22.023, 30.942, 31.387, 38.283, 44.917, 50.417 and 55.524 degree, where the matching XRD peaks can be seen when compared to the PZT ceramic. In addition, rhombohedral calcium carbonate ($CaCO_3$) (2θ= 29.072), dicalcium silicate (2θ= 32.013, 32.117 and 32.939) and hydrated peak of hexagonal calcium hydroxide (2θ= 34.111) can also be noticed and these peaks can be clearly seen in the pure Portland cement XRD pattern. Nonetheless, these detectable phases do not account for all the phases present in the cement matrix. For example, calcium silicate hydrate which is the primary cement hydration product is generally known to be amorphous with poor crystalline form and thus amorphous characteristic can also be noticed from the XRD pattern. The overall detectable crystallized products when compared to the total phases of Portland cement are therefore relatively small; although the presence can still be seen. It thus further explains as to why these peaks of hydrated cement phases are even lesser in intensity in the XRD pattern of PZT-cement composite at 50% PZT by vol. since the crystallized perovskite structure of PZT would dominantly give a stronger diffraction resulting in high intensity peaks as seen in the XRD pattern.

It can be seen from Fig. 2 that when the composite was subjected to different electric field, the *P-E* hysteresis loops can be seen at all different electric field. It must first be noted that all ferroelectric hysteresis loops (*P-E* loops) of the PZT-cement

composites show a "lossy" feature with round tips as a result of cement matrix in the composites. It is believed that when an external electrical field acts on the cement matrix many weak conducting ions such as Ca^{2+}, OH^-, Si^{4+}, Al^{3+} begin to migrate besides the polarization of electron. These ions cause higher conducting loss in the composites, hence a lossy feature is then observed in all the P-E loops obtained [19]. However, this study primarily aims at comparing the effects of the frequency and amplitude of the applied electric field on the hysteresis behavior, as reported in PZT ceramics and other monolithic materials [15-18]. Therefore, the ferroelectric parameters obtained here are used exclusively for comparison purpose among themselves. From the *P*-*E* loops seen in Fig. 2 (a), one can define two parameters based on the x- and y-axes intercepts. With a lossy behavior, it is impossible to achieve the fully saturated loops, hence the typical hyteresis parameters; i.e. the remnant polarization (P_r) and the coercive field (E_c) cannot be extracted. For comparison, we define the y-axis intercept at a given applied field as the "*instantaneous*" remnant polarization (P_{ir}), while the x-axis intercept is called the "*instantaneous*" coercive field (E_{ic}).

From Fig. 2(a), an increase in the amplitude of the field E_0 makes the loop larger and increases its angle to the *E* axis of inclination. Furthermore, it can be seen that there is an increase in the so called "*instantaneous*" remnant polarization (P_{ir}) and the "*instantaneous*" coercive field (E_{ic}) which represents the polarization at zero field and electric field at zero polarization at each measured frequency and E_0 when the electric field (E_0) increases from 10 kV/cm to 25 kV/cm. At frequency of 60 Hz, P_{ir} can be seen to increase from 1.25 to 4.65 μC/cm^2 and E_{ic} increases from 6.05 to 14.27 kV/cm for the hysteresis loops with the electric field of 10 kV/cm and 25 kV/cm, respectively. The increase in both the "*instantaneous*" parameters is due to the electric charge in a polar

material when induced with increasing an external electric field. The plots of the "*instantaneous*" polarization and coercive field against different E_0 at fixed f (60 Hz) can be seen in Fig. 2 (b). It can be observed that when the electric field increases there is an increase in the "*instantaneous*" remnant polarization and that this increase appear to be almost linear. The "*instantaneous*" coercive field was found to increase in a similar manner. Previous investigations on the ferroelectric hysteresis behavior of the ferroelectric materials under sub-coercive field condition also showed similar changes of the hysteresis parameters with the applied field [16,18].

When the hysteresis loops were plotted at 25 kV/cm and with varying frequency from 20 to 100 Hz (Fig. 3 (a)), a typical hysteresis loops can still be seen at lower frequency (20 and 40 Hz). However at higher frequency i.e. 100 Hz, the loop tends to stretched out more and the loop no longer resemble a typical hysteresis. The "*instantaneous*" remnant polarization (P_{ir}) and "*instantaneous*" coercive field (E_{ic}) can be seen to decrease with an increase in frequency. The observation that the P_{ir} and E_{ic} decreases with increasing frequency is ascribed to the delayed response of the polarization reversal to the varying external field. Similar behavior was observed in previous study on ferroelectric ceramics [13-15].

It should be noted here that a loss from the cement can be seen to be more sensitive at higher frequency especially at 100 Hz where an oval shaped typical of a resistance is seen. It is understood that at the high frequency the interfacial polarizations cannot follow the change of the electric field due to the longer time taken for the space charge polarization to occur [16]. It is believed that when an external electrical field acts on the cement matrix many weak conducting ions such as Ca^{2+}, OH^{-}, Si^{4+}, Al^{3+} begin to

migrate besides the polarization of electron. These ions move slowly when it reaches the interface of PZT and cement or in the defect areas and there is an accumulation effect which in turn results in the polarization of a space charge, and at lower frequency all the polarization can follow these changes of electrical field [19].

I think we need to compare our results with previous P-E studies on PZT-PC composites here. Could you please provide some comparison of our results with those from the published paper by Chinese group [refs 20, 21]?

Fig. 3 (b) shows the "*instantaneous*" remnant polarization P_{ir} and the "*instantaneous*" coercive field E_{ic} measured at different frequencies at fixed E_0=25 kV/cm. It can be seen that P_{ir} can be seen to decrease increases from 6.10 to 4.24 to μC/cm^2 when increasing f from 20 to 100 Hz. The E_{ic} on the other hand can be seen to increase from 12.25 to 16.86 kV/cm with increasing frequency and the saturation seems to occur when the frequency reaches 80 Hz, where there is little difference in the coercive field between the results at 80 and 100 Hz.

From the above results, it was found that both the "*instantaneous*" remnant polarization (P_{ir}) and the "*instantaneous*" coercive field (E_{ic}) increase when the electric field (E_0) increases from 10 kV/cm to 25kV/cm. When the hysteresis loops were plotted at 25 kV/cm and with varying frequency from 20 to 100 Hz, P_{ir} was found to decrease with an increase in frequency while E_{ic} still increases. At higher frequency (≥80 Hz), the loop tends to stretch out more and no longer exhibit ferroelectric *P-E* hysteresis loop. It is understood that at the higher frequency a space charge polarization from conducting ions at the interface cannot follow the change of the electric field, thereby leading to a non-ferroelectric appearance. It should also be noted here that fully saturated P-E loops

cannot be achieved for the 0-3 PZT–PC composite studied here as a result of its highly lossy characteristics due to the presence of the weak conducting ions in the cement matrix, which in turns leads to poling difficulties in this type of the composites.

The authors gratefully acknowledge the Thailand Research Fund (TRF) and the Commission on Higher Education (CHE) for financial support.

References

[1] Z. Li, D. Zhang, K. Wu, J. Am. Ceram. Soc., **85** (2002), p.305.

[2] C. Xin, S. Huang, C. Jun, X. Ronghua, L. Futian, L. Lingchao, J. Eur. Ceram. Soc., **25** (2005), p. 3223.

[3] A.Chaipanich, T. Tunkasiri, Curr App Phys., **7** (2007), p285.

[4] B. Dong, Z. Li, Compos. Sci. Technol.**65** (2005), p.1363.

[5] S. Huang, J. Chang, R. Xu, F. Liu, L. Lu, Z. Ye, X. Cheng, Smart Mater. Struct.,**13** (2004) 270

[6] Z. Li, B. Dong, D. Zhang, Cem. Concr. Compos., **27** (2005), p. 27.

[7] A. Chaipanich , N. Jaitanong, T. Tunkasiri, Matls. Letts., **61** (2007), p.5206.

[8] A. Chaipanich and N. Jaitanong, Adv. Mats. Res., **55-57**(2008), p.381.

[9] N. Jaitanong, K. Wongjinda, P. Tammakun, G. Rujijanagul and A. Chaipanich, Adv. Mats.Res., **55-57** (2008), p.377.

[10] N. Jaitanong, A. Chaipanich , T. Tunkasiri, Ceram Inter., **34** (2008), p.793.

[11] A. Chaipanich, Curr App Phys., **7** (2007), p. 574.

[12] A. Chaipanich Curr App Phys., **7** (2007), p. 537.

[13] J.-M. Liu, H. L. W. Chan, C. L. Choy, Y. Y. Zhu, S. N. Zhu, Z. G. Liu, N. B. Ming, Appl. Phys. Lett., **79** (2001), p.236.

[14] R.Yimnirun, S. Ananta, Y. Laosiritaworn, A.Ngamjarurojana, and S.Wongsaenmai, Ferroelectrics, **358** (2007), p.3.

[15] R.Yimnirun, Y. Laosiritaworn, S. Ananta, and S.Wongsaenmai, Appl. Phys. Lett., **89** (2006), p 162901-1

[16] R. Yimnirun, N. Wongdamnern, N. Triamnak, M. Unruan, A. Ngamjarurojana, S. Ananta, and Y. Laosiritaworn, J. Appl. Phys. **103** (2008), p 086105-1

[17] N. Wongdamnern, A. Ngamjarurojana, Y. Laosiritaworn, S. Ananta, and R. Yimnirun, J. Appl. Phys. *Submitted*

[18] R. Yimnirun, N. Wongdamnern, N. Triamnak, M. Unruan, A. Ngamjarurojana, S. Ananta, and Y. Laosiritaworn, J. Phys. D: Appl. Phys. **41** (2008), p 205415-1

[19] X. Cheng, S.Huang, J. Chang, and Z. Li, J. Appl. Phys., **101**(2007)

[20] ? P-E loop of PC-PZT composites

[21] ? P-E loop of PC-PZT composites

Figure Captions

Figure 1 XRD Diffraction pattern of 0-3 PZT-PC composites with comparison to PZT and PC patterns

Figure 2 Effects of electric field amplitude on (a) the ferroelectric (*P*-*E*) hysteresis loops and (b) on *instantaneous* remnant polarization (P_{ir}) and *instantaneous* coercive field (E_{ic}) of PZT-PC composites (with fixed *f* of 60 Hz)

Figure 3 Effects of electric field frequency on (a) the ferroelectric (*P*-*E*) hysteresis loops and (b) on *instantaneous* remnant polarization (P_{ir}) and *instantaneous* coercive field (E_{ic}) of PZT-PC composites (with E_0 fixed at 25 KV/cm)

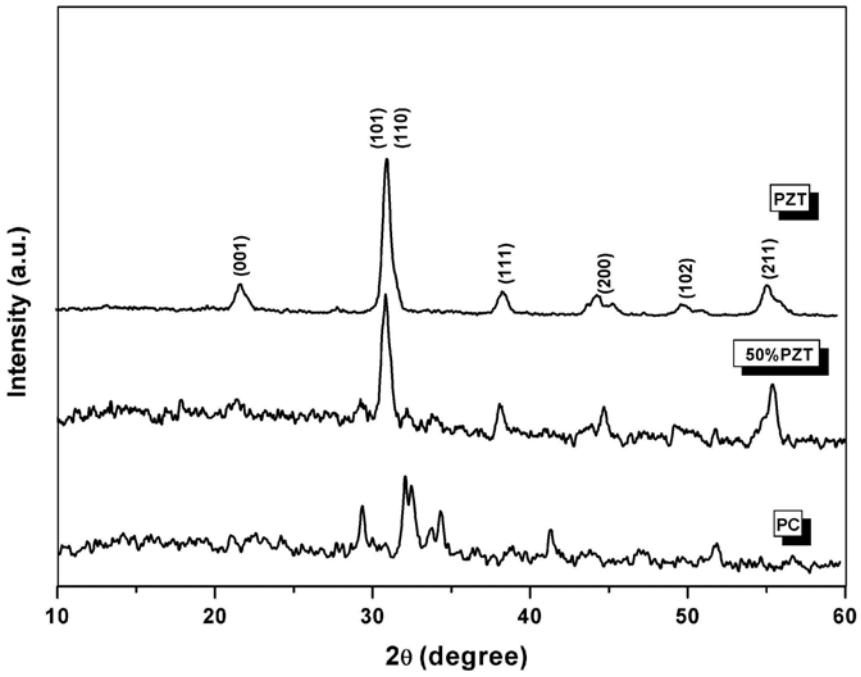
Intensity (a.u.)
(001)
(101)
(110)
(111)
(200)
(102)
(211)
PZT
50%PZT
PC
10
20
30
40
50
60
2θ (degree)

Figure 1

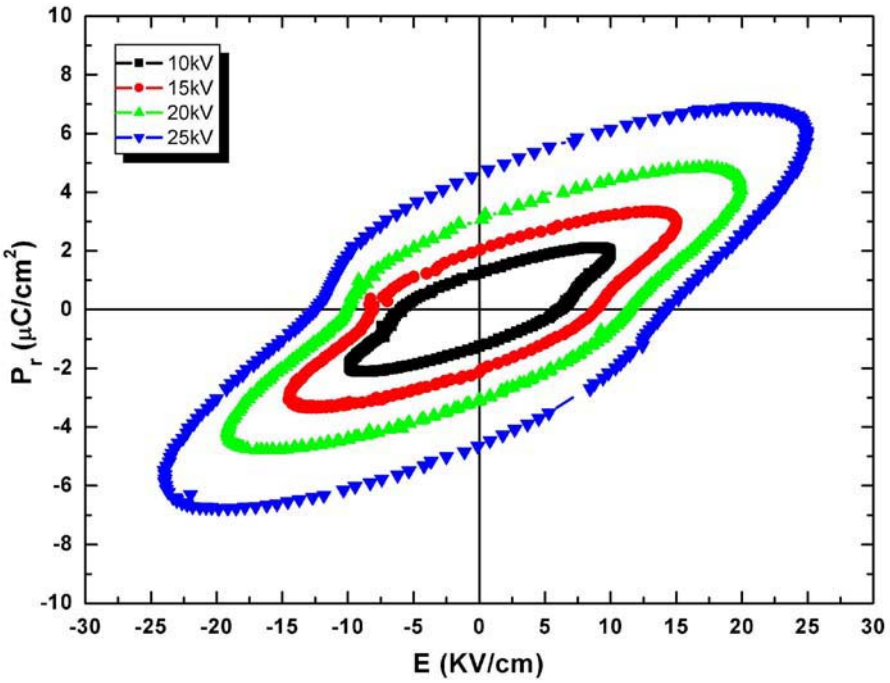
10kV
15kV
20kV
25kV
P_r (μC/cm^2)
E (KV/cm)

(a)

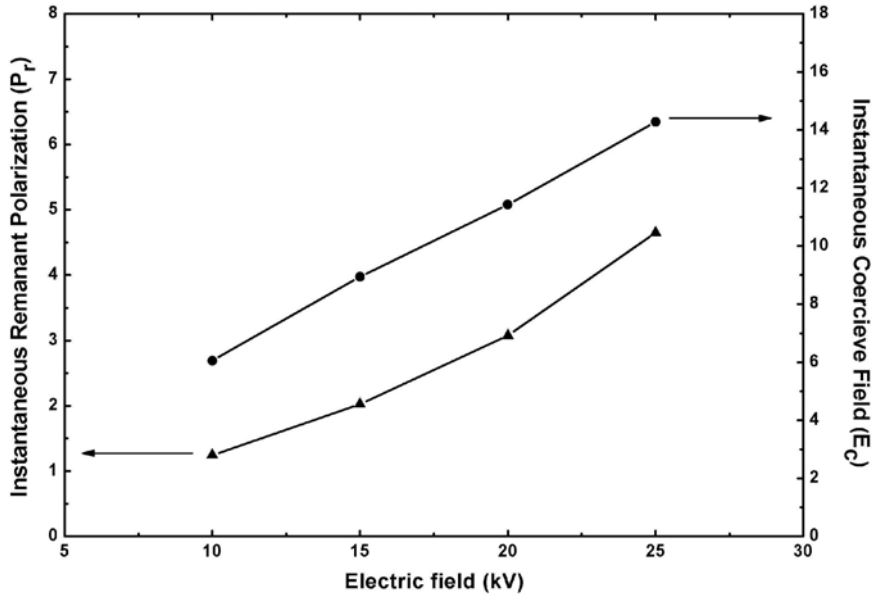
Instantaneous Remanant Polarization (P_r)
Instantaneous Coercieve Field (E_C)
Electric field (kV)

(b)

Figure 2

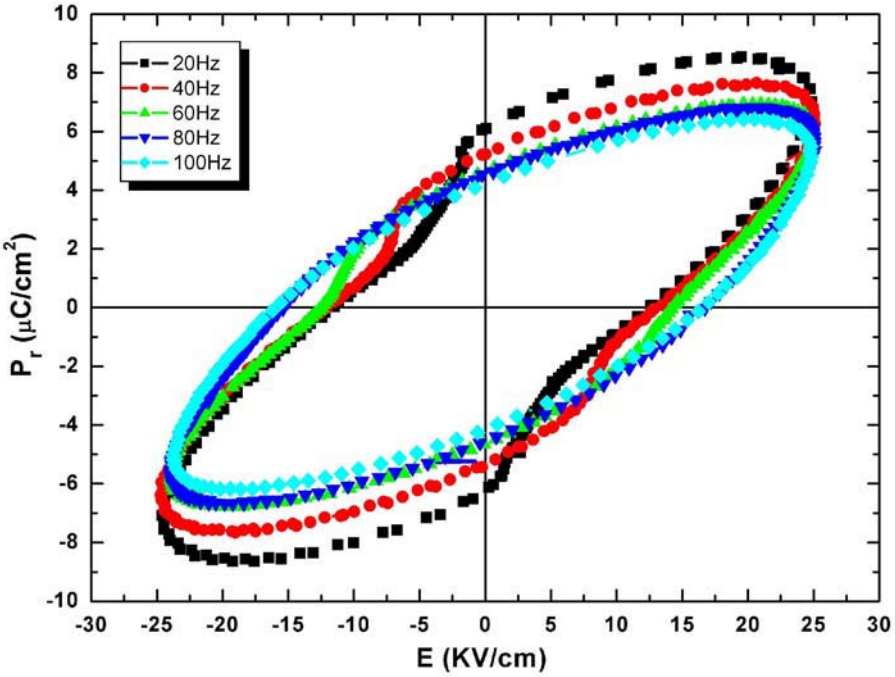
20Hz
40Hz
60Hz
80Hz
100Hz
P_r (μC/cm^2)
E (KV/cm)

(a)

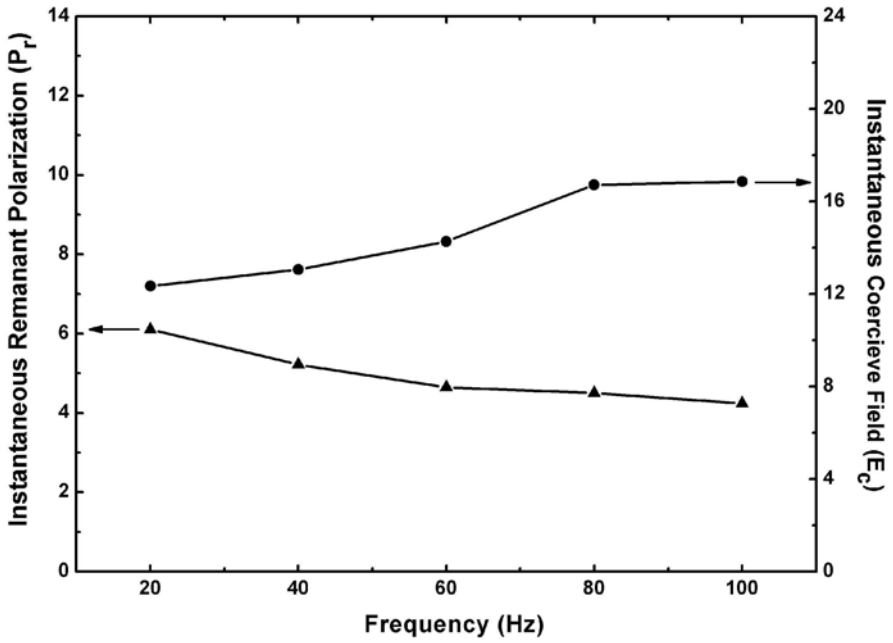
Instantaneous Remanant Polarization (P_r)
Instantaneous Coercieve Field (E_c)
Frequency (Hz)

(b)

Figure 3

Phys. Scr. **T129** (2007) 184–189 doi:10.1088/0031-8949/2007/T129/042

Stress- and temperature-dependent scaling behavior of dynamic hysteresis in soft PZT bulk ceramics

R Yimnirun, S Wongsaenmai, R Wongmaneerung, N Wongdamnern, A Ngamjarurojana, S Ananta and Y Laosiritaworn

Department of Physics, Faculty of Science, Chiang Mai University, Chiang Mai 50200, Thailand

E-mail: rattikornyimnirun@yahoo.com

Received 1 March 2007
Accepted for publication 13 July 2007
Published 27 November 2007
Online at stacks.iop.org/PhysScr/T129/184

Abstract

Effects of electric field-frequency, electric field-amplitude, mechanical stress, and temperature on the hysteresis area, especially the scaling form, were investigated in soft lead zirconate titanate (PZT) bulk ceramics. The hysteresis area was found to depend on the frequency and field-amplitude with the same set of exponents as the power-law scaling for both with and without stresses. The inclusion of stresses into the power-law was obtained in the form of $\langle A - A_{\sigma=0}\rangle \propto f^{-0.25} E_0 \sigma^{0.44}$ which indicates the difference in energy dissipation between the under-stress and stress-free conditions. The power-law temperature scaling relations were obtained for hysteresis area $\langle A\rangle$ and remanent polarization P_r, while the coercivity E_C was found to scale linearly with temperature T. The three temperature scaling relations were also field-dependent. At fixed field amplitude E_0, the scaling relations take the forms of $\langle A\rangle \propto T^{-1.1024}$, $P_r \propto T^{-1.2322}$ and $(E_{C0} - E_C) \propto T$.

PACS numbers: 77.22.Ch, 77.84.Dy, 77.84.−s

(Some figures in this article are in colour only in the electronic version.)

1. Introduction

Lead zirconate titanate ($Pb(Zr_{1-x}Ti_x)O_3$ or PZT) ceramics are among the lead-based complex perovskites that have been investigated extensively, both from academic and commercial viewpoints with various applications [1–3]. However, PZT ceramics are usually modified with dopants. Generally, donor (higher-valency) additives induce 'soft' piezoelectric behavior with higher dielectric and piezoelectric activities, while acceptor (lower-valency) additives result in 'hard' piezoelectric behavior [1–3]. Most of the previous investigations have been focused on soft PZT ceramics because of their extensive uses in sensors and actuators [1–3]. In many of these applications, the dynamic hysteresis, i.e. hysteresis area $\langle A\rangle$ as a function of the field amplitude E_0 and frequency f has become an important consideration [1–4]. Hence, there have been reports on the scaling behavior, which indicates the dependence of the hysteresis area $\langle A\rangle$ on relevant parameters, of the dynamic hysteresis in ferromagnetic and ferroelectric thin films [5–13]. Many theoretical studies have been focused on the scaling law.

$$\langle A\rangle \propto f^{\alpha} E_0^{\beta}, \tag{1}$$

where α and β are exponents that depend on the dimensionality and symmetry of the system of hysteresis curves in polarization systems [5–8]. Earlier investigations have reported the scaling relations for high-f region with α and β values, respectively, of -1 and 2 for $(\Phi^2)^2$ and $(\Phi^2)^3$ models, and of -0.33 and 3 for PZT thin-film [6, 8, 9]. In contrast, there are only very few reports on the scaling behavior studies of ferroelectric hysteresis loops of bulk ferroelectric ceramics [14–17].

More importantly, in many applications the ceramic specimens are often subjected to mechanical loading, either from the design of the device itself or from operating conditions which induce stresses [1–3, 18]. Therefore, a prior knowledge of how the material properties change under different load conditions in materials is inevitably crucial for proper design of a device and for suitable

selection of materials for a specific application. In many previous investigations the electrical properties of ceramics were found to depend strongly on stresses (σ) [19–23]. Additionally, it is well known that the size and shape of the hysteresis loop in the ferroelectric state depend strongly on temperature T [1–3, 24]. The temperature dependence of ferroelectric properties is of interest in view of not only technological applications, but also in fundamental senses. The theoretical investigation by Rao *et al* has already proposed a temperature scaling for ferromagnetic materials, which indicates that the hysteresis area decreases with increasing temperature [5, 8]. Experimental results on ferromagnetic thin-films have revealed various temperature scaling relations [5, 6, 8, 10]. Interestingly, there has been no report on the temperature scaling of dynamic hysteresis in ferroelectrics, both theoretical and experimental. Since f, E_0, σ and T have been reported to impose significant influence on the dynamic hysteresis responses of ferroelectric ceramics, it is therefore the aim of this study to establish the scaling behavior of the dynamic hysteresis responses of soft PZT bulk ceramics under the influence of external stress and temperature. In this present study, the scaling behavior indicates the dependence of the hysteresis area $\langle A \rangle$ on frequency f, field amplitude E_0, stress σ and temperature T.

2. Experimental

Disk-shaped samples of a commercially available soft PZT ceramic (PKI-552, Piezo Kinetics Inc., USA) with diameter of 10 mm and thickness of 1 mm were used in this study. For the stress-dependent studies, the dynamic hysteresis (P–E) loops were characterized at room temperature (25 °C) by using a modified Sawyer–Tower circuit with f covering from 2 to 100 Hz and E_0 from 0 to 18 kV cm^{-1}. The electric field was applied to a sample by a high voltage AC amplifier (Trek 610D) with the input sinusoidal signal from a function generator (HP 3310A). The P–E loops were recorded by a digital oscilloscope (HP 54645A, 100 MHz). Effects of the external stress on the dynamic hysteresis were investigated with the compressometer, which was developed for simultaneous applications of the mechanical stress and the electric field [22, 23]. The compressive stress, applying parallel to the electric field direction, was supplied by the servohydraulic load frame and monitored with the pressure gauge. The P–E loops were recorded as a function of mechanical stress applied discretely between 0 and 24 MPa for each applied field and frequency. At each constant stress, the loop was obtained after 20 sampling cycles to average out the noise deformation. For the temperature-dependent studies, the stress-free P–E hysteresis loops were obtained over a temperature range of 298–453 K with E_0 up to 40 kV cm^{-1} (f was fixed at 4 Hz).

3. Results and discussion

3.1. Stress-dependent case

The hysteresis profiles for various frequencies f, field-amplitude E_0, and stress σ are obtained. For a particular applied stress, as expected, the dependence of the loop pattern

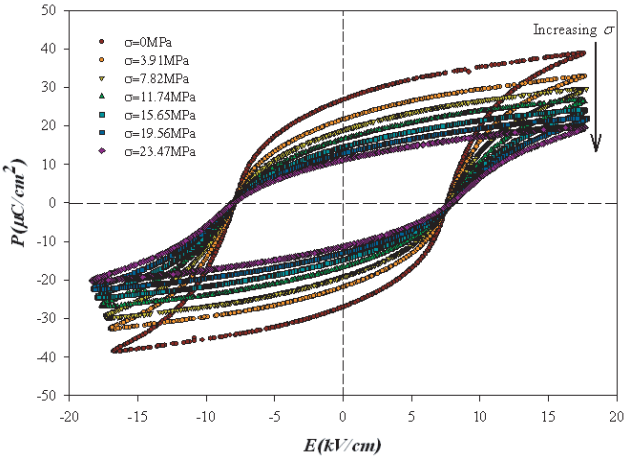

Figure 1. Hysteresis loops for soft PZT ceramic at various σ ($f = 100$ Hz and $E_0 = 18$ kV cm^{-1}).

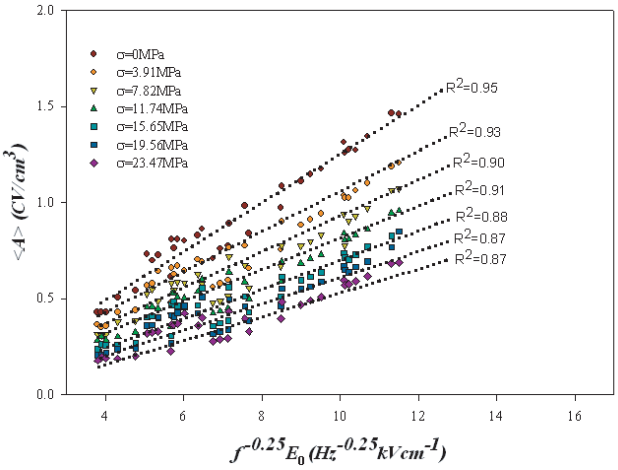

Figure 2. Scaling of hysteresis area $\langle A \rangle$ against $f^{-0.25}E_0$ for soft PZT ceramic at various σ.

and area $\langle A \rangle$ on f and E is remarkable. At fixed E_0, the loop area $\langle A \rangle$, remanent polarization (P_r), and coercive field (E_C) decrease with increasing frequency. For the dependence of the hysteresis loop on E_0, the loop does not saturate at small fields (6 and 8 kV cm^{-1}). With further increase in E_0, $\langle A \rangle$, P_r and E_C increase until well saturated loop is achieved. Similar stress-free observations have been reported in thin-films and bulk ceramics [7, 11, 14–17].

Figure 1 displays the hysteresis loops under different compressive stress during loading at fixed f of 100 Hz and fixed E_0 of 18 kV cm^{-1}. The P–E loop area $\langle A \rangle$ is found to decrease steadily with increasing stress. To investigate the scaling behavior under the effect of applied stresses, instead of including only the field amplitude E_0 and the frequency term f, the scaling relation should also include the stress (σ) term, i.e.

$$\langle A \rangle \propto f^m E_0^n \sigma^p. \tag{2}$$

However, due to increasing number of exponents, to simplify the problem, the validity of the scaling law $\langle A \rangle(\sigma) \propto f^{-0.25}E_0$ is assumed, inspired by a stress-free investigation on bulk PZT [14], for all applied stresses. Consequently, the area $\langle A \rangle$ for each stress is plotted against $f^{-0.25}E_0$, as shown in figure 2, and it can be seen from the least-square linear fits

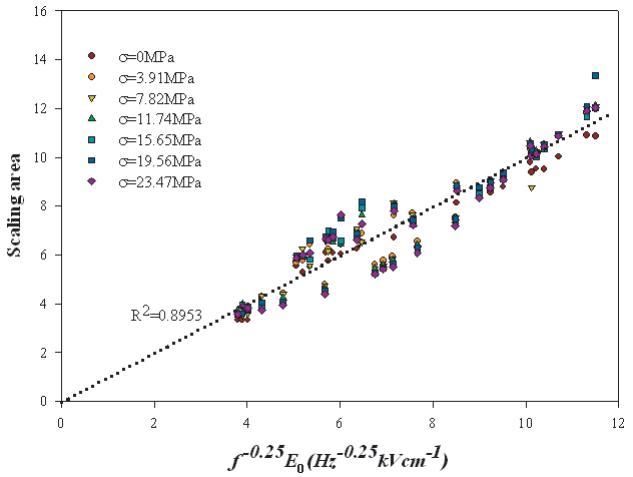

Figure 3. The collapse of the scaling area $(\langle A\rangle - F(\sigma))/(\sigma)$ against $f^{-0.25}E_0$ on the same linear-line (with small fluctuation) for soft PZT ceramic.

that reasonably good linear relations can be found. As a result, the condition of universality having $m = -0.25$ and $n = 1$ in soft PZT bulk ceramic systems is confirmed whereas the proportional constant in equation (2) may still be a function of σ. Therefore, equation (2) is generalized by writing,

$$\langle A\rangle = G(\sigma)\, f^{-0.25}E_0 + F(\sigma), \tag{3}$$

where both $G(\sigma)$ and $F(\sigma)$ are assumed to be a function of σ representing slope-function and y-intercept-function for a 'linear-relation' in equation (3), and their values are presented via linear-fit functions in figure 2. Next, to obtain the scaling form as indicating in equation (2), the slope-function $G(\sigma)$ is assumed to take a form of power-law function, i.e. $G(\sigma) = a + b\sigma^c$, and a nonlinear fit for $G(\sigma)$ gives $a = 0.136 \pm 0.021$, $b = -0.019 \pm 0.015$ and $c = 0.439 \pm 0.173$ with $R^2 \approx 0.994$. However, for the y-intercept-function $F(\sigma)$, the scattering data in $F(\sigma)$ do not follow a trivial power-law scaling form. Instead, the reasonably well-fitted function that suits $F(\sigma)$ in the current study is found to take a quadratic function. So $F(\sigma) = a_0 + a_1\sigma + a_2\sigma^2$ is written and a least square fit is performed to give $a_0 = -0.019 \pm 0.006$, $a_1 = 0.002 \pm 0.001$ and $a_2 = -1.149 \times 10^{-4} \pm 4.850 \times 10^{-4}$ with $R^2 \approx 0.878$. As a result, from equation (3), it is therefore possible to write the scaling area

$$\frac{\langle A\rangle - F(\sigma)}{G(\sigma)} = f^{-0.25}E_0 \tag{4}$$

and by plotting this scaling area $(\langle A\rangle - F(\sigma))/G(\sigma)$ against $f^{-0.25}E_0$ all the data should collapse on to a single linear line having a y-intercept at zero. The data-collapsing of the scaling area from all f, E_0 and σ was found to confirm equation (4) as evident in figure 3. On the other hand, it is of interest if the scaling of $\langle A\rangle$ in a form given by equation (2) is allowed. Therefore, by discarding minor loops which usually occur at very low E_0, $F(\sigma) \equiv \langle A\rangle\ (E_0 \to 0)$ will be small in comparison to $\langle A\rangle$ and can be discarded in equation (4) at some intermediately high fields. Consequently, $\langle A\rangle \propto (a + b\sigma^c)\, f^{-0.25}E_0$ may be written and by substituting the fitted parameters, it is found that

$$\langle A\rangle - \langle A_{\sigma=0}\rangle = \langle A - A_{\sigma=0}\rangle \propto f^{-0.25}E_0\sigma^{0.44}, \tag{5}$$

where $\langle A_{\sigma=0}\rangle$ refers to stress-free hysteresis area which will be a dominant term for zero stress. Note that from the appearance of stress σ, $\langle A - A_{\sigma=0}\rangle$, referring to the difference in energy dissipation between under-stress and stress-free conditions, increases with increasing stress suggesting a decay of $\langle A\rangle$ with σ at a rate of $\sigma^{0.44}$ as observed in experiments. As a result, it can be concluded that the difference in the hysteresis area between under-stress and stress-free conditions scales with frequency, field-amplitude and stress via exponents $m = -0.25$, $n = 1$ and $p = 0.44$. However, at a particular fixed stress, equation (5) gives $f^{-0.25}E_0$ which is the original form for how the area scales with the frequency and the field-amplitude [14].

To understand the scaling relation obtained, at least qualitatively, one needs to consider the following statements. Since the P–E loop area indicates the polarization dissipation energy subjected to one full cycle of electric field application, the loop area is therefore directly related to volume involved in the switching process during the application of electric field [22–24]. Hence, when the mechanical stress is applied, more and more ferroelectric domains are constrained by the applied stress and cannot be re-oriented by the electric field so as to participate in the polarization reversal. Consequently, both the saturation and remanent polarizations become lower with increasing compressive stress. The polarization dissipation energy is consequently found to decrease with increasing applied stress, indicating that the sample volume contributing to polarization reversal decreases with the increasing stress. Similar observations have also been reported in other investigations [19–23]. Though this study has revealed a significant influence of the external stress on the scaling behavior in bulk ceramics, there has been no quantitative theoretical treatment to include the stress-term in the scaling relation. An earlier theoretical investigation by Rao and Pandit [8] has already proposed the inclusion of temperature term in the scaling relation, in addition to f and E_0 terms. Many of the theoretical treatments to explain the stress effect on the hysteresis behavior have been primarily based on constitutive models, thermodynamic phenomenology and Rayleigh law approach [25–27]. This clearly has triggered a need to include a stress-term in the previous theoretical models [5–7].

3.2. Temperature-dependent case

The hysteresis loops for various electric field amplitudes E_0 and temperatures T were obtained and it was found that both E_0 and T played a crucial role on the hysteresis area $\langle A\rangle$. For example, with increasing E_0, a transition from a minor loop at low field to a saturated s-shape loop at high field occurs. This is expected because with higher field there is more electrical energy supplied into the system resulting in more 'electrical driving force' acting on electric dipole moments [24]. Consequently, the polarization has more tendency to follow the external electric field which in turn reduces the phase lag between the polarization and the field signals. As a result, the saturated loops are obtained at high fields instead of the minor loops at low fields. On the other hand, with increasing temperature, the loop area is notably reduced in size. This is caused by the fact that higher temperature

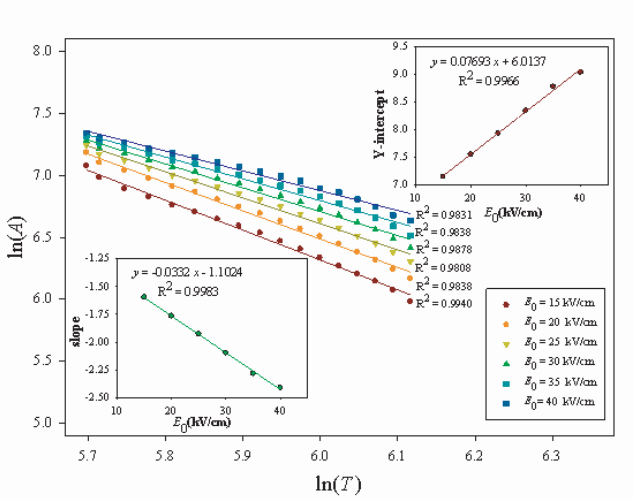

Figure 4. Double logarithmic plot between ln (A) and ln (T) for various E_0 where the linear relations are found but the y-intercepts and slopes seem to be E_0-dependent. The insets show those linear relations with E_0.

provides higher thermal fluctuation to the polarization which reduces the ferroelectric interaction among the dipoles [24]. Therefore, even E_0 is fixed, the polarization direction is easily tuned with the electric field at higher temperatures due to the smaller ferroelectric interaction providing a reduction in both remanent polarization (P_r) and coercivity (E_C). For this reason, the hysteresis loop area is reduced with increasing temperature. Similar observations have been reported in many other ferroelectric systems [28–31]. More interestingly, the observed temperature dependence of these hysteresis parameters prompts a question whether there exist temperature scaling relations for these parameters.

Figure 4 shows the relation between $\langle A \rangle$ and T in a double logarithmic form where good linear fits are apparent (R^2 close to 1). This implies a power-law relation between the hysteresis area and temperature, i.e. $\langle A \rangle \propto T^{\gamma}$, and for each E_0 the exponent γ can be extracted from the slope, i.e. $\gamma = \mathrm{d}\ln\langle A \rangle / \mathrm{d}\ln T$. However, both the slope γ and the y-intercept seem to vary with E_0. Thus, to prove this E_0 dependence, both the slope γ and the y-intercept are plotted as a function of E_0 (insets in figure 4), and the linear dependences on E_0 are noticeable. The linear least square fits of both slopes and y-intercepts with E_0 give $y = -0.0332x - 1.1024$ with $R^2 = 0.9983$ for the slope (lower inset), and $y = 0.0769x + 6.0137$ with $R^2 = 0.9966$ for the y-intercept (upper inset). However, the y-intercept refers to the value of $\ln\langle A \rangle$ at the limit $\ln T$ approaching zero and from the fitting $\ln\langle A \rangle$ is not ceased at this limit which is not really sound because at low temperatures dynamic of the dipoles or domain walls freeze. This could be caused by the fact that domain wall motion at high temperature is very different from that at very low temperature [32, 33]. Consequently, this study does not imply there is a finite hysteresis area at T approaching zero (i.e. in this case $\ln T = 0$ or $T = 1$) but the quantity $\ln\langle A \rangle$ at $\ln T = 0$ here comes from an empirical fit to fulfill the validity of the linear fit. Therefore, upon the proposed assumptions and fitting techniques, by integrating all the relevant fits, it is

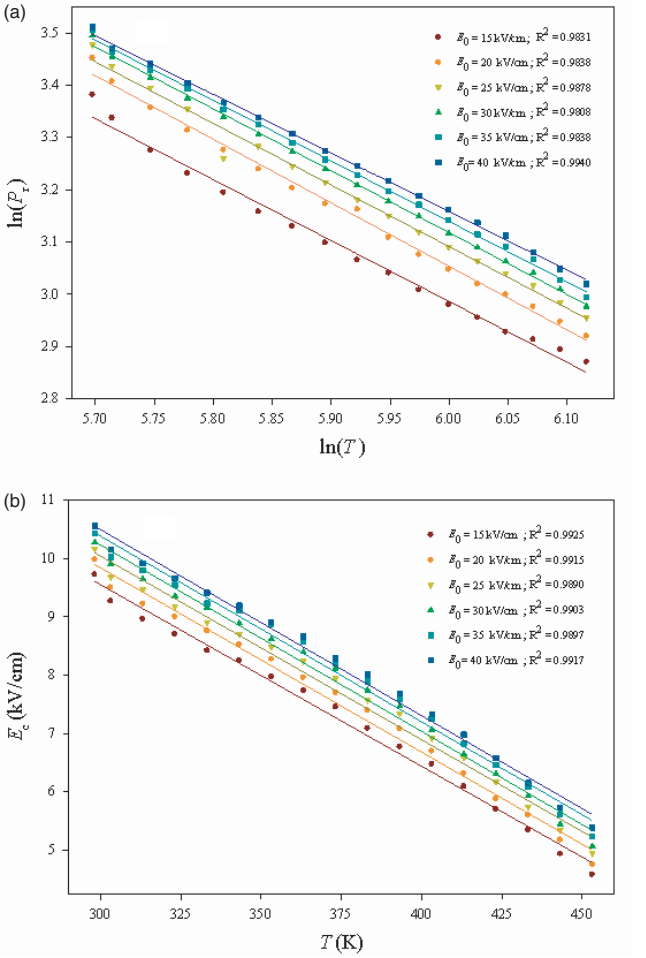

Figure 5. (a) Double logarithmic plot between ln (P_r) and ln (T), and (b) linear plot between E_C and T.

found that

$$\langle A \rangle = \exp\left(0.0769E_0 + 6.0137\right) T^{-(0.0332E_0 + 1.1024)}. \quad (6)$$

Through similar mathematical treatment performed on $\langle A \rangle$, temperature dependent relations for P_r and E_C are also obtained. Figure 5(a) shows the relation between P_r and T in a double logarithmic plot. As is evident, the power-law relation seems suitable for the fit since good R^2 are attained. It is found that

$$P_r = \exp(-0.0068E_0 + 10.305) T^{(0.0022E_0 - 1.2322)}. \quad (7)$$

The relation between E_C and T is shown in figure 5(b). Surprisingly, linear relations are apparent so an approximation on $y = ax + b$ could be used to fit the data. Nonlinear fits between E_C and T are also performed (not shown) and the linear dependence of E_C and T is confirmed. Therefore, it could be estimated that

$$E_C = (-0.00003E_0 - 0.03085)\, T + (0.0459E_0 + 18.319)\,. \quad (8)$$

The temperature dependences of $\langle A \rangle$, P_r and E_C shown in equations (6)–(8) are also slightly E_0-dependent. Obviously, small coefficients to E_0 (for the whole range of E_0 used in this study) suggest that at fixed E_0

$$\langle A \rangle \propto T^{-1.1024}, \quad (9)$$

$$P_{\mathrm{r}} \propto T^{-1.2322}, \tag{10}$$

$$(E_{\mathrm{C0}} - E_{\mathrm{C}}) \propto T. \tag{11}$$

E_{C0} in equation (11) can be viewed as the coercivity at $T \sim 0$ K. However, as $T \to 0$, thermal energy is low causing a non-symmetric hysteresis loop, hence E_{C0} cannot be meaningfully defined. Here, E_{C0} is used for proposing the fit, which is valid for the experimental range in this study.

The quantitative results obtained in equations (9)–(11) could also be explained in terms of domain switching as a function of temperature and field. Generally, the domain switching is caused by the domain wall movement leading to either extension or contraction of the ferroelectric domains, and determines the average polarization value. In soft PZT ceramics, the oxygen vacancy is a key factor which controls how the ferroelectric domain grows and shrinks. In particular, oxygen vacancy is mobile and usually gets stuck at the ferroelectric domain [34–36]. This causes domain wall clamping and decelerates the domain switching. Therefore, if the trapped oxygen vacancies are high in number, the polarization switching is rarely allowed and the polarization will be suppressed due to the pinned domain wall [37]. Nevertheless, the oxygen vacancy can become less trapped if an external electric field is applied [38]. This is since there is more electric driving energy on the ferroelectric dipoles and, starting from boundaries with low oxygen vacancy density, the domain walls move across the boundaries allowing bigger domain switching whereas the oxygen vacancies move aside and get accumulated at other boundaries. This is why higher P_{r} and E_{C} are found with increasing applied field. On the other hand, temperature also has some prominent effect on the domain wall movement. With increasing temperature, there is higher level of thermal fluctuation in the system, that causes the oxygen vacancy to become less entrapped [39]. Therefore, the external field need not be as high as those at low temperatures to unlock the domain switching. This leads to the reduction in E_{C} with increasing temperature. In the case of P_{r}, the higher temperature induces higher level of thermal fluctuation on the domain wall motion and reduces the stability of the polarization in each domain. Thus the average P_{r} tends to decrease with increasing temperature. As a result, the hysteresis area $\langle A \rangle$ is also reduced with increasing temperature. In general, this temperature- and field-dependent domain switching phenomenon is universal to all ferroelectric systems. However, the behavior may be different in detail due to different levels of complex defect, types and percentages of doping, crystal structures and domain states [31, 34, 36–39].

More importantly, equations (9)–(11) present simple relations for the temperature scaling of ferroelectric hysteresis parameters. It should be noted that there have only been few theoretical treatments to include temperature term in dynamic hysteresis scaling of ferromagnetics [5, 6, 8]. Considering relatively successful applications of the treatments to E- and f-dependent ferroelectric hysteresis [5–9], it would be worthwhile to compare our experimental results with the theoretically derived scaling. Theoretical scaling relations have been proposed as $\langle A \rangle \propto T^{-\gamma}$ with γ being 0.7, 1.18 and 1.98 for continuum 3D $(\Phi^2)^2$, 2D and 3D Ising models, respectively [5, 6, 8]. An explanation for the variation may come from the different polarization-interaction terms as considered in these models. It could be seen that our experimentally obtained temperature scaling of $\langle A \rangle$ (with $\gamma \sim 1.1$) falls between the values obtained from the models. The difference could be attributed to additional contributions from depolarizing effects within the ceramics (arisen from domain walls, grain boundaries, space charges, immobile defects etc) [14–17], as compared to physically over-simplified polarization-interaction proposed in the theoretical models [5, 6, 8].

Furthermore, the relation $E_{\mathrm{c}} \propto (T - \mathrm{T_c})^{-0.35}$ drawn from the 3D $(\Phi^2)^2$ model is significantly different from the linear relation obtained from our study, which further clarifies that the theoretical models cannot be applied to ferroelectric bulk ceramics. This study clearly serves as a survey to show that more improvement of the theoretical approach is needed to predict the scaling behavior in bulk ferroelectric ceramics. Interestingly, different forms of temperature scaling of E_{C} extracted from the previous experimental data on PZT thin films also indicate dimensional dependence of the coercivity, as reported in previous investigations [26, 35].

4. Conclusions

The scaling behavior of the dynamic hysteresis of soft PZT bulk ceramics under the effects of mechanical stress and temperature has been investigated. With the presence of external stress, the scaling law for the loop-area yields the same set of exponents as frequency and field-amplitude in stress-free condition which confirms the condition of universality in the bulk system. The difference in energy dissipation between the under-stress and stress-free conditions is found to scale with $f^{-0.25} E_0 \sigma^{0.44}$. Additionally, power-law temperature scaling relations have been found for hystersis area $\langle A \rangle$ and remanent polarization P_{r}, while the coercivity E_{C} scales linearly with temperature. The three temperature scaling relations are field-dependent. At fixed E_0, the scaling relations take the forms of $\langle A \rangle \propto T^{-1.1024}$, $P_r \propto T^{-1.2322}$ and $(E_{\mathrm{C0}} - E_{\mathrm{C}}) \propto T$.

Acknowledgments

Financial support from the Thailand Research Fund (TRF), Commission on Higher Education (CHE), Faculty of Science and Graduate School of Chiang Mai University is gratefully acknowledged.

References

[1] Jaffe B, Cook W R and Jaffe H 1971 *Piezoelectric Ceramics* (New York: Academic)
[2] Xu Y H 1991 *Ferroelectric Materials and Their Applications* (Los Angeles: North-Holland)
[3] Uchino K 2000 *Ferroelectric Devices* (New York: Dekker)
[4] Auciello O, Scott J F and Ramesh R 1998 *Phys. Today* **22** 1
[5] Rao M, Krishnamurthy H R and Pandit R 1990 *Phys. Rev.* B **42** 856
[6] Acharyya M and Chakrabarti B K 1995 *Phys. Rev.* B **52** 6560
[7] Liu J-M, Chan H L W, Choy C L, Zhu Y Y, Zhu S N, Liu Z G and Ming N B 2001 *Appl. Phys. Lett.* **79** 236

[8] Rao M and Pandit R 1991 *Phys. Rev.* B **43** 3373
[9] Liu J-M, Chan H L W, Choy C L and Ong C K 2001 *Phys. Rev.* B **65** 014416
[10] Jiang Q, Yang H N and Wang G C 1995 *Phys. Rev.* B **52** 14911
[11] Pan B, Yu H, Wu D, Zhou X H and Liu J-M 2003 *Appl. Phys. Lett.* **83** 1406
[12] Kim Y-H and Kim J-J 1997 *Phys. Rev.* B **55** R11933
[13] Park J-H, Kim C-S, Choi B-C, Moon B K, Jeong J H and Kim I W 2003 *Appl. Phys. Lett.* **83** 536
[14] Yimnirun R, Laosiritaworn Y, Wongsaenmai S and Ananta S 2006 *Appl. Phys. Lett.* **89** 162901
[15] Yimnirun R, Wongsaenmai S, Ananta S and Laosiritaworn Y 2006 *Appl. Phys. Lett.* **89** 242901
[16] Yimnirun R, Wongmaneerung R, Wongsaenmai S, Ngamjarurojana A, Ananta S and Laosiritaworn Y 2007 *Appl. Phys. Lett.* **90** 112906
[17] Yimnirun R, Wongmaneerung R, Wongsaenmai S, Ngamjarurojana A, Ananta S and Laosiritaworn Y 2007 *Appl. Phys. Lett.* **90** 112908
[18] Uchino K 1997 *Piezoelectric Actuators and Ultrasonic Motors* (Boston, MA: Kluwer Academic)
[19] Zhao J, Glazounov A E and Zhang Q M 1999 *Appl. Phys. Lett.* **74** 436
[20] Viehland D and Powers J 2001 *J. Appl. Phys.* **89** 1820
[21] Zhou D, Kamlah M and Munz D 2005 *J. Eur. Ceram. Soc.* **25** 425
[22] Yimnirun R, Laosiritaworn Y and Wongsaenmai S 2006 *J. Phys. D: Appl. Phys.* **39** 759
[23] Yimnirun R, Ananta S, Ngamjarurojana A and Wongsaenmai S 2005 *Appl. Phys.* A **81** 1227
[24] Lines M E and Glass A M 1977 *Principles and Applications of Ferroelectrics and Related Materials* (Oxford: Clarendon)
[25] Damjanovic D 1997 *J. Appl. Phys.* **82** 1788
[26] Tsurumi T, Sasaki T, Kakemoto H, Harigai T and Wada S 2004 *Japan. J. Appl. Phys.* **43** 7618
[27] Achuthan A and Sun C T 2005 *J. Appl. Phys.* **97** 114103
[28] Liu J-M, Pan B, Yu H and Zhang S T 2004 *J. Phys.: Condens. Matter* **16** 1189
[29] Yuan G L, Liu J-M, Zhang S T, Wu D, Wang Y P, Liu Z G, Chan H L W and Choy C L 2004 *Appl. Phys. Lett.* **84** 954
[30] Lin D, Xiao D, Zhu J and Yu P 2006 *Appl. Phys. Lett.* **88** 062901
[31] Pandey S K, Thakur O P, Kumar A, Prakash C, Chatterjee R and Goel T C 2006 *J. Appl. Phys.* **100** 014104
[32] Gruverman A, Auciello O and Tokumoto H 1998 *Ann. Rev. Mater. Sci.* **28** 101
[33] Lee K and Baik S 2006 *Ann. Rev. Mater. Res.* **36** 81
[34] Chang W, King A H and Bowman K 2006 *Appl. Phys. Lett.* **88** 242901
[35] Tsurumi T, Nam S-M, Kil Y-B and Wada S 2002 *Key Eng. Mater.* **214–215** 123
[36] Jullian C, Li J F and Viehland D 2004 *J. Appl. Phys.* **95** 4316
[37] He L X and Vanderbilt D 2003 *Phys. Rev.* B **68** 134103
[38] Dimos D, Al-Shareef H N, Warren W L and Tuttle B A 1996 *J. Appl. Phys.* **80** 1682
[39] Hauke T, Mueller V, Beige H and Fousek J 1998 *Phys. Rev.* B **57** 10424

IOP Publishing Physica Scripta
Phys. Scr. **T129** (2007) 205–208 doi:10.1088/0031-8949/2007/T129/046

Changes in ferroelectric properties of barium titanate ceramic with compressive stress

Wanwilai Chaisan, Rattikorn Yimnirun and Supon Ananta

Department of Physics, Faculty of Science, Chiang Mai University, Chiang Mai 50200, Thailand

E-mail: wanwilai_chaisan@yahoo.com

Received 26 February 2007
Accepted for publication 17 August 2007
Published 28 November 2007
Online at stacks.iop.org/PhysScr/T129/205

Abstract
In this work, barium titanate (BT) ceramic was prepared using a conventional mixed oxide method. The effect of uniaxial compressive stress on the ferroelectric properties of BT ceramics were investigated. The changes in ferroelectric properties were observed at stress up to 60 MPa using a compressometer in conjunction with a modified Sawyer–Tower circuit. The results showed that applied stress had a significant influence on the ferroelectric properties of BT ceramics. Ferroelectric characteristics, i.e. the area of the ferroelectric hysteresis (P–E) loop, the saturation polarization (P_{sat}), the remanent polarization (P_r) and the loop squareness (R_{sq}), decreased with increasing compressive stress, while the coercive field (E_c) remained constant. Stress-induced domain wall motion suppression and non-180° ferroelectric domain switching processes are responsible for the changes observed.

PACS numbers: 77.80.−e, 77.84.−s, 77.84.Dy

1. Introduction

Barium titanate ($BaTiO_3$; BT), which exhibits a perovskite structure and a Curie temperature ∼120 °C, is a classical ferroelectric material which has been extensively exploited both for fundamental research and for technological utilization over the past decades [1, 2]. Owing to its high dielectric constant, large mechanical-quality factor, large pyroelectric coefficient, non-toxic handling, low cost of manufacturing and being a lead-free ferroelectric ceramic, BT is an environmentally friendly material, thus making it a strong candidate for various electronic applications in this global climatic situation. These include commercial capacitors, positive temperature coefficient resistors, high-density optical data storage, ultrasonic transducers, piezoelectric devices and semiconductors [3–6]. In many of these applications, BT ceramics are often subjected to mechanical loading, either deliberately in the design of the device itself or the device is used under environmental stresses. Despite this fact, material constants used in any design calculations are often obtained from a stress-free measuring condition, which in turn may lead to incorrect or inappropriate actuator and transducer designs [7]. It is therefore important to determine the electrical properties of BT ceramics as a function of applied stress. Previous investigations on stress-dependence of electrical properties of many ferroelectric ceramics, such as lead zirconate titanate (PZT), lead magnesium niobate (PMN) and PMN–lead titanate (PT) [7, 8], have clearly emphasized the importance of this subject. These works reported that the electrical properties of these ceramics changed significantly on the application of stress. Yimnirun *et al* [7] and Zhou *et al* [9] investigated the effect of external stress on the ferroelectric properties of soft PZT ceramics. Their results showed that the ferroelectric characteristics, i.e. the area of the ferroelectric hysteresis (P–E) loops, the saturation polarization (P_{sat}), the remanent polarization (P_r) and the loop squareness (R_{sq}), decrease with increasing compressive stress. For BT, the stress dependence on its electrical properties has been widely studied for many decades. Konkol and Piotrowska [10] have studied the effect of one-dimensional stress on the permittivity (ε) of BT ceramics. Their work showed that the ε value increased with pressure below 100 kg cm^{-2} and increased more slowly after pressure above 100 kg cm^{-2} as domain movement is restricted. After removal of stress, the ε slowly decreased to the original value. Moreover, Kim *et al* [11] observed the change in domain configuration under external stress and explained it in terms of elastic strain energy minimization. However, there are few works studying the ferroelectric

properties of BT under stress. Desu [12] studied the influence of stress on the ferroelectric properties of BT thin film and reported that the coercive fields of BT thin film increased while remanent polarization decreased with increasing compressive stress. Sinyakov and Flerova [13] studied the hysteresis loop behavior of BT single crystal with tensile stress. Nevertheless, as well known, the experimental results of thin films and single crystals are always totally different from bulk ceramics because of their different microstructures [14].

Thus far, there have been no systematic studies on the ferroelectric properties of BT bulk ceramics and even though, as mentioned above, there have been many works on electrical properties of BT ceramics since 1940s [1, 2], there are no previous reports on the P–E hysteresis loop results under various environmental stresses of BT bulk ceramics. Therefore, this work will be the first to investigate the dependence of hysteresis loop with stress for BT ceramic. The major purpose of this work is to report the results of P–E hysteresis loops of BT ceramic under various compressive stresses and to discuss these new experimental results. Moreover, the ferroelectric data, i.e. the saturation polarization (P_s), the remanent polarization (P_r), the coercive field (E_c) and the loop squareness (R_{sq}), of BT ceramic under compressive stress will also be reported.

2. Experimental procedure

Investigations were performed on BT ceramics produced by the conventional mixed oxide method. The x-ray diffraction test at room temperature showed that BT ceramics have a pure perovskite phase with tetragonal symmetry, matched with JCPDS file no 5-0626 with unit cell parameters $a = 3.994$ Å and $c = 4.038$ Å, space group *P4 mm* (no 99) [15]. Disk samples with a diameter of 12.5 mm and a thickness of 0.8 mm were chosen for the electrical measurements and the samples were electroded by silver painting.

The ferroelectric hysteresis (*P–E*) loops were characterized by using a computer controlled modified Sawyer–Tower circuit. The electric field was applied to a sample by a high voltage ac amplifier (Trek, model 610D) with the input sinusoidal signal with a frequency of 100 Hz from a signal generator (Goodwill, model GAG-809). To study the effect of the compressive stress on the ferroelectric properties, the uniaxial compressometer was constructed. The detailed descriptions of this system are explained elsewhere [7, 16]. During the measurements, the specimen was immersed in silicone oil to prevent high-voltage arcing during electric loading. Measurements were performed as a function of mechanical stress applied discretely between 0 and 60 MPa. During the measurements, a desired stress was first applied to the sample and then the electric field was applied. The ferroelectric hysteresis (*P–E*) loop was recorded at room temperature (25 °C). The parameters obtained from the loops were the saturation polarization (P_s), the remanent polarization (P_r) and the coercive field (E_c), which are defined as the points where the loops reach the maximum polarization, cross the zero field and the zero polarization, respectively.

3. Results and discussion

The polarization versus electric field (*P–E*) hysteresis loops of the BT ceramics under different compressive stress are shown in figure 1. It should first be noted that the area of these *P–E* hysteresis loops slightly decreases with increasing stress. The *P–E* loop area represents the unit-volume polarization dissipation energy of a ferroelectric material subject to one full cycle of electric field loading [17]. The change in polarization dissipation energy is plotted in figure 2 as a function of compressive stress, in which the dissipation energy is found to decrease linearly with the stress increment. The polarization dissipation energy is also termed energy loss consumed for self-heating of the specimen and related directly to the number of domains participating in the switching process during an electric loading cycle [9]. From figure 2, it is clear that the number of domains contributing to polarization reversal gradually decreases with increasing compressive stress. In the stress-free state (0 MPa), the dissipation energy is 1.10×10^5 J m^{-3}, whereas at maximum stress (60 MPa), the dissipation energy decreases to 0.9×10^5 J m^{-3} (~20% of the stress-free state), which implies that a lower number of domains participate in polarization reversal under high compressive stress.

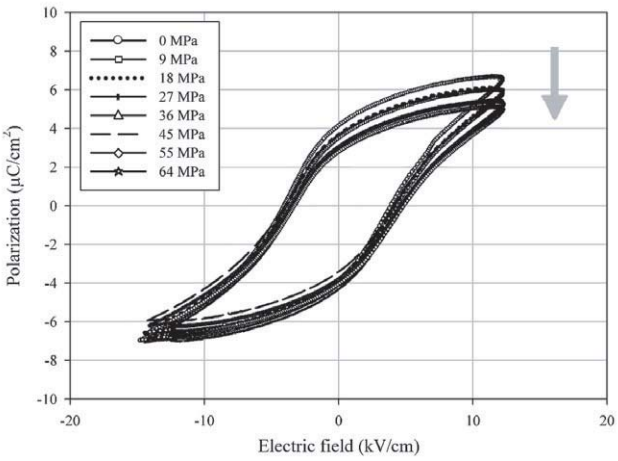

Figure 1. Polarization versus electric field (*P–E*) hysteresis loops as a function of compressive stress for BT ceramic.

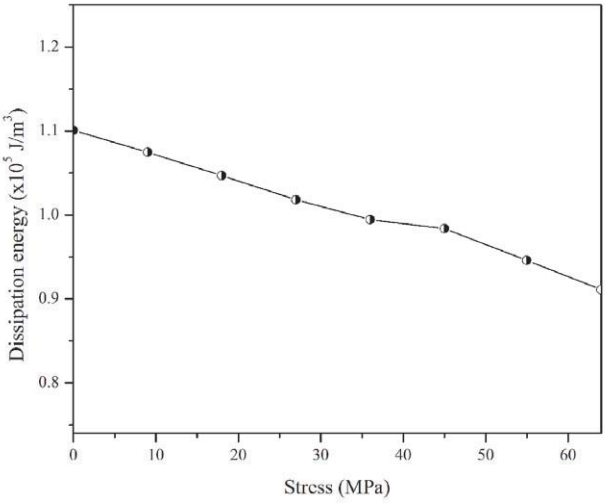

Figure 2. Changes in dissipation energy (hysteresis loop area) with compressive stress for BT ceramic.

The changes in the saturation polarization (P_s), remanent polarization (P_r) and coercive field (E_c) with the compressive

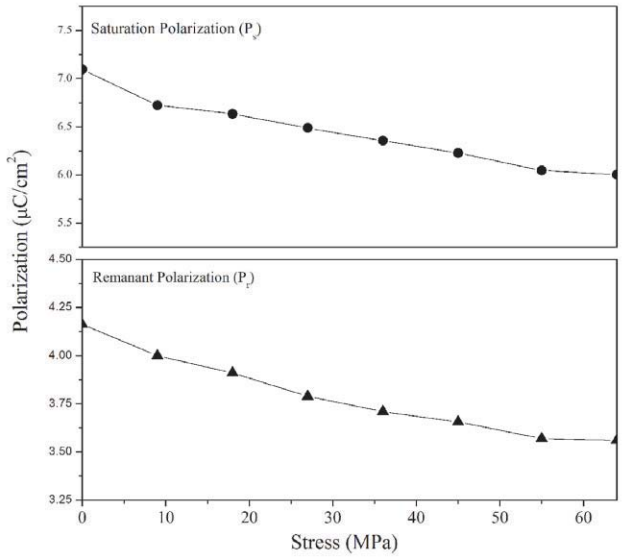

Figure 3. Changes in saturated polarization (P_s) and remanent polarization (P_r) with compressive stress for BT ceramic.

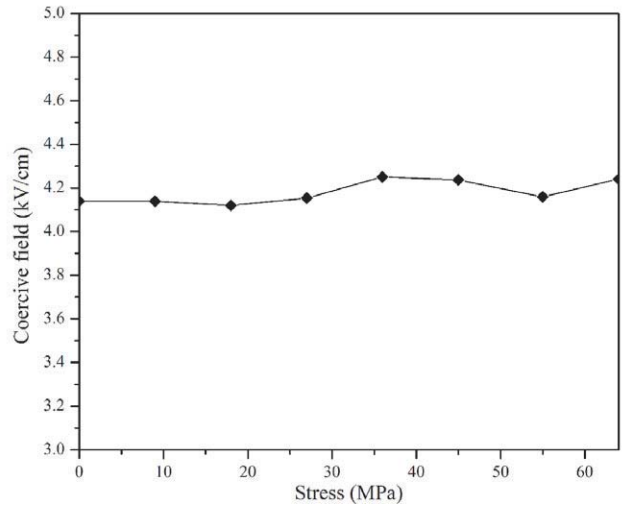

Figure 4. Changes in coercive field (E_c) with compressive stress for BT ceramic.

stress are plotted in figures 3 and 4, respectively. Similarly to the trend observed in the dissipation energy, figure 3 clearly shows that both the P_s and P_r decrease as the compressive stress increases. This suggests a significant stress induced decrease in the switchable part of the spontaneous polarization of the BT ceramic resulting in the observed decrease in the polarization value under high stress [18]. In contrast, the applied stress shows little or no influence on the coercive field (E_c), as plotted in figure 4. These results clearly indicate that BT ceramics are not suitable for high compressive stress applications. It should be noted here that previous works on other ceramics systems, such as PZT, PLZT and PMN–PT, showed a similar tendency [9, 19, 20].

The ferroelectric characteristics of the BT ceramic can also be assessed with the hysteresis loop squareness (R_{sq}), which can be calculated from the empirical expression [21, 22]:

$$R_{sq} = \frac{P_r}{P_s} + \frac{P_{1.1E_c}}{P_r}, \quad (1)$$

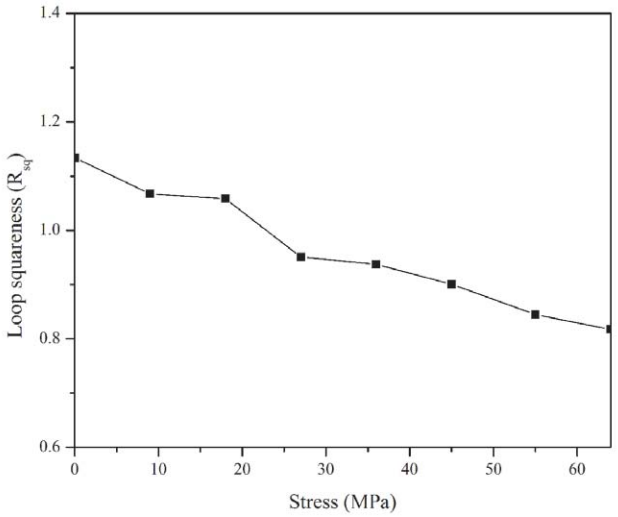

Figure 5. Changes in loop squareness (R_{sq}) with compressive stress for BT ceramic.

where P_r is the remanent polarization, P_s is the saturated polarization obtained at some finite field strength below the dielectric breakdown and $P_{1.1E_c}$ is the absolute value of the polarization at the field equal to $1.1E_c$. For the ideal square loop, R_{sq} is equal to 2. As shown in figure 5, the R_{sq} values gradually decrease with increasing compressive stress. This observation is clearly a result of the decrease in polarization under the compressive stress. From these results, it can be said that the ferroelectric characteristics of BT ceramic decrease considerably under application of compressive stress.

To understand these experimental results on the BT ceramic, one can interpret the changes in terms of domain-reorientation processes. When the compressive stress is applied in the direction parallel to the poling direction, the applied stress tends to keep the ferroelectric domains aligned with their polar axes away from the stress direction through the non-180° domain switching processes. Therefore, it takes a larger than usual applied electric field to reorient the domain along the stress direction, resulting in a lower value of the saturated polarization (figure 3). When the electric field is reduced to zero the domain tends to rotate back away from the stress direction, resulting in a lower than usual remanent polarization (figure 3). Moreover, the decrease in the dissipation energy with increasing compressive stress indicates that more and more ferroelectric domains are constrained by the stress and cannot be reoriented by the electric field so as to participate in the polarization reversal. Consequently, both the saturated and remanent polarizations become lower with increasing compressive stress. The results of the changes in the ferroelectric characteristics of the BT ceramic with increasing compressive stress are in agreement with previous investigations of many ferroelectric ceramics [7, 9, 23].

4. Conclusions

In this study, the effects of compressive stress on the ferroelectric properties of BT ceramic are investigated. Ferroelectric properties under compressive stress are observed up to 60 MPa using a compressometer in conjunction with

a modified Saywer–Tower circuit. The results show that the area of the hysteresis loops, which corresponds to the dissipation energy, the saturation polarization (P_s), the remanent polarization (P_r) and the loop squareness (R_{sq}) decrease with increasing compressive stress, whereas the coercive field (E_c) appears unaffected by stress. The non-180° ferroelectric domain switching and stress-induced domain wall suppression processes are responsible for the changes observed. These values (P_s, P_r, R_{sq} and E_c) confirmed that the ferroelectric characteristics of BT ceramic decrease considerably under the application of compressive stress.

Acknowledgments

This work is supported by the Thailand Research Fund (TRF), the Commission on Higher Education (CHE) and the Faculty of Science, Chiang Mai University.

References

[1] Moulson A J and Herbert J M 2003 *Electroceramics: Materials, Properties, Applications* (Chichester, UK: Wiley)
[2] Haertling G H 1999 *J. Am. Ceram. Soc.* **82** 797–818
[3] Uchino K 1998 *Piezoelectrics and Ultrasonic Applications* (Dordrecht: Kluwer)
[4] Uchino K 2000 *Ferroelectric Devices* (New York: Dekker)
[5] Hennings D 1987 *J. High Technol. Ceram.* **3** 91–111
[6] Sreekantan S, Noora A, Ahmad Z, Othman R and West A 2007 *J. Mater. Process. Technol.* at press
[7] Yimnirun R, Laosiritaworn Y and Wongsaenmai S 2006 *J. Phys. D: Appl. Phys.* **39** 759–64
[8] Steiner O, Tagantsev A K, Colla E L and Setter N 1999 *J. Eur. Ceram. Soc.* **19** 1243–6
[9] Zhou D, Kamlah M and Munz D 2005 *J. Eur. Ceram. Soc.* **25** 425–32
[10] Konkol R and Piotrowska A 1976 *Mater. Sci.* **2** 127–8
[11] Kim S B, Chung T J and Kim D Y 1993 *J. Eur. Ceram. Soc.* **12** 147–51
[12] Desu S B 1993 *J. Electrochem. Soc.* **140** 2981–7
[13] Sinyakov E V and Flerova S A 1970 *Phys. Solid State* **12** 2728–30
[14] Chiang Y-M, Birnie D P and Kingery W D 1997 *Physical Ceramics* (New York: Wisley)
[15] JCPDS-ICDD card no. 5-0626. International Centre for Diffraction Data, Newtown, PA, 2002
[16] Park S E and Shrout T R 1997 *J. Appl. Phys.* **82** 1804–11
[17] Lines M E and Glass A M 1997 *Principles and Applications of Ferroelectrics and Related Materials* (Oxford: Clarendon)
[18] Yang G, Ren W, Liu S F, Masys A J and Mukherjee B K 2000 *Proc. 2000 IEEE Ultrason. Symp. (San Juan, Puerto Rico)* p 1005–8
[19] Lynch C S 1996 *Acta Mater.* **44** 4137–48
[20] Zhao J and Zhang Q M 1996 *Ferroelectrics* **2** 971–4
[21] Chaisan W, Yimnirun R, Ananta S and Cann D P 2007 *Mat. Chem. Phys.* **104** 103–8
[22] Haertling G H and Zimmer W J 1966 *Am. Ceram. Soc. Bull.* **45** 1084–9
[23] Yimnirun R, Ananta S, Ngamjarurojana A and Wongsaenmai S 2005 *Appl. Phys. A: Mat. Sci. Proc.* **81** 1227–31

Available online at www.sciencedirect.com
ScienceDirect
Ceramics International 34 (2008) 731–734
CERAMICS INTERNATIONAL
www.elsevier.com/locate/ceramint

Comparative studies of dynamic hysteresis responses in hard and soft PZT ceramics

N. Wongdamnern *, N. Triamnak, A. Ngamjarurojana, Y. Laosiritaworn, S. Ananta, R. Yimnirun

Department of Physics, Faculty of Science, Chiang Mai University, Chiang Mai 50200, Thailand

Available online 29 September 2007

Abstract

Lead zirconate titanate (PZT) is a ferroelectric material with very interesting and useful dynamic hysteresis properties. Normally, PZT is doped with donors or acceptors to yield better electrical properties. Soft and hard PZT ceramics are respectively donor- and acceptor-doped PZT, which are commercially available and widely employed in various applications. Previous investigations have mainly been focused on the dynamic hysteresis at room temperature and under stress-free condition. However, when used, these ceramics are normally subjected to stress. More importantly, the ambient temperature is usually not at room temperature. Therefore, this study was to investigate dynamic hysteresis behavior of both hard and soft PZT ceramics with varying compressive stress and temperature. The results clearly revealed the influence of external stress and temperature on the dynamic hysteresis of both types of PZT ceramics. Increasing stress and temperature resulted in a decrease of the hysteresis area of the two types of PZT ceramics.

Keywords: A. Dynamic hysteresis; B. Hard PZT; C. Soft PZT

1. Introduction

Lead zirconate titanate ($Pb(Zr_{1-x}Ti_x)O_3$ or PZT) ceramics are among the lead-based complex perovskites that have been investigated extensively, from both academic and commercial viewpoints. They are employed extensively in sensor and actuators applications, as well as smart systems [1–6]. The most widely studied and used PZT compositions are in the vicinity of the morphotropic phase boundary (MPB) between the tetragonal and rhombohedral ferroelectric phases [1,4,6–8]. However, to meet the requirements for specific applications, PZT ceramics are usually modified with dopants [1,4,9,10]. Generally, donor (higher valency) additives induce 'soft' piezoelectric behaviors with higher dielectric and piezoelectric activities suitable for sensor and actuator applications. On the other hand, acceptor (lower valency) additives result in 'hard' piezoelectric behaviors particularly suitable for ultrasonic motor applications [1,2,4–6].

However, in these applications, PZT ceramics are often subjected to mechanical loading under different temperatures, either deliberately in the design of the device itself or the use in changing shapes for many smart structure applications or the uses under environmental stresses or environmental heats [1–7]. A prior knowledge of how the material properties change under different conditions is therefore crucial for proper design of a device and for suitable selection of materials for a specific application. Despite that fact, material constants used in many design calculations are often obtained from a stress-free measuring condition or room temperature condition, which in turn may lead to incorrect or inappropriate designs of actuator and transducer. It is therefore important to determine the properties of these materials as functions of applied stress and temperature. Previous investigations on the stress dependence of dielectric and electrical properties of many ceramic systems, i.e. undoped-PZT, PLZT, BT, PMN–PT, PZT–BT and PMN–PZT, have clearly emphasized the importance of the subject [11–19]. The present study aims at studying technically important and commercially available soft and hard PZT ceramics. Many investigations have already revealed interesting results on the dielectric and piezoelectric properties of the

* Corresponding author. Tel.: +66 53 943367; fax: +66 53 943445.
E-mail address: nat_4169@hotmail.com (N. Wongdamnern).

0272-8842/$34.00
doi:10.1016/j.ceramint.2007.09.048

soft and hard PZT ceramics under stress [13–15,19]. However, there has been no work on the stress and temperature dependence of the ferroelectric properties of the ceramics. Therefore, this study is undertaken to investigate the influences of the uniaxial compressive stress and temperature on the ferroelectric properties of the soft and hard PZT ceramics.

2. Experimental procedure

A commercially available soft PZT (PKI-552, Piezo Kinetics Inc., USA) and hard PZT ceramics (APCI-840, USA) were used in this study. Soft PZT properties presented (measured by the supplier) a longitudinal charge coefficient d_{33} = 550 pm/V; a planer coupling factor k_p = 0.63, a dielectric constant (1 kHz) ε_r = 3400, a Curie temperature T_c = 200 °C and a bulk density = 7.6 g/cm^3. Hard PZT properties presented d_{33} = 290 pm/V, k_p = 0.59, ε_r = 1250, T_c = 325 °C and a bulk density = 7.6 g/cm^3. The disc-shaped samples with a diameter of 6.27 mm and a thickness of 1 mm were pre-poled by the supplier.

The ferroelectric hysteresis (*P–E*) loops were characterized using a computer controlled modified Sawyer-Tower circuit. The electric field was applied to a sample by a high-voltage ac amplifier (Trek, model 610D) with the input sinusoidal signal with a frequency of 50 Hz from a signal generator (Goodwill, model GAG-809). To study the effects of the uniaxial stress and temperature on the ferroelectric properties, the uniaxial compressometer was constructed with heating system. The compressometer with heater were developed for simultaneous applications of the mechanical stress, the temperature and the electric field. The compressometer cell with heating system consisting of a cylindrical brass cell with a heavy brass base, a brass ram, precisely guided loading platform provides true uniaxial stress during mechanical loading, while the heater provides desired heat to increase the temperature up to 200 °C. The prepared specimen was carefully placed between the two alumina blocks and the electric field was applied to the specimen via the copper shims attached to the alumina blocks. With this setting, the uniaxial compressive stress was applied parallel to the electric field direction and heat was applied to the brass and passed to sample through silicone oil. During the measurements, the specimen was immersed in silicone oil to prevent high-voltage arcing during electric loading. The uniaxial compressive stress was supplied by the servohydraulic load frame and the applied stress was monitored with the pressure guage of the load frame. Heating of the sample was applied by 300 W heater, which was tightened to brass and the applied heat was monitored and controlled by multimeter and computer interface. Measurements were performed as functions of mechanical compressive stress and temperature. Mechanical stress was applied discretely between 0 and 324 MPa and temperature was applied discretely between 25 and 160 °C. The ferroelectric hysteresis (*P–E*) loop was recorded at discrete temperature for each mechanical loading condition. The measurements reported were for the samples during mechanical loading. It should also be noted that the reported ferroelectric parameters were obtained after a total of 10 cycles of the electric field were applied to the sample at constant stress and temperature.

3. Results and discussion

The polarization versus electric field (*P–E*) hysteresis loops of the soft and hard PZT ceramics under different compressive stress during loading are shown in Figs. 1 and 2, respectively. It should first be noticed that the area of the *P–E* loops decreases steadily with increasing the compressive stress in both soft and hard PZT ceramics. The *P–E* loop area indicates the polarization dissipation energy of a ferroelectric material subjected to one full cycle of electric field application. This amount of energy loss is directly related to volume involved in the switching process during the application of electric field [2]. Therefore, the decrease in the loop area with increasing stress is a result of the stress-induced domain wall motion suppression [19]. The polarization dissipation energy is consequently found to decrease with increasing the applied stress, indicating that the sample volume contributing to polarization reversal decreases with the increasing compressive stress.

The change in the saturated polarization (P_{sat}), the remanent polarization (P_r), and the coercive field (E_c) with the uniaxial

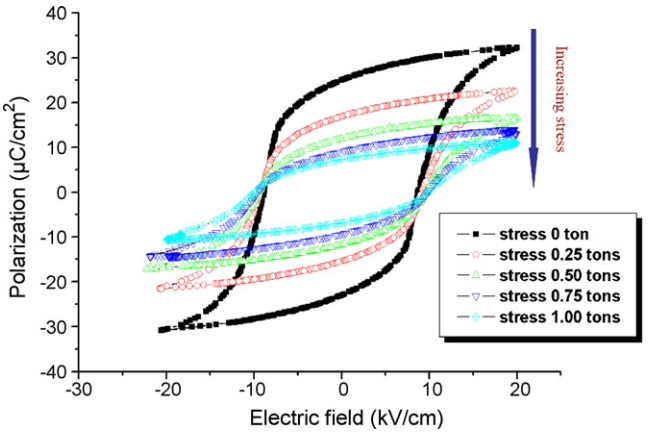

Fig. 1. Polarization vs. electric field (*P–E*) hysteresis loops as a function of compressive stress for soft PZT ceramic during loading.

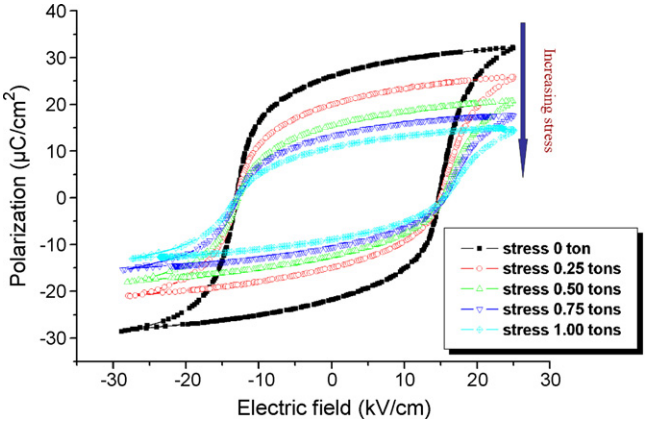

Fig. 2. Polarization vs. electric field (*P–E*) hysteresis loops as a function of compressive stress for hard PZT ceramic during loading.

compressive stress is similar to the trend observed in the dissipation energy (loop area). Both the saturated and remanent polarization decrease as the compressive stress increases. This suggests a significant stress-induced decrease in the switchable part of the spontaneous polarization of the soft and hard PZT ceramics resulting in the observed decrease in the polarization values, as well as the dissipation energy, under high stress [15,23]. In contrast, the applied stress shows little or no influence on the coercive field (E_c). It should also be noted that previous investigations on other ceramic systems, such as BT, PLZT, PMN–PT and PMN–PZT, showed a similar tendency [11,12,19–22,24].

To understand, these experimental results on the soft and hard PZT ceramics, one can interpret the changes in term of domain-reorientation processes [13–19]. When uniaxial compressive stress is applied in the direction parallel to the poling direction, the applied stress tends to keep the ferroelectric domain aligned with their polar axes away from the stress direction through the non-180° ferroelectric domain switching processes. Therefore, it takes a larger than usual applied electric field to reorient the domains along the stress direction, resulting in a lower value of the saturated polarization (P_s). When the electric field is reduced to zero the domain tend to rotate back away from the applied stress direction, resulting in a lower than usual remanent polarization (P_r). Furthermore, the decrease in the dissipation energy with increasing compressive stress indicates that more and more ferroelectric domains are constrain by the stress and cannot be reoriented by the electric field so as to participate in the polarization reversal. Consequently, both the saturated and remanent polarizations become lower with increasing compressive stress [19]. The results of changes in the ferroelectric characteristics of the soft and hard PZT ceramics with increasing compressive stress are in agreement with the previous investigations of many ferroelectric ceramics [11,12,18–25].

The (P–E) hysteresis loops of the soft and hard PZT ceramics under different temperatures are shown in Figs. 3 and 4, respectively. In both cases, area of the P–E loops decreases steadily with increasing the temperature, indicating that polarization dissipation energy decreases when the temperature increases. This is caused by that higher temperature provides

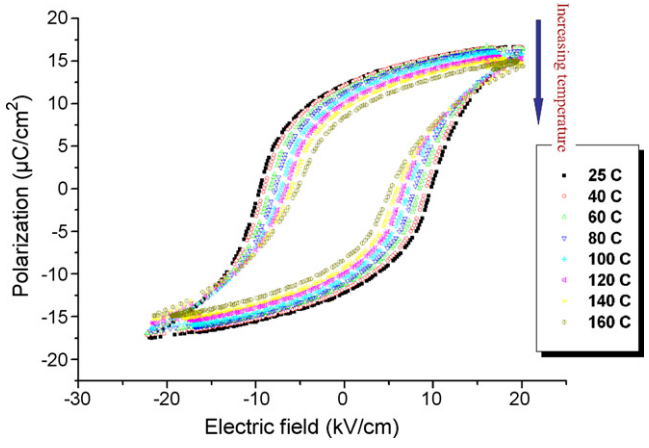

Fig. 3. Polarization vs. electric field (P–E) hysteresis loops as a function of temperature for soft PZT ceramic.

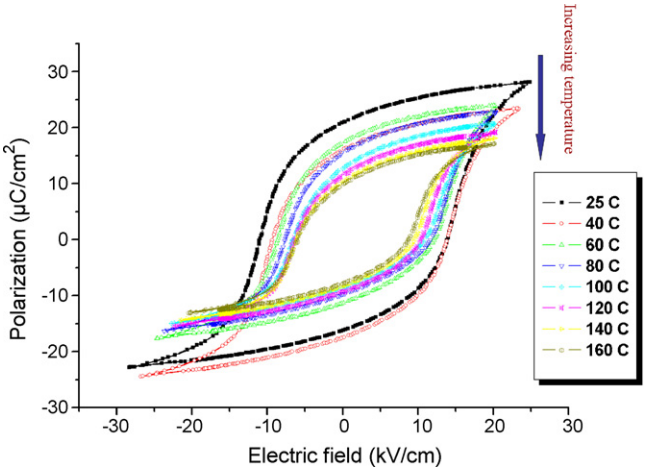

Fig. 4. Polarization vs. electric field (P–E) hysteresis loops as a function of temperature for hard PZT ceramic.

higher thermal fluctuation to the polarization order parameter, which reduces the ferroelectric interaction among the dipoles. Therefore, even E_0 is fixed, the polarization direction is easily turned with the electric field at higher temperatures due to the smaller ferroelectric interaction providing a reduction in both remanent polarization (P_r) and coercivity (E_c). For this reason, the hysteresis loop area is reduced with increasing the temperature. Additionally, slightly asymmetric P–E loops are also observed in the hard PZT, as displayed in Figs. 2 and 4. The observation could be attributed to the presence of the complex defects, which provide the internal field-bias. Therefore, the ferroelectric interaction between these defect dipoles which are trapped near domain walls, and the other dipoles in the domain makes the polarization switching and domain reorientation processes, as well as the domain wall motions, more difficult in one field direction than the other direction. This results in asymmetric loops, and the differences between E_c^+ and E_c^-, and P_r^+ and P_r^-, as observed in Figs. 2 and 4.

4. Conclusions

In this study, the effects of stress and temperature on the ferroelectric properties of soft and hard PZT ceramics are investigated. The results show that in both types of PZT ceramics the ferroelectric characteristics, i.e. the area of the ferroelectric hysteresis (P–E) loops, which corresponds to the energy dissipation, the saturated polarization (P_{sat}) and the remanent polarization (P_r), decrease with increasing compressive stress, while the coercive field (E_c) is virtually unaffected by the applied stress. The non-180° ferroelectric domain switching and stress-induced domain wall suppression processes are responsible for the changes observed. Similar decrease of the ferroelectric parameters is also observed with increasing temperature. The cause for the thermal effect is believed to reduce ferroelectric interaction due to higher thermal fluctuation. More importantly, this study undoubtedly shows that the applied stress and the temperature have significant influences on the ferroelectric properties of the soft and hard PZT ceramics.

Acknowledgments

The Thailand Research Fund (TRF), Commission on Higher Education (CHE), The Development and Promotion of Science and Technology Talents Project (DPST), Faculty of Science and Graduate School of Chiang Mai University are gratefully acknowledged for financial supports.

References

[1] B. Jaffe, W.R. Cook, H. Jaffe, Piezoelectric ceramics, J. Sound Vib. 20 (4) (1971) 562–563.
[2] G.H. Heartling, Ferroelectric ceramics: history and technology, J. Am. Ceram. Soc. 82 (1999) 797–818.
[3] L.E. Cross, Ferroelectric materials for electromechanical transducer applications, Mater. Chem. Phys. 43 (1996) 108–115.
[4] A.J. Moulson, J.M. Herbert, Electroceramics, Properties, Applications, 2nd ed., Wiley–Interscience, New York, 2003.
[5] K. Uchino, Ferroelectric Devices, vol. 16, Marcel Dekker, Inc., New York, 2000.
[6] Y.H. Xu, Ferroelectric Materials and Their Applications, JAJR Trading, Inc., USA, 1991.
[7] L.E. Cross, Relaxor ferroelectrics, Ferroelectrics 76 (1987) 241–267.
[8] W. Cao, L.E. Cross, Theoretical model for the morphotropic phase boundary in lead zirconate–lead titanate solid solution, Phys. Rev. B 47 (1993), 4825–4830.
[9] S. Takahashi, Effect of impurity doping in lead zirconate titanate ceramics, Ferroelectrics 41 (1982) 143–156.
[10] F. Kulcsar, Electromechanical properties of lead titanate zirconate ceramics modified with certain three or five-valent additives, J. Am. Ceram. Soc. 42 (7) (1959) 343–349.
[11] I.J. Fritz, Uniaxial stress effects in a 95/5 lead zirconate titanate ceramic, J. Appl. Phys. 49 (9) (1978) 4922–4928.
[12] C.S. Lynch, The effect of uniaxial stress on the electro-mechanical response of 8/65/35 PLZT, Acta Mater. 44 (10) (1996) 4137–4148.
[13] Q.M. Zhang, J. Zhao, K. Uchino, J. Zheng, Change of the weak field properties of $Pb(ZrTi)O_3$ piezoceramics with compressive uniaxial stresses and its links to the effect of dopants on the stability of the polarizations in the materials, J. Mater. Res. 12 (1997) 226–234.
[14] J. Zhao, A.E. Glazounov, Q.M. Zhang, Change in electromechanical properties of 0.9PMN–0.1PT relaxor ferroelectric induced by uniaxial compressive stress directed perpendicular to the electric field, Appl. Phys. Lett. 74 (1999) 436–438.
[15] G. Yang, S.F. Lui, W. Ren, B.K. MukHerjee, Effect of uniaxial stress and DC bias field on the piezoelectric, dielectric, and elastic properties of piezoelectric ceramics, in: Proceedings of the IEEE Ultrasonic Symposium 1005 on Smart Structures and Materials, SPIE 3992, 2000, pp. 103–113.
[16] D. Viehland, J. Powers, Effect of uniaxial stress upon the electromechanical properties of various piezoelectric ceramics and single crystals, J. Appl. Phys. 89 (2001) 1820–1825.
[17] R. Yimnirun, S. Ananta, E. Meechoowas, S. Wongsaenmai, Effect of uniaxial stress on dielectric properties of lead magnesium niobate–lead zirconate titanate ceramics, J. Phys. D: Appl. Phys. 36 (2003) 1615–1619.
[18] D. Viehland, J.F. Li, E. McLaugHlin, J. Powers, R. Janus, H. Robinson, Effect of uniaxial stress on the large-signal electromechanical properties of electrostrictive and piezoelectric lead magnesium niobate lead titanate ceramics, J. Appl. Phys. 95 (2004) 1969–1972.
[19] D. Zhou, M. Kamlah, D. Munz, Effects of bias electric fields on the nonlinear ferroelastic behavior of soft lead zirconate titanate piezoceramics, J. Eur. Ceram. Soc. 25 (2005) 425–432.
[20] D. Fang, C. Li, Nonlinear electric-mechanical behavior of a soft. PZT-51 ferroelectric ceramic, J. Mater. Sci. 34 (1999) 4001–4010.
[21] O. Guillon, P. Delobelle, F. Thiebaud, V. Walter, D. Perreux, Uniaxial electromechanical behavior of a soft PZT: experiments and modeling, Ferroelectrics 308 (2004) 95–111.
[22] J. Zhao, Q.M. Zhang, Effect of mechanical stress on the electromechanical performance of PZT and PMN–PT ceramics, in: Proceedings of IEEE 10th International Symposium on Applications of Ferroelectrics (ISAF), vol. 2, 1996, pp. 971–974.
[23] G. Yang, W. Ren, S.F. Liu, A.J. Masys, B.K. Mukherjee, Effect of uniaxial stress and dc bias field on the piezoelectric, dielectric, and elastic properties of piezoelectric ceramics, in: Proceedings of the IEEE Ultrasonic Symposium 1005 on Ultrasonics Symposium, vol. 2, 2000, pp. 1005–1008.
[24] R. Yimnirun, S. Ananta, A. Ngamjarurojana, S. Wongsaenmai, Uniaxial stress dependence of ferroelectric properties of XPMN–$(1-X)$PZT ceramic systems, Appl. Phys. A: Mater. Sci. Process. 81 (6) (2005) 1227–1231.
[25] R. Yimnirun, Y. Laosiritaworn, S. Wongsaenmai, Effect of uniaxial compressive pre-stress on ferroelectric properties of soft PZT ceramics, J. Phys. D: Appl. Phys. 39 (2006) 759–764.

Available online at www.sciencedirect.com
ScienceDirect
Ceramics International 34 (2008) 809–812
CERAMICS INTERNATIONAL
www.elsevier.com/locate/ceramint

Artificial neural network modeling of ceramics powder preparation: Application to $NiNb_2O_6$

W. Laosiritaworn [a,*], O. Khamman [b], S. Ananta [b], R. Yimnirun [b], Y. Laosiritaworn [b]

[a] *Department of Industrial Engineering, Faculty of Engineering, Chiang Mai University, Chiang Mai 50200, Thailand*
[b] *Department of Physics, Faculty of Science, Chiang Mai University, Chiang Mai 50200, Thailand*

Available online 7 October 2007

Abstract

This paper studied the modeling of the synthesis process of $NiNb_2O_6$ (NN) powder using an artificial neural network (ANN). The characteristic of interest was the amount of NN phase percentage produced from the synthesis process. Three controlling factors affecting the mentioned characteristic were dwell time, calcined temperature and heating/cooling rate. Design of experiments (DoE) technique was used to analyze the relationship of controlling factors to the amount of NN phase. The results show that calcined temperature is the most important factor affecting the amount of NN phase. The dwell time and heating/cooling rate are less significant on the phase but longer dwell time and higher heating/cooling rate are appreciable for the slightly higher purity. Multiple regression was also used to compare the results and the ANN was found to significantly outperform the regression analysis.

Keywords: Powders preparation; Artificial neural network

1. Introduction

Typically, in preparing ceramic powder, several techniques ranging from mechanical milling to chemical method can be used [1]. However, due to many factors involved such as milling time, dwell time, calcined temperature, heating/cooling rate, etc., lots of experimental combinations are possible. Therefore, to search for the optimal condition in obtaining the powder with a pure preferred phase at low cost could be difficult. This method of trial-and-error experiment is not economical and the optimal experimental setting cannot be guaranteed. Consequently, there is a need for a technique which can be used to find the relation between the relevant parameters to obtain the powder with a high purity phase in a cost efficient way. Thus, there comes the objective of this study to suit such a situation using an artificial neural network.

Artificial neural network (ANN) is one of several artificial intelligence tools which has been widely used in various applications due to its ability to learn from samples, and fault tolerance. In this study, it is used to predict the percentage of the desired material in ceramic powder preparation. The $NiNb_2O_6$ (NN) powder was chosen as a case study due to its interesting in being used as a precursor to prepare $Pb(Ni_{1/3}Nb_{2/3})O_3$ [9] which is a potential candidate for electroceramics applications [1–3].

In this study, by following the NN powder preparation technique suggested in Ref. [9], the percentage of the obtained NN phase relevant to the condition of preparation including dwell time, calcined temperature and heating/cooling rate was investigated. Fifty-one experimental samples have been used to construct the ANN model. Once the ANN has been assembled, it was used to predict the percentage of NN phase of the unseen input conditions. Therefore, this minimizes the need to conduct an actual experimentation. Design of experiments (DoE) was then used to analyze the effect of controlling factors to the percentage of NN phase. Multiple regression model was also used for a comparison purpose.

1.1. Background theories

1.1.1. Artificial neural network

Artificial neural network (ANN) is 'an interconnected assembly of simple processing elements, *units* or *nodes*, whose

* Corresponding author.
E-mail address: wimalin@eng.cmu.ac.th (W. Laosiritaworn).

0272-8842/$34.00
doi:10.1016/j.ceramint.2007.09.102

functionality is loosely based on the animal neuron. The processing ability of the network is stored in the inter-unit connection strengths, or *weights*, obtained by a process of adaptation to, or *learning* from, a set of training patterns' [4].

Inspired by how the brain and nerve cells work, ANN is constructed by connecting simple processing elements or neurons together. Neurons can be located in the input layer, the output layer or the hidden layers. The input layer takes data from the outside of a neural network and sends it to hidden layer neurons. The output layer sends the information back outside the network.

ANN training can be supervised or unsupervised (self-organising). This paper is focused on supervised training. The back-propagation algorithm is the most extensively adopted algorithm for network training [5] and is the type of network used in this research.

1.1.2. Statistical design of experiments

Statistical DoE was first developed in the early 1920s by Sir Ronald Fisher to determine the effect of multiple factors on the outcome of agricultural trials. The work of statisticians [6,7] with an interest in this area has provided a firm foundation for practitioners. DoE is a statistical and structural method used to analyze relationships between factors affecting processes (independent variables) and the output of those processes (dependent variables). DoE techniques are widely used, both by researchers, for characterisation, optimisation, and modelling [8].

2. Experimental procedures

2.1. NN powder preparation

The NN powder was synthesized by the solid-state reaction of thoroughly ground mixtures of NiO and Nb_2O_5 powders milling in the required stoichiometric ratio. The detailed description of the NN powder preparation is given elsewhere [9]. In this study, the NN powder was synthesized by varying dwell time from 1 to 48 h, calcined temperature from 500 to 1200 °C, and heating/cooling rate from 3 to 30 °C/min. Then the obtained powder is investigated by X-ray diffraction (XRD) technique to calculate the percentage of NN phase. However, if there exist more than two phases in the XRD pattern, the NN percentage is set as unclassified. Controlling factors in the experiments were set by trial-and-error and percentage of NN phase were recorded. Fifty-one records of experimental data were available.

2.2. Multiple regression analysis

A multiple regression model has the following form:

$$y = \beta_0 + \beta_1 x_1 + \beta_2 x_2 + \cdots + \beta_k x_k,$$

where β_0 is the intercept, $\beta_1, \ldots, \beta_k$ refer to parameters representing the contribution of the independent variables, and $x_1, \ldots, x_k$ are independent variables.

Of the 51 records available, 41 records were randomly selected and used to fit regression equation while the remaining 10 records was used as independent test set. The regression equation is as follows:

$$y = -103.905 + 0.189x_1 + 0.810x_2 + 0.616x_3,$$

where y is the percentage of NN phase obtained, while x_1, x_2 and x_3 refer to calcined temperature, dwell time and heating/cooling rate, respectively. The results from regression analysis are compared with the result from ANN in the next section.

2.3. Artificial neural network training and testing

The same data set used to fit regression equation was used to train ANN. The training was carried out with 41 records and the remaining 10 records for testing ANN performance. Qnet v2000 software was used to develop an ANN model. The network developed consisted of three layers. Input layer has three neurons representing calcined temperature, dwell time and heating/cooling rate while the output layer has one neuron which represents the prediction of percentage of NN phase obtained. Hidden layer neurons were selected by trial-and-error and the appropriate number of hidden neurons were 17. Root mean square error of the training and testing data were 0.039701 and 0.049907, respectively, and the correlation coefficient of training and testing data were 0.977587 and

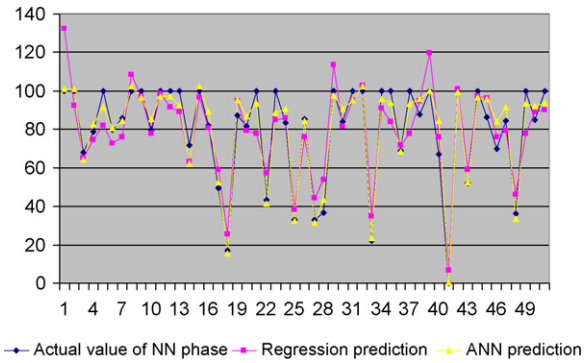

Fig. 1. The comparison of actual value with regression prediction and ANN prediction.

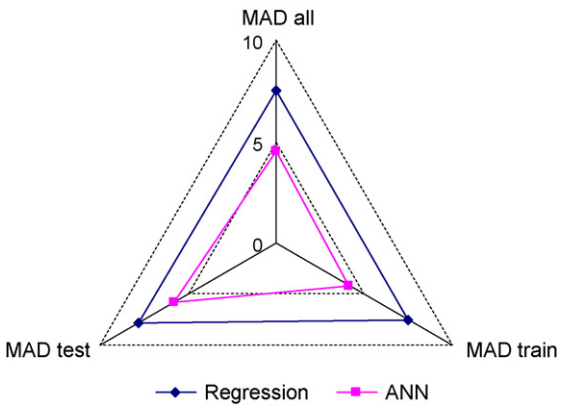

Fig. 2. MAD of results from regression model and ANN model.

Table 1
ANOVA analysis

Source	d.f.	Seq SS	Adj SS	Adj MS	*F*	*P*
Calcined temperature	4	148162.3	148162.3	37040.6	3532.83	0
Dwell time	6	2207	2207	367.8	35.08	0
Heating/cooling rate	2	525.1	525.1	262.6	25.04	0
Calcined temperature × dwell time	24	280.9	280.9	11.7	1.12	0.363
Calcined temperature × heating/cooling rate	8	2907.1	2907.1	363.4	34.66	0
Dwell time × heating/cooling rate	12	1317.7	1317.7	109.8	10.47	0
Error	48	503.3	503.3	10.5		
Total	104	155903.4				

d.f.: degree of freedom; Seq SS: sequencial sum of squares; Adj SS: adjusted sum of squares; Adj MS: adjusted mean square; *F*: *F*-statistic; *P*: *p*-value.

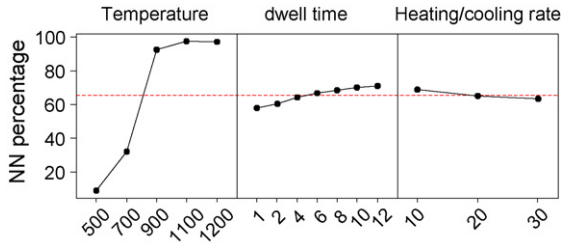

Fig. 3. Main effect plot (data means) of NN percentage.

0.947345, respectively. As the correlation coefficient of both training and testing data were very close to 1, the model is a good approximation of real experimentations.

Fig. 1 shows the actual data of percentage of NN phase compared with the prediction from regression and ANN. Fig. 2 is the radar chart that illustrates mean absolute deviation (MAD) of the overall, training and testing data of the results from both regression and ANN. It can be concluded from both figures that ANN significantly outperform multiple regression, as a result ANN model was used for further analysis.

2.4. Design of experimental analysis

After the ANN had been properly trained, it was used to predict experimental results. Experiments were set at five levels for the calcined temperature ranging from 500 to 1200 °C, seven levels for the dwell time ranging from 1 to 12 h and three levels for the heating/cooling rate ranging from 10 to 30 °C/min, with all possible combinations of experimental setting of 105. These experimental settings were fed to the trained ANN to obtain the prediction of the NN phase.

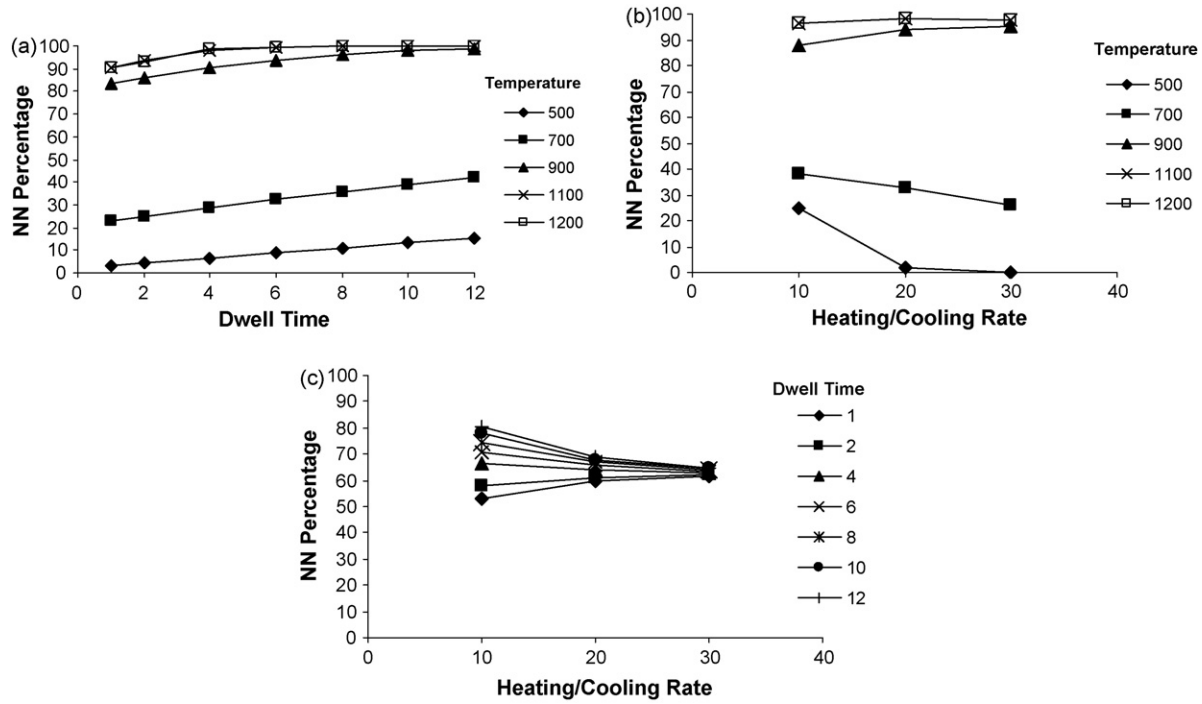

Fig. 4. Interaction plot (data means) of NN percentage: (a) between temperature and dwell time; (b) between temperature and heating/cooling rate; (c) between heating/cooling rate and dwell time.

3. Results and discussion

Analysis of variance (ANOVA) was carried out to identify significant factors and factor interactions to the percentage of NN. The ANOVA analysis was prepared by using MINITAB release 14. Table 1 summarises the significant factors of each response at the 95% confidence level. Significant factors at the 95% confidence level were the factor that has P value lower than 0.05. As a result, calcined temperature, dwell time, heating/cooling rate, interaction of calcined temperature and heating/cooling rate and interaction of dwell time and heating/cooling rate are found to be significant with different levels.

The relation among the experimental parameters in obtaining the high purity NN phase can be analysed by the main effect plot (Fig. 3), which shows the effect of each controlling factors on the NN percentage. The graph indicated that calcined temperatures has the highest effect on NN percentage and there is a steep decrease in NN percentage at temperature below 900 °C. Dwell time and heating/cooling rate have less effect than calcined temperature but their effects are still significant according to the ANOVA analysis.

The interaction plot (data mean) of NN percentage is shown in Fig. 4. Each sub-figure represents the interaction between a pair of preparation conditions in obtaining the NN phase. Since there are three relevant parameters considered in this study, when a pair is chosen, each data point in the considered sub-figure is calculated from the average over the remaining parameter. For instance, Fig. 4(a) shows the interaction of temperature and time of the obtained NN phase in which each data point is calculated from the average over all considered heating/cooling rate.

It can be summarised from Fig. 4(a) that the calcined temperature has prominent effect on the percentage of NN phase, where a very high percentage is obtained only for the temperature above (or equal to) 900 °C. A huge leap in the percentage is found in calcined temperature between 700 and 900 °C, but the longer dwell time only slightly enhances the percentage. Slight dependence on heating/cooling rate of the NN phase is also found (Fig. 4(b)). The strong reliance on the temperature is again apparent. On the other hand, Fig. 4(c) shows the relation of heating/cooling rate of the NN phase with varying dwell time. As can be seen, the high percentage is found for low heating/cooling rate but high dwell time. The description underlying all these phenomena can be given via thermodynamics of phase transformation. Presumably, to grow the NN phase, the thermal energy must be at the right condition corresponding to the energy barrier. If the calcined temperature is too low, the thermal energy might not be enough to trick out the NN phase. However, even the heating/cooling rate does not have a significant effect on the percentage of NN phase, but when the rate is too high, there might not be enough time for the NN phase to get growing so a longer dwell time is needed.

4. Conclusions

The ANN technique was used to study the relation among calcined temperature, dwell time and heating/cooling rate in obtaining the high percentage of NN phase. In this study, the high accuracy ANN model of NN synthesis process, was constructed from a minority of training examples, in predicting the results from an untrained experiment. Also from the prediction, a significant effect from the relevant parameters to the percentage of NN phase is apparent. The most important factor to obtain the high percentage is the calcined temperature while the dwell time has a moderate effect on the phase, and the heating/cooling rate has the least significant. The major advantage of ANN is that it allows the through analysis of the relationship of controlling factors to the amount of NN phase without conducting experiments randomly. The traditional trial-and-error experiment might results in conducting many experiments, yet the optimal solution might never be found. The techniques adopted in this article could also be applied to other process which will results in a more economical and structure way for data analysis.

Acknowledgements

The authors would like to acknowledge Thailand Research Fund (TRF) and the Commission on Higher Education (CHE) for financial support.

References

[1] J.S. Reed, Principles of Ceramic Processing, 2nd ed., Wiley, New York, 1995.
[2] G.H. Haertling, Ferroelectric ceramics: history and technology, J. Am. Ceram. Soc. 82 (1999) 797–818.
[3] A.J. Moulson, J.M. Herbert, Electroceramics, 2nd ed., Wiley, Chichester, 2003.
[4] K. Gurney, An Introduction to Neural Networks, UCL Press Limited, London, 1997.
[5] C.A.O. Nascimento, R. Giudici, R. Guardani, Neural network based approach for optimization of industrial chemical processes, Comput. Chem. Eng. 24 (2000) 2303–2314.
[6] G.E.P. Box, W.G.J. Hunter, S. Hunter, Statistics for Experimenters: An Introduction to Design, Data Analysis, and Model Building, Wiley, New York, 1987.
[7] D.C. Montgomery, Design and Analysis of Experiments, 5th ed., John Wiley & Sons Inc., New York, 2001.
[8] J. Antony, R.K. Roy, Improving the process quality using statistical design of experiments: a case study, Qual. Assur. 6 (1999) 87–95.
[9] O. Khamman, R. Yimnirun, S. Ananta, Phase and morphology evolution of corundum-type $Ni_4Nb_2O_9$ powders synthesized by solid-state reaction, Mater. Lett. 61 (2006) 2565–2570.

Available online at www.sciencedirect.com
ScienceDirect
Ceramics International 34 (2008) 705–708
CERAMICS INTERNATIONAL
www.elsevier.com/locate/ceramint

Piezoelectric properties of low temperature sintering in $Pb(Zr,Ti)O_3$–$Pb(Zn,Ni)_{1/3}Nb_{2/3}O_3$ ceramics for piezoelectric transformer applications

A. Ngamjarurojana [a,*], S. Ural [b], S.H. Park [b], S. Ananta [a], R. Yimnirun [a], K. Uchino [b]

[a] *Department of Physics, Faculty of Science, Chiang Mai University, Chiang Mai 50200, Thailand*
[b] *International Center for Actuators and Transducers, Materials Research Institute, Pennsylvania State University, University Park, PA 16802, USA*

Available online 25 September 2007

Abstract

In this study, in order to develop low-temperature sintering ceramics for a multilayer piezoelectric transformer application, we explored CuO and Bi_2O_3 as sintering aids at low temperature (900 °C) sintering condition for Sb, Li and Mn-substituted $0.8Pb(Zr_{0.48}Ti_{0.52})O_3$–$0.16Pb(Zn_{1/3}Nb_{2/3})O_3$–$0.04Pb(Ni_{1/3}Nb_{2/3})O_3$ ceramics. These substituted ceramics have excellent piezoelectric and dielectric properties such as $d_{33} \sim 347$ pC/N, $k_p \sim 0.57$ and $Q_m \sim 1469$ when sintered at 1200 °C. The addition of CuO decreased the sintering temperature through the formation of a liquid phase. However, the piezoelectric properties of the CuO-added ceramics sintered below 900 °C were lower than the desired values. The additional Bi_2O_3 resulted in a significant improvement in the piezoelectric properties. The composition Sb, Li and Mn-substituted $0.8Pb(Zr_{0.48}Ti_{0.52})O_3$–$0.16Pb(Zn_{1/3}Nb_{2/3})O_3$–$0.04Pb(Ni_{1/3}Nb_{2/3})O_3$ + 0.5 wt% CuO + 0.5 wt% Bi_2O_3 showed the value of $k_p = 0.56$, $Q_m = 1042$ (planar mode), $d_{33} = 350$ pC/N, when it was sintered at 900 °C for 2 h. These values indicated that the newly developed composition might be suitable for multilayer piezoelectric transformer application.

Keywords: Low temperature sintering; Piezoelectric transformer and vibration velocity

1. Introduction

The materials for piezoelectric actuators, ultrasonic motors and piezoelectric transformers applications should have compromised characteristics between hard and soft piezoelectrics, implying high electromechanical coupling factor (k) and piezoelectric constant (d) with high mechanical quality factor (Q_m) [1].

However, the sintering temperature of lead zirconate titanate (PZT)-based high-power compositions is usually too high, approximately 1200 °C, to use base metal electrodes such as Ag and Cu. Therefore, Ag/Pd alloy is generally used as the electrode to suppress the migration of Ag into the ceramics at high temperature. Consequently, lowering of the sintering temperature of piezoelectric ceramics is essential for the fabrication of cost-effective multilayer piezoelectric devices. Furthermore, low temperature sintering can provide advantages such as compatibility with low temperature cofired ceramics (LTCC), the reduction of energy consumption, and the reduced PbO volatilization.

Previously, various techniques were employed to obtain the low temperature sinterable PZT composition. The addition of dopants, which improves solid-state sintering, and the addition of oxides and compounds, which have low melting points for liquid-phase sintering are the most popular methods [2–4]. Some of the oxides and compounds that have been used for assisting liquid-phase sintering [5–9]. Even though these techniques were able to obtain dense ceramics at low sintering temperature, piezoelectric properties were not satisfactory enough to be used in industry.

Previously, we developed the Sb, Li and Mn-substituted $Pb(Zr_{0.48}Ti_{0.52})O_3$–$Pb(Zn_{1/3}Nb_{2/3})O_3$–$Pb(Ni_{1/3}Nb_{2/3})O_3$ ceramics with excellent dielectric and piezoelectric properties when sintered at 1200 °C [10]. The aim of this study was to

* Corresponding author. Tel.: +66 53 941921x445; fax: +66 53 943445.
E-mail address: Ngamjarurojana@yahoo.com (A. Ngamjarurojana).

0272-8842/$34.00
doi:10.1016/j.ceramint.2007.09.012

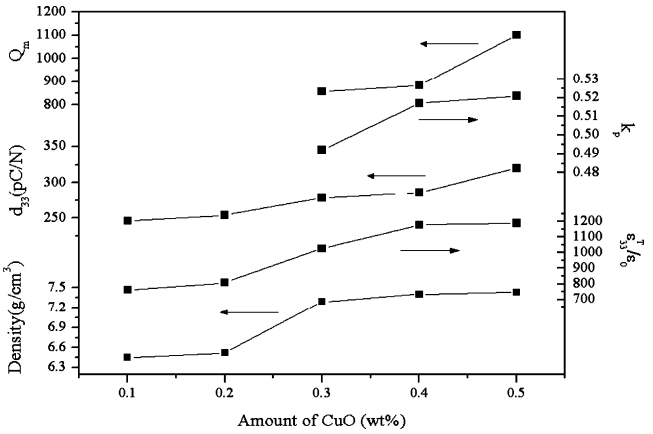

Fig. 1. Density, dielectric permittivity ($\varepsilon_{33}^{T}/\varepsilon_0$), piezoelectric constant (d_{33}), electromechanical coupling factor (k_p) and mechanical quality factor (Q_m) and of the specimens sintered at 900 °C for 2 h in $Pb(Zr,Ti)O_3$–$Pb(Zn,Ni)_{1/3}Nb_{2/3}O_3$ + x wt% CuO ceramics.

lower the sintering temperature of this composition for providing Ag or Cu cofiring compatible high-power piezoelectric ceramics, aiming at layered structure piezoelectric actuators and transformer applications. We therefore investigated the effect of CuO and Bi_2O_3 addition in the Sb, Li and Mn-substituted $Pb(Zr_{0.48}Ti_{0.52})O_3$–$Pb(Zn_{1/3}Nb_{2/3})O_3$–$Pb(Ni_{1/3}Nb_{2/3})O_3$ ceramics as a solution for low temperature sinterable high power ceramics.

2. Experimental procedure

The specimens studied in this research were fabricated according to the formula: $0.8Pb(Zr_{0.48}Ti_{0.52})O_3$–$0.16Pb(Zn_{1/3}Nb_{2/3})O_3$–$0.04Pb(Ni_{1/3}Nb_{2/3})O_3$ with Sb, Li and Mn substitution $(Pb(Zr,Ti)O_3$–$Pb(Zn,Ni)_{1/3}Nb_{2/3}O_3)$ + x wt% CuO + y wt% Bi_2O_3, where $x = 0.1$–0.5; $y = 0$–0.5, respectively. Raw materials of PbO, ZrO_2, TiO_2, ZnO, NiO, Nb_2O_5, Sb_2O_5, Li_2CO_3, MnO_2, CuO and Bi_2O_3 with >99% purity were used to prepare samples by a conventional ceramic sintering process. The obtained mixture was ball-milled using zirconia ball media with isopropanal as a medium in a polyethylene jar for 24 h. The mixed slurry was dried and calcined at 750 °C for 2 h. The calcined powders were ball-milled again with additives and consolidated into disks of 12.5 mm diameter and rectangular plates using isostatic pressing about 150 MPa. PbO-rich atmosphere sintering of the ceramics was performed in a high-purity alumina crucible at the temperature of 850–900 °C for 2 h. The crystal structure and symmetry of the sintered bodies were examined by X-ray diffraction (XRD) and sintered densities were measured by the Archimedes method. Silver electrode (Dupont, QS 171) was printed on the lapped surfaces for electrode. The electrode specimens were poled in silicone oil at 150 °C by applying a dc field of 3 kV/mm for 30 min. The piezoelectric constant (d_{33}) was measured using a quasi-static piezoelectric d_{33} meter (Model ZJ-3d, Institute of Acoustics Academic Sinica, China). The planar coupling coefficient (k_p)

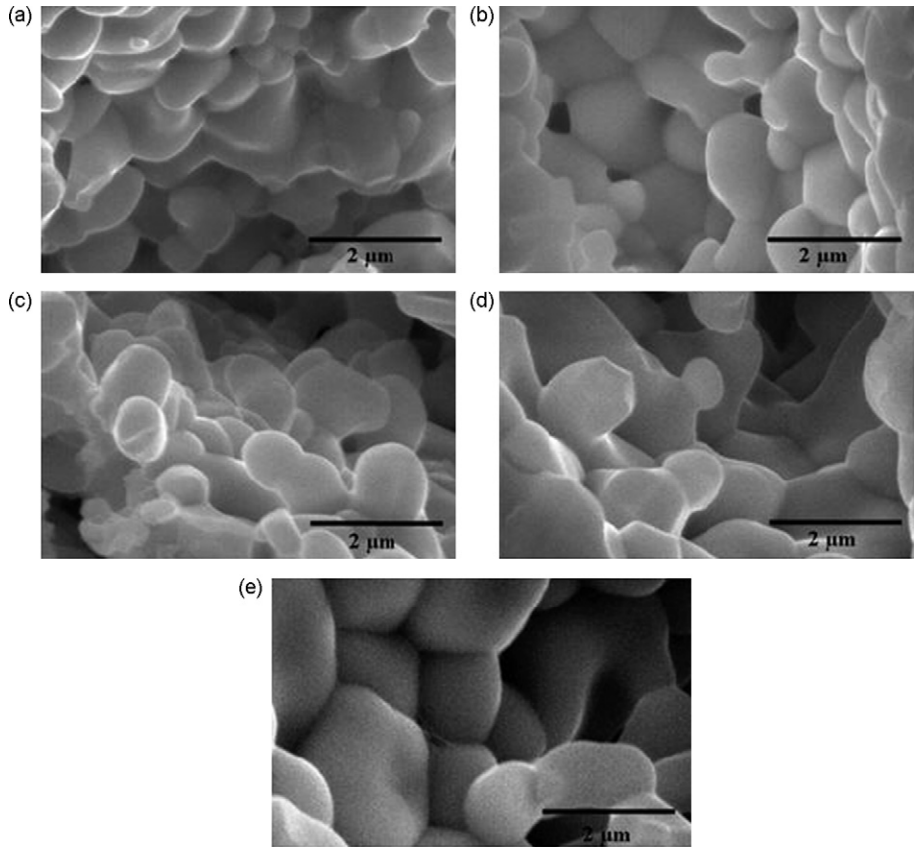

Fig. 2. SEM images of the samples sintered at 900 °C for 2 h in $Pb(Zr,Ti)O_3$–$Pb(Zn,Ni)_{1/3}Nb_{2/3}O_3$ + x wt% CuO ceramics.: (a) $x = 0.1$, (b) $x = 0.2$, (c) $x = 0.3$, (d) $x = 0.4$ and (e) $x = 0.5$.

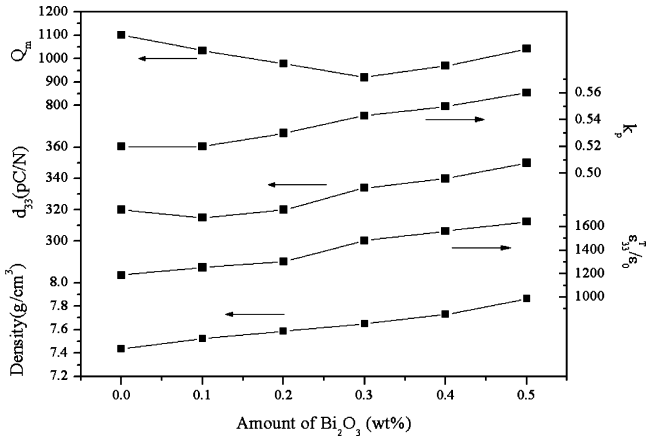

Fig. 3. Density, dielectric permittivity $(\varepsilon_{33}^{T}/\varepsilon_0)$, piezoelectric constant (d_{33}), electromechanical coupling factor (k_p) and mechanical quality factor (Q_m) and of the specimens sintered at 900 °C for 2 h in $Pb(Zr,Ti)O_3$–$Pb(Zn,Ni)_{1/3}Nb_{2/3}O_3$ + 0.5 wt% CuO + y wt% Bi_2O_3 ceramics.

and the mechanical quality factor (Q_m) were determined by the resonance and anti-resonance technique using an impedance analyzer (Model HP4294A, Hewlett-Packard, CA).

3. Results and discussion

3.1. Effect of CuO addition

Initially, the effect of the addition of CuO on the sinterability, crystal structure, piezoelectric and dielectric properties was investigated in $Pb(Zr,Ti)O_3$–$Pb(Zn,Ni)_{1/3}Nb_{2/3}O_3$-based ceramics. The sintering temperature of all the specimens was fixed at 900 °C, which is cofiring compatible temperature for Ag and low temperature cofired ceramics (LTCC) substrate. Density, dielectric permittivity $(\varepsilon_{33}^{T}/\varepsilon_0)$, electromechanical coupling factor (k_p), mechanical quality factor and piezoelectric constant (d_{33}) were plotted as a function of the amount of CuO addition in Fig. 1. The density was increased with the increase of CuO contents approximately from 6.4 to 7.8 g/cm^3. This improvement of the density might be related to the formation of the liquid phase. Moreover, the variation of piezoelectric and dielectric properties showed similar trend to that of density. Therefore, the improved piezoelectric and dielectric properties, which were observed in the range of $x \geq 0.3$, might be due to the increased density as well as increased grain size shown in Fig. 2. This hardening effect that could be confirmed by the enhancement of Q_m value approximately from 600 to 1200 as shown in Fig. 1. Therefore, Cu ions could be expected to enter B site and act as a hardener. Fig. 2 shows the SEM images of the $Pb(Zr,Ti)O_3$–$Pb(Zn,Ni)_{1/3}Nb_{2/3}O_3$ + x wt% CuO ceramics sintered at 900 °C for 2 h. As the CuO addition amount increased, grain growth happened whereas small grains disappeared. This grain growth with CuO addition can be explained with liquid phase sintering. Previously, we showed that the addition of CuO can reduce the sintering temperature of the $Pb(Zr,Ti)O_3$–$Pb(Ni,Nb)O_3$ system by the formation of a liquid phase [11]. Thus, this liquid phase formation can also be an explanation for the $Pb(Zr,Ti)O_3$–$Pb(Zn,Ni)_{1/3}Nb_{2/3}O_3$ + x wt% CuO ceramics.

3.2. Effect of Bi_2O_3 addition

Bi_2O_3 has low melting temperature (817 °C) and it was reported Bi_2O_3 can form liquid phase with ZnO at approximately 750 °C. Therefore, Bi_2O_3 was added to $Pb(Zr,Ti)O_3$–$Pb(Zn,Ni)_{1/3}Nb_{2/3}O_3$ + 0.5 wt% CuO in order to further improve the piezoelectric properties of the specimens sintered at low temperature. Density, dielectric permittivity $(\varepsilon_{33}^{T}/\varepsilon_0)$, electromechanical coupling factor (k_p), mechanical quality

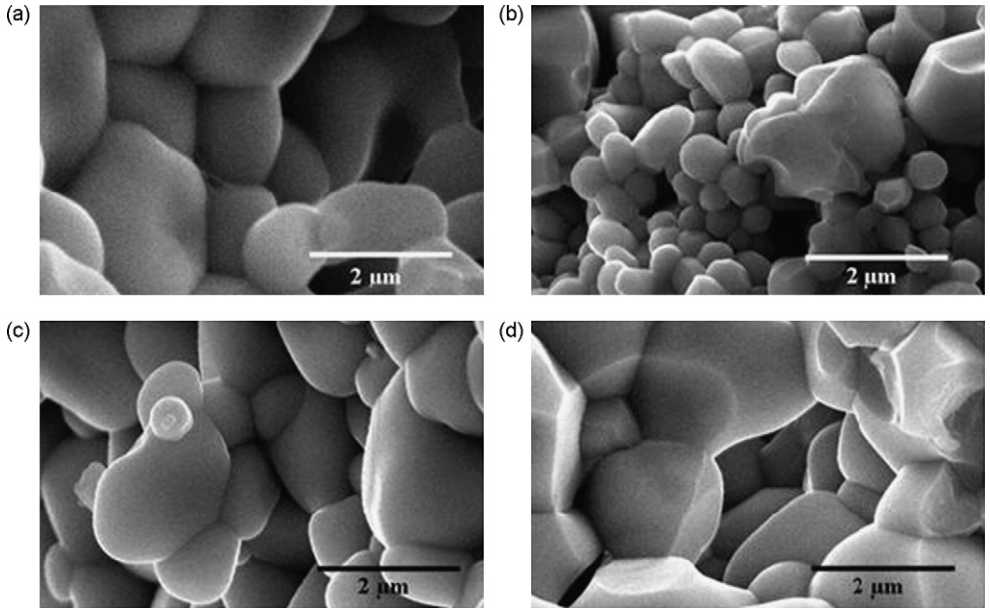

Fig. 4. SEM images of the samples sintered at 900 °C for 2 h in $Pb(Zr,Ti)O_3$–$Pb(Zn,Ni)_{1/3}Nb_{2/3}O_3$ + 0.5 wt% CuO + y wt% Bi_2O_3 ceramics.: (a) $y = 0$, (b) $y = 0.1$, (c) $y = 0.3$ and (d) $y = 0.5$.

factor and piezoelectric constant (d_{33}) of $Pb(Zr,Ti)O_3$–$Pb(Zn,Ni)_{1/3}Nb_{2/3}O_3$ + 0.5 wt% CuO + y wt% Bi_2O_3 ceramics sintered at 900 °C for 2 h are plotted as a function of the amount of Bi_2O_3 addition in Fig. 3. When Bi_2O_3 was added, density was increased and this increased density improved the dielectric and piezoelectric properties as seen in Fig. 3. The density of the specimens was improved when the amount of Bi_2O_3 was added and this increase might be due to the formation of liquid phase. In addition, Q_m was decreased and $\varepsilon_{33}^T/\varepsilon_0$ and d_{33} were increased with the amount of Bi_2O_3 addition in the range of $0.0 \leq y \leq 0.3$. Therefore, their variations could happen because Bi ions entered A site, since they acted as softener in this range. On the contrary, Q_m exhibits a minimum profile at 0.3 wt% of Bi_2O_3 addition. In addition, $\varepsilon_{33}^T/\varepsilon_0$, d_{33} and Q_m were increased with the amount of Bi_2O_3 addition above 0.3 wt%. Thus, Bi ions might act as both hardener and softener in this range and their variations might be able to occur because Bi ions entered B site and A site, respectively. Fig. 4 shows the SEM images of the $Pb(Zr,Ti)O_3$–$Pb(Zn,Ni)_{1/3}Nb_{2/3}O_3$ + 0.5 wt% CuO + y wt% Bi_2O_3 ceramics sintered at 900 °C for 2 h. When the amount of Bi_2O_3 was more than 0.3 wt%, the small grains almost disappeared and average grain size increased. Even though apparent liquid phase formation was not observed in the SEM images, Bi_2O_3 addition might induce small amount of liquid phase and it could be expected to help grain growth due to its low melting point.

4. Conclusions

In this study, we developed CuO and Bi_2O_3 as sintering aids at low temperature sintering condition (900 °C) for Sb, Li and Mn-substituted $Pb(Zr,Ti)O_3$–$Pb(Zn,Ni)_{1/3}Nb_{2/3}O_3$ ceramics. The addition of CuO decreased the sintering temperature through the formation of a liquid phase. However, the piezoelectric properties of the CuO-added ceramics sintered below 900 °C were lower than the desired values. The additional Bi_2O_3 resulted in a significant improvement in the piezoelectric properties.

At the sintering temperature of 900 °C, the electromechanical coupling factor (k_p), piezoelectric constant (d_{33}), mechanical quality factor (Q_m) of Sb, Li and Mn-substituted $0.8Pb(Zr_{0.48}Ti_{0.52})O_3$–$0.16Pb(Zn_{1/3}Nb_{2/3})O_3$–$0.04Pb(Ni_{1/3}Nb_{2/3})O_3$-based ceramics with 0.5 wt% CuO and 0.5 wt% Bi_2O_3 show the optimal value of 0.56, 350 pC/N and 1042, respectively. These values indicated that the newly developed composition might be suitable for multilayer piezoelectric transformer application.

Acknowledgements

This work was supported by the Thailand Research Fund (TRF) and Commission on Higher Education (CHE). The authors are thankful to the Graduate School and Faculty of Science, Chiang Mai University and the Ministry of Education for financial support.

References

[1] K. Uchino, J.R. Giniewicz, Micromechatronics, Marcel Dekker, New York, 2003.
[2] S. Takahashi, Sintering $Pb(Zr,Ti)O_3$ ceramics at low temperature, Jpn. J. Appl. Phys. 19 (4) (1980) 771–1771.
[3] P.G. Lucuta, F. Constantinescu, D. Barb, Structural dependence on sintering temperature of lead zirconate–titanate solid solutions, J. Am. Ceram. Soc. 68 (10) (1985) 533–537.
[4] G. Zhilun, L. Longtu, G. Suhua, Z. Xiaowen, Low-temperature sintering of lead-based piezoelectric ceramics, J. Am. Ceram. Soc. 72 (3) (1989) 486–491.
[5] S. Kaneko, D. Dong, K. Murakami, Effect of simultaneous addition of $BiFeO_3$ and $Ba(Cu_{0.5}W_{0.5})O_3$ on lowering of sintering temperature of $Pb(Zr,Ti)O_3$ ceramics, J. Am. Ceram. Soc. 68 (4) (1998) 1013–1018.
[6] X. Wang, K. Murakami, S. kaneko, High-performance $PbZn_{1/3}Sb_{2/3}O_3$–$PbNi_{1/2}Te_{1/2}O_3$–$PbZrO_3$–$PbTiO_3$ ceramics sintered at a low temperature with the aid of complex additives Li_2CO_3–Bi_2O_3–$CdCO_3$, Jpn. J. Appl. Phys. 39 (9) (2000) 5556–5559.
[7] T. Hayashi, T. Inoue, Y. Akiyama, Low-temperature sintering and properties of (Pb, Ba, Sr)(Zr, Ti, Sb)O_3 piezoelectric ceramics using sintering aids, Jpn. J. Appl. Phys. 38 (9) (1999) 5547–5552.
[8] L. Wu, C.H. Wang, The dielectric and piezoelectric properties of 0.125PMN–0.875PZT ceramics-doped with $4PbO{\cdot}B_2O_3$, Jpn. J. Appl. Phys. 32 (6) (1993) 2757–2761.
[9] D.E. Wittmer, R.C. Buchanan, Low temperature densification of lead zirconate titanate with vanadium pentoxide additive, J. Am. Ceram. Soc. 64 (3) (1981) 485–490.
[10] S.-H. Park, S. Ural, C.-W. Ahn, S. Nahm, K. Uchino, Piezoelectric properties of Sb-, Li-, and Mn-substituted $Pb(Zr_xTi_{1-x})O_3$–$Pb(Zn_{1/3}Nb_{2/3})O_3$–$Pb(Ni_{1/3}Nb_{2/3})O_3$ ceramics for high-power applications, Jpn. J. Appl. Phys. 45 (9) (2006) 2667–2673.
[11] C.-W. Ahn, H.-C. Song, S. Nahm, S. Priya, S.-H. Park, K. Uchino, H.-G. Lee, H.-J. Lee, Effect of ZnO and CuO on the sintering temperature and piezoelectric properties of a hard piezoelectric ceramic, J. Am. Ceram. Soc. 89 (3) (2006) 921–925.

Available online at www.sciencedirect.com
ScienceDirect
Ceramics International 35 (2009) 181–184
CERAMICS INTERNATIONAL
www.elsevier.com/locate/ceramint

Monte Carlo investigation of hysteresis properties in ferroelectric thin-films under the effect of uniaxial stresses

Y. Laosiritaworn [a,*], S. Ananta [a], J. Poulter [b], R. Yimnirun [a]

[a] Department of Physics, Faculty of Science, Chiang Mai University, Chiang Mai 50200, Thailand
[b] Department of Mathematics, Faculty of Science, Mahidol University, Bangkok 10400, Thailand

Accepted 1 October 2007
Available online 23 February 2008

Abstract

The uniaxial stress dependence of the hysteresis behavior of ferroelectric films was studied. The DIFFOUR model was modified to include the uniaxial stress effect. Both the uniaxial stress and the external electric field were applied on the out-of-plane direction of the films. The polarization was measured with varying the magnitude of the applied stress and the electric field frequency via the dynamics of the polarization reversal in terms of hysteresis. The study was taken by means of Monte Carlo simulations using the spin-flip Metropolis algorithm. From the results, the district dependence of hysteresis behavior on frequency between low frequency and high frequency was prominent. On the other hand, the remanent and the coercivity significantly decreased with increasing applied stresses. Moreover, the areas under the hysteresis loops also decreased indicating smaller magnitude of energy dissipation. The results agree well with related experiments where applicable.

Keywords: Ferroelectric thin-films; Monte Carlo; Uniaxial stress; Hysteresis

1. Introduction

Ferroelectric thin-films have recently been of wide interest in view of both technological and fundamental importance [1,2]. Of a particular interest is the technological applicability such as high-speed ferroelectric recording media in which high areal densities and high reliability are in demand [1]. Therefore, it is necessary to understand the response of ferroelectric domain switching to electric field corresponding to specific material structures in detail. Nevertheless, for the sake of simplicity, theoretical studies on ferroelectric multi-layers are usually performed on an ideal stress-free system. However, real materials used in many applications are often affected by crystalline anisotropy caused by external mechanical stress, or internal strain induced by misfit in lattice spacing at the interfaces between ferroelectric layers and the substrate. Furthermore, ferroelectric thin-films under stresses were found to have their polarization behavior altered leading to substantial changes in phase transition between ferroelectric and paraelectric phases [3,4]. Consequently, it is very important to include the applied stress to model real materials.

In this work, the uniaxial stress dependence of the ferroelectric dynamic properties in thin-films was studied. To outline, the study was firstly done by proposing the DIFFOUR Hamiltonian that includes the uniaxial stress effect. Then, by means of Monte Carlo simulations, the polarization along the out-of-plane direction is investigated with varying the field frequency and uniaxial stress via the dynamics of the hysteresis. Finally, all the descriptions to these results are given in detail.

2. Methodologies

2.1. Spin Hamiltonian

In this study, the DIFFOUR Hamiltonian [5–7]

$$H = \sum_i \left(\frac{P_0^2}{2m} - \frac{a}{2}u_i^2 + \frac{b}{2}u_i^4 \right) - \sum_{<ij>} U_{ij}\vec{u}_i \cdot \vec{u}_j - E(t)\sum_i u_{iz} \quad (1)$$

was considered where $\vec{u}_i$ is the ferroelectric dipole spin at site i, $P_0^2/2m$ is the kinetic energy, a and b are the double-well

* Corresponding author. Fax: +66 53943445.
E-mail address: yongyut_laosiritaworn@yahoo.com (Y. Laosiritaworn).

0272-8842/$34.00
doi:10.1016/j.ceramint.2007.10.034

potential parameters for the ferroelectric spins, and U_{ij} is the ferroelectric interaction. However, in this study, only the case that $\vec{u}_i$ is constant in magnitude was considered to underline the dynamics of the spin orientation in response to the field. Therefore, by proposing appropriate reference energy and introducing the stress effect, the Hamiltonian can be rewritten as

$$H = \sum_{<ij>} U_{ij}(\Delta l)\hat{u}_i \cdot \hat{u}_j - E(t)\sum_i u_{iz}, \tag{2}$$

where $\hat{u}_i$ is a unit vector referring to one of the possible 14 ferroelectric spin directions (6 from tetragonal and 8 from rhombohedral structures), $<ij>$ represents summation over the nearest pairs, and u_{iz} is the spin's z component. $E(t) = E_0 \sin(2\pi ft)$ is the electric field acting only on the out-of-plane direction of the films, where f and E_0 refer to frequency and amplitude respectively. Helical and free-boundary conditions were used for the in-plane (xy) and the out-of-plane (z) directions. In this picture, the magnitude of $\hat{u}_i$ is dimensionless, so both U_{ij} and E have a unit of energy. $U_{ij}(\Delta l)$ is a function of lattice distortion Δl, arising from the applied stress, and assumed to take a Lennard–Jones potential-like [8], i.e.

$$U_{ij}(r_{ij}) = U_0\left[\left(\frac{r_0}{r_{ij}}\right)^{12} - 2\left(\frac{r_0}{r_{ij}}\right)^{6}\right]. \tag{3}$$

Here, r_0 is the lattice spacing at a specific thermal equilibrium, U_0 is the ferroelectric interaction associated to r_0 ($\Delta l = 0$), and r_{ij} is the distance between site i and j. For zero stress (strain), $r_{ij} = r_0$ and $U_{ij} = -U_0$ so the system prefers ferroelectric phase. Since the Young's modulus is defined as $Y \equiv P/((r_{ij} - r_0)/r_0)$ where P is the stress (pressure), it is possible to write $r_{ij}/r_0 = 1 - (P/Y)$ and Eq. (3) as $U^z_{ij} = U_0[(1-(P/Y))^{-12} - 2(1-(P/Y))^{-6}]$. However, along the xy direction, there also exists the lattice distortion caused by the stress along the z direction. The ratio of the distortions between these two directions is defined as the Poisson ratio $\varepsilon \equiv -\Delta r^{xy}/\Delta r^z$ (where for many systems ranging from metal to ceramics, $\varepsilon \approx 0.3$ [9]). As a result, it is possible to write $\varepsilon = -\Delta r^{xy}/\Delta r^z = -(r^{xy}_{ij} - r_0)/(r^z_{ij} - r_0) = ((1 - r^{xy}_{ij})/r_0)/(r^z_{ij}/(r_0 - 1))$ which gives $r^{xy}_{ij}/r_0 = 1 - \varepsilon((r^z_{ij}/r_0) - 1) = 1 + \varepsilon(P/Y)$. Consequently, the ferroelectric interaction along the xy direction is $U^{xy}_{ij} = U_0[(1+(\varepsilon P/Y))^{-12} - 2(1+(\varepsilon P/Y))^{-6}]$. As a result, the Hamiltonian can be written as

$$H = \sum_{<ij> \in \text{in-plane}} U^{xy}_{ij}\hat{u}_i\hat{u}_j + \sum_{<ij> \in \text{out-of-plane}} U^z_{ij}\hat{u}_i\hat{u}_j - E(t)\sum_i u_{iz}. \tag{4}$$

2.2. Monte Carlo simulation

Throughout this study, U_0 was set as 1, so this re-defines the unit of temperature T as J/k_B (where k_B is the Boltzmann's constant), and electric field amplitude E_0 as a unit of U_0. The simulations were done at a temperature in the ferroelectric phase (where there exists hysteresis loops), i.e. $T = 1.0\ J/k_B$. The ratio P/Y was varied from 0.00 to 0.16. The simulation was done on bi-layer ferroelectric films where each single layer consists of ferroelectric unit cells connecting along the in-plane direction. The ferroelectric spins are assumed to reside in the unit cells and the system consists of $N = L \times L \times 2$ spins where $L \times L$ refers to number of spins in one monolayer. To minimize finite size effect, large L is required so in this study $L = 40$ was chosen. Trial simulations for larger sizes were also performed and it is found that for the range of parameters used in this study, the difference in hysteresis behavior is not significant. The unit time step was defined from one full simulation update of all sites of the lattice, i.e. 1 Monte Carlo step per site (mcs). The field frequency was varied from 0.001 to 4 mcs^{-1} and the field amplitude is fixed at $E_0/U_0 = 4$.

With the Hamiltonian proposed in Eq. (3), each system was assigned an initial random configuration and later on was passed to the thermal Monte Carlo updates, using the Metropolis algorithm [10]. In updating the system, each spin is assigned a new random direction, and the probability of accepting that new direction is proportional to

$$\text{probability} = \exp\left(-\frac{\Delta H}{k_B T}\right) \tag{5}$$

where ΔH is the energy differences between of the original and the new updating state. If the energy difference is less than zero, or a uniform random number in the range [0,1) is less than the probability given in Eq. (5), the new direction is accepted and the system is successfully updated, or else the considered spin is left untouched. The whole procedure is repeated until the simulation ends.

In measuring, with varying the uniaxial stress and the applied field frequency, each simulation waited for a few cycles to obtain steady hysteresis loops, and then the polarization per spin along the z direction was calculated, i.e.

$$p_r = \frac{1}{N}\left[\sum_i u_{iz}\right]. \tag{6}$$

Then, 1000 steady hysteresis loops were used to calculate average hysteresis loop for each condition.

3. Results and discussion

From the simulation results, with varying field frequency and stress, significant changes to the hysteresis loop were found. Fig. 1a shows the patterns for hysteresis loops for frequencies ranging from 0.001 to 0.320 mcs^{-1}. As can be seen, 2 distinct behaviors can be found for low frequency region, e.g. $f \leq 0.125\ \text{mcs}^{-1}$ and for high frequency region, e.g. $f > 0.125\ \text{mcs}^{-1}$. At low frequencies, the loops get bigger with increasing frequency. This is because, at low frequency, the field period is high and hence the sweeping time of the field per one hysteresis cycle is large. Ferroelectric spins then have time to follow the field leading to low phase-lag between the polarization and field and hence to a small hysteresis loop.

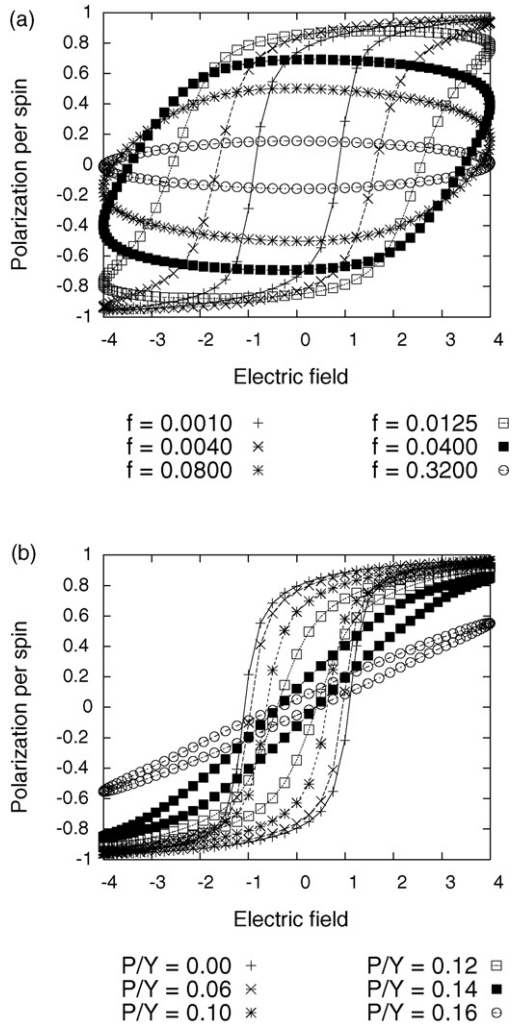

Fig. 1. Hysteresis loops of the bi-layered films (a) at zero-stress but varying frequency from $f = 0.0010$ to $f = 0.3200$ mcs^{-1}, and (b) at $f = 0.0010$ mcs^{-1} but varying stress from $P/Y = 0.00$ to $P/Y = 0.16$.

However, with increasing the frequency in the low frequency region, the phase lag gets bigger and hence the hysteresis loop becomes larger. However, if the frequency is still increased, the loop reaches a maximum size at a certain frequency. Beyond this point, the frequency is very high which limits the dynamics of the spins and results in a smaller loop with an oval shape-like.

However, with a non-zero stress, e.g. in Fig. 1b, the decrease of the remanent p_r, the coercivity E_C, and the hysteresis loop-area were found. The reason is that the stress causes the z direction to become a 'hard axis'. As a result, the spins prefer to align in the xy direction or have their z-components align in an anti-parallel pattern to lower the energy. Consequently, both p_r and E_C reduce. In comparison with experiments, qualitatively, the decrease of the coercivity and the loop-area with increasing stress has trends that agree reasonably well with an experiment on ferroelectric material [11].

On the other hand, Fig. 2 shows the hysteresis loop area as a function of frequency for various stresses. The loop area increases for low frequency region and decreases for high

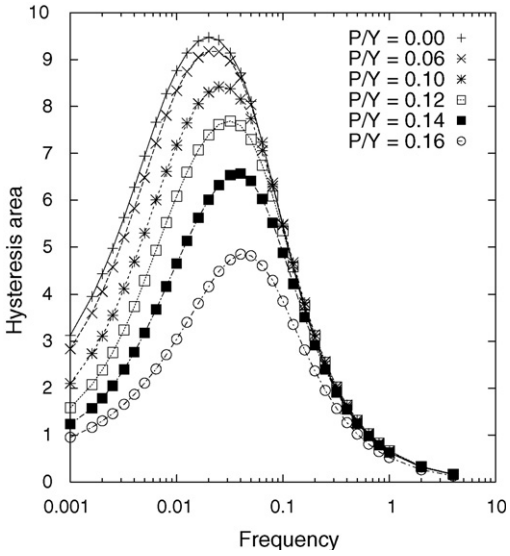

Fig. 2. Stress dependent of the hysteresis areas (arbitrary unit) of the bi-layered films as a function of the electric field frequency (mcs^{-1} unit) with varying stresses from $P/Y = 0.00$ to $P/Y = 0.16$.

frequency region with increasing frequency. At a particular frequency, the loop area is smaller for larger stresses. This is because the z direction is the stress induced 'hard axis'. In this way, the spins are loosely coupled along the z direction and hence it will be easier for the spins to catch up with the field so the inclined oval loop occurs with small loop area. However, with increasing the frequency at low frequencies, the phase lag gets larger but with higher stresses it will require higher frequency to reach the loop-area maximum point. This is why the frequency at the maximum area shifts to higher frequency for larger stress. Notice that the maximum area is smaller for larger stress because of smaller p_r and E_C.

4. Conclusions

In this study, Monte Carlo simulations were performed to study ferroelectric thin-films under the influence of uniaxial stress on ferroelectric hysteresis properties. The objective is to investigate the behavior of the spin-reversal along the out-of-plane direction with changes in the magnitude of the stress and the electric field frequency. With increasing frequency, it is found that the hysteresis area increases for low frequency and decreases for high frequency. On the other hand, the applied stress reduces p_r, E_C and the hysteresis area. This is due the stress causing the out-of-plane direction to be a 'hard axis' and the hysteresis results in smaller loop-area. The results qualitatively agree well with experiments where applicable.

Acknowledgement

The authors would like to acknowledge financial supports from the Commission on Higher Education and the Thailand Research Fund (TRF).

References

[1] J.F. Scott, Ferroelectric Memories, Springer-Verlag, Berlin, 2002.
[2] G.H. Haertling, Ferroelectric Ceramics: History and Technology, Journal of American Ceramic Society 82 (1999) 797–818.
[3] X. Lu, J. Zhu, Z. Liu, X. Xu, Y. Wang, Phase transition related stress in ferroelectric thin films, Thin Solid Films 375 (2000) 15–18.
[4] J. Mendiola, M.L. Calzada, P. Ramos, M.J. Martin, F. Agulló-Rueda, On the effects of stresses in ferroelectric (Pb,Ca)TiO_3 thin films, Thin Solid Films 315 (1998) 195–201.
[5] T. Janssen, J.A. Tjon, One-dimensional model for a crystal with displacive modulation, Physical Review B 24 (1981) 2245–2248.
[6] J.-M. Liu, Q.C. Li, W.M. Wang, X.Y. Chen, G.H. Cao, X.H. Liu, Z.G. Liu, Scaling of dynamic hysteresis in ferroelectric spin systems, Journal of Physics: Condensed Matter 13 (2001) L153–L161.
[7] J.-M. Liu, W.M. Wang, Z.G. Liu, H.L. Chan, C.L. Choy, Dynamic hysteresis in ferroelectric systems: experiment and Monte Carlo simulation, Applied Physics A 75 (2002) 507–514.
[8] S.J. Mitchell, D.P. Landau, Phase separation in a compressible 2D Ising model, Physical Review Letter 97 (2006) 025701.
[9] W.D. Callister, Materials Science and Energineering: An Introduction, John Wiley & Sons, New York, 2003.
[10] N. Metropolis, A.W. Rosenbluth, M.N. Rosenbluth, A.H. Teller, E. Teller, Equation of state calculations by fast computing machines, Journal of Chemical Physics 21 (1953) 1087–1092.
[11] R. Yimnirun, Y. Laosiritaworn, S. Wongsaenmai, Effect of uniaxial compressive pre-stress on ferroelectric properties of soft PZT ceramics, Journal Physics D 39 (2006) 759–764.

Available online at www.sciencedirect.com
ScienceDirect
Ceramics International 35 (2009) 121–124
CERAMICS INTERNATIONAL
www.elsevier.com/locate/ceramint

Preparation and characterization of ceramic nanocomposites in the PZT–BT system

Wanwilai Chaisan *, Rattikorn Yimnirun, Supon Ananta

Department of Physics, Faculty of Science, Chiang Mai University, Chiang Mai 50200, Thailand

Accepted 1 October 2007
Available online 23 February 2008

Abstract

Nanocomposites of the $(1-x)$PZT-xBT system were fabricated by the bimodal particle concept. The effect of fabricating conditions on structural characteristics and dielectric properties of the ceramics was investigated using XRD, SEM, and a standard dielectric measurement. The ceramic–solid solutions and -nanocomposites in the PZT–BT system were comparatively explored. It was clearly seen that the microstructures and the dielectric properties of PZT–BT ceramic-nanocomposites are totally different from those of ceramic–solid solutions. The dielectric behavior of ceramic-nanocomposites displayed superimposition of two phase transitions with a lower maximum value of the dielectric constant than that of the solid solutions.

Keywords: B. Nanocomposites; C. Dielectric properties; D. PZT; BT

1. Introduction

Piezoelectric ceramics (e.g. $Pb(Zr_x,Ti_{(1-x)})O_3$, $BaTiO_3$ and its related compounds), which are widely used as transducers, pressure sensors and actuators, suffer from mechanical and electrical deterioration in service because of fatigue damage. When piezoelectric devices are used in severe circumstances, such as high stress or high power applications, problems that are related to reliability (i.e. degradation of electrical properties and fatigue fracture) become more critical and important. Therefore, it is necessary to investigate the electrical behavior of piezoelectric ceramics and to design microstructure that possesses excellent electrical properties. Both $BaTiO_3$ (BT) and $Pb(Zr,Ti)O_3$ (PZT) are among the most common ferroelectric materials and have been studied extensively since the late 1940s [1,2]. These two ceramics have distinct characteristics that make each individual ceramic suitable for different applications. The compound PZT has highly desirable piezoelectric properties which can be applied in transducer applications. Furthermore, it has a high T_C of 390 °C which allows piezoelectric devices to be operated at relatively high temperatures. BT is a normal ferroelectric material which exhibits a high dielectric constant, a lower T_C (∼120 °C) and better mechanical properties [1–3]. Thus, mixing PZT with BT is expected to decrease the sintering temperature of BT-based ceramics, allowing a desirable move towards electrodes of lower cost [4]. Moreover, the nano-reinforced structure is believed to improve densification and mechanical properties of the ceramic composite. Therefore, ceramic-nanocomposites of the lead zirconate titanate–barium titanate ($(1-x)$PZT-xBT) system with various compositions, were fabricated using a modified mixed-oxide synthetic route and a bimodal particle concept. The effect of processing parameters on the arrangement of phases, microstructural evolution and electrical properties of the ceramics was carefully investigated using XRD, SEM and dielectric measurements.

2. Experimental procedure

Ceramic-nanocomposites in the system $(1-x)$PZT-xBT ($0.1 \leq x \leq 0.5$; $\Delta x = 0.1$) have been fabricated from PZT powder and BT nanopowder, employing a normal sintering method. Reagent grade PbO, ZrO_2, TiO_2 and $BaCO_3$ powders (Fluka, >99% purity) were used as starting materials. Powder of each end member (PZT and BT) was first formed in order to avoid unwanted pyrochlore phases. For the preparation of BT

* Corresponding author. Tel.: +66 53 943367; fax: +66 53 943445.
E-mail address: wanwilai_chaisan@yahoo.com (W. Chaisan).

0272-8842/$34.00
doi:10.1016/j.ceramint.2007.10.032

nanopowder, a vibratory laboratory mill (McCrone Micronizing Mill) powered by a 1/30 HP motor was employed for 30 h with zirconia media in ethanol. The well-mixed powder was calcined at 1300 °C for 2 h in an alumina crucible. With a modified mixed-oxide method [5], the PZT powders were prepared using a lead zirconate ($PbZrO_3$) as precursor in order to reduce the occurrence of undesirable phase. Pure $PbZrO_3$ phase was first formed by reacting PbO with ZrO_2 at 800 °C for 2 h. $PbZrO_3$ powder was then mixed with PbO and TiO_2 and milled, dried and calcined at 900 °C for 2 h to form single phase PZT.

The $(1 - x)$PZT–xBT mixed powders were then formulated from the BT and PZT components by employing the similar mixed-oxide procedure. In the mixing process, the calculated relevant proportions of constituents were weighed, suspended in ethanol and intimately mixed in a ball-mill with zirconia media. Drying was carried out for 2 h and the dried powder was then ground into the fine powders. The powders were then isostatically cold-pressed into pellets with a diameter of 15 mm and a thickness of 2 mm at a pressure of 4 MPa and sintered at 1200 °C for 2 h.

Densities of sintered ceramics were measured by Archimedes method and X-ray diffraction (XRD using CuK_α radiation) was employed to identify the phases formed. The grain morphology and size were directly imaged using scanning electron microscopy (SEM). For electrical measurements, silver paste was fired on both sides of the polished samples at 750 °C for 12 min as the electrodes. Dielectric properties of the sintered ceramics were studied as a function of both temperature and frequency. The capacitance was measured with a HP4284A LCR meter in connection with a Delta Design 9023 temperature chamber and a sample holder capable of high temperature measurement. Dielectric constant (ε_r) was calculated using the geometric area and thickness of the discs.

3. Results and discussion

XRD patterns of all sintered ceramic-nanocomposites are shown in Fig. 1. Here the peak positions and intensities of the XRD patterns vary according to the amount and chemical composition of the phases present. It is seen that the diffraction peaks shifted towards a higher angle with increasing x and the XRD peaks of all ceramic-nanocomposites are broader than those of solid-solution case in our earlier work [6]. These can be interpreted in terms of co-existing perovskite phases, i.e. PZT, BT and their reacted intermediate phases. Moreover, with careful observation, it is found that the sintered samples of $0.3 \leq x \leq 0.5$ nanocomposites exhibit the perovskite structure with traces of unwanted phase ($\bigtriangledown$) occurring at $2\theta \sim 28°$. It is believed that this unwanted phase is ZrO_2 matched with JCPDS file no. 37-1484 [7]. Compositional fluctuations due to the evaporation of lead oxide within surface regions are believed to be responsible for the occurrence of free ZrO_2 phase in the sintered $(1 - x)$PZT-xBT ceramics of $0.3 \leq x \leq 0.5$ nanocomposites. Another possibility was put forward by Fushimi and Ikeda [8], who suggested that melting of PT-PZ solid solution can change from congruent to incongruent and induce ZrO_2 to form at ~1340 °C. On the other hand, Brankovic et al. [9] suggested that incomplete reaction of the starting precursors can also result in the persistence of free ZrO_2 phase. Since no trace of ZrO_2 has been observed for sintered samples of $x = 0.1$ and 0.2, it is believed that the segregation of ZrO_2 may be associated with loss of Pb content and also depend on the level of BT content, similar with observations made in other perovskite systems [10,11].

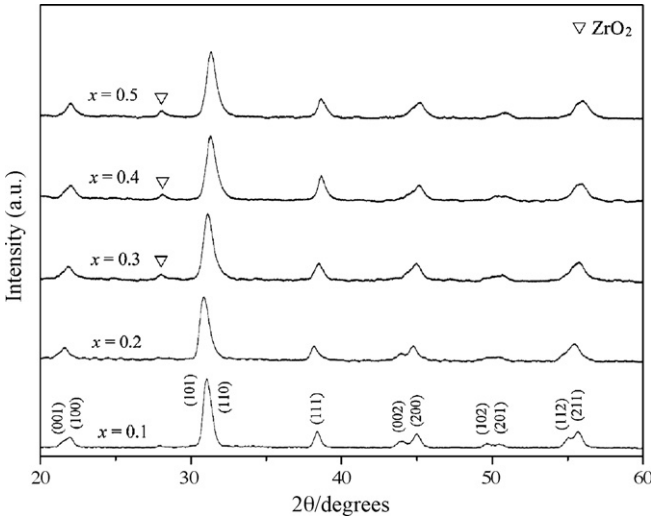

Fig. 1. XRD patterns of the $(1 - x)$PZT-xBT ceramic-nanocomposites sintered at 1200 °C for 2 h.

The microstructural morphology of $(1 - x)$PZT-xBT ceramic-nanocomposites was initially examined by SEM. Micrographs of as-fired surface of all ceramic-nanocomposites are shown in Fig. 2(a–e). In general, high porosity, heterogeneous microstructures consisting mainly of two ranges of particles (in respect of size and shape) were found in all samples. A distribution of very small spherical BT particles (brighter phase with diameter ~200–500 nm) is found over the PZT grains, especially for rich-BT samples. Large pore-sizes of the order of 2 μm were also observed. These poorly sintered samples could be attributed to several factors, including the effect of different particle size fractions between the two end components, ineffective mixing and the use of low density green bodies produced by conventional uniaxial die-pressing.

Densities in the range 4.80–6.21 g/cm^3 were obtained, which are considerably lower than the values obtained for sintered PZT–BT solid solution ceramics in our earlier work [6]. In order to preserve the ceramics with a nanostructural arrangement, it is possible that the sintering temperature employed in this work is not enough for driving the densification mechanism to achieve dense PZT/BT ceramic-nanocomposites. However, so far, there are no reports on the production of highly dense PZT/BT ceramic-nanocomposites by a pressureless sintering method. Moreover, the scope for improving pressureless sintering by raising the temperature is limited by the melting point of PZT (~1400 °C) whilst the hot-pressing technique can cause severe PbO-volatilization problems [12].

The temperature dependence of the dielectric constant (ε_r) measured at 1 MHz for $(1 - x)$PZT–xBT nanocomposites with

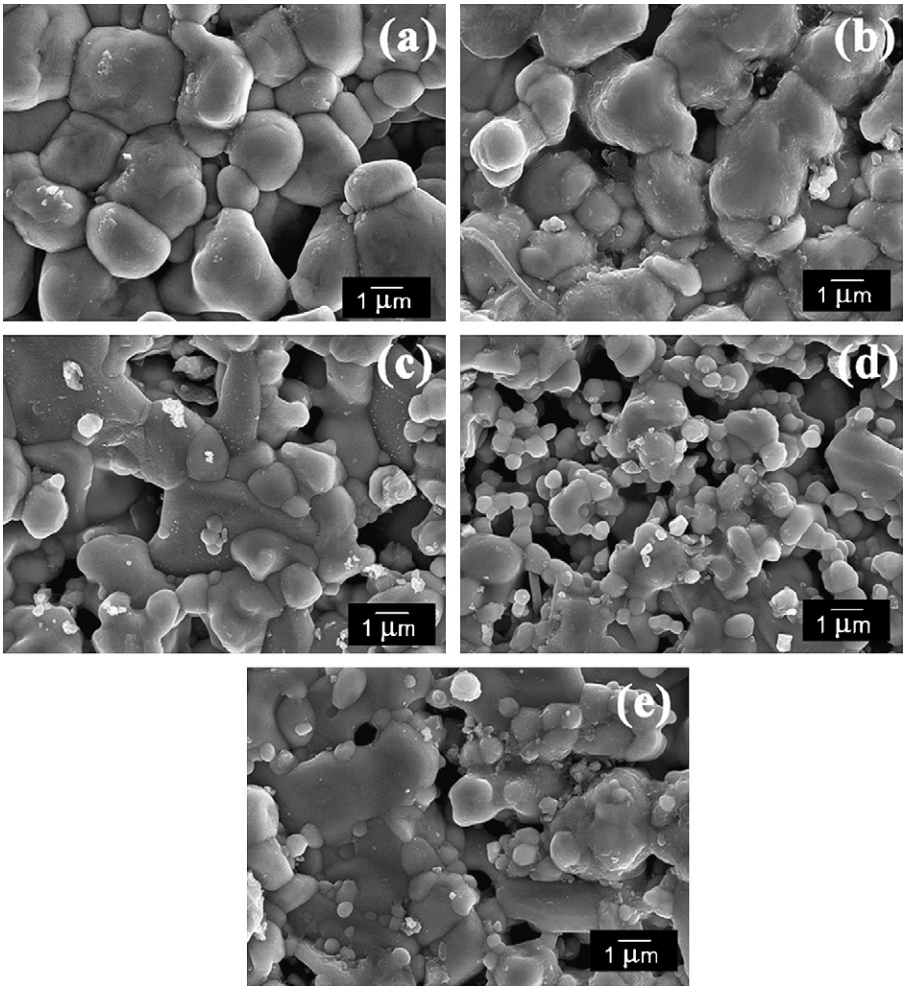

Fig. 2. SEM micrographs of as-fired surfaces of the sintered $(1-x)$PZT-xBT ceramic-nanocomposites with x = (a) 0.1, (b) 0.2, (c) 0.3, (d) 0.4 and (e) 0.5.

$0.1 \leq x \leq 0.5$ is shown in Fig. 3. All ceramic-nanocomposites display dielectric peak superimposition of the two phase transitions (T_1 and T_2) with no frequency dependence. The shape of dielectric peak for each composition seems to be the two peaks merged into a mound. The height of the mound was lower than those of solid solutions [6]. The phase transition temperatures, T_1 and T_2, and dielectric data are illustrated in Fig. 3 and list in Table 1. As is well known, the dielectric constant of pure PZT and pure BT showed anomalies at 390 and 130 °C, respectively. Therefore, ceramic-nanocomposites between PZT and BT are expected to show a transition temperature between 390 and 130 °C. An attempt was made to characterize the dielectric temperature of PZT–BT as a function of x. However, difficulties were encountered in indexing the measured dielectric peak broadening obtained. As seen in Fig. 3, with increasing of x, T_1 and T_2 decrease moving toward

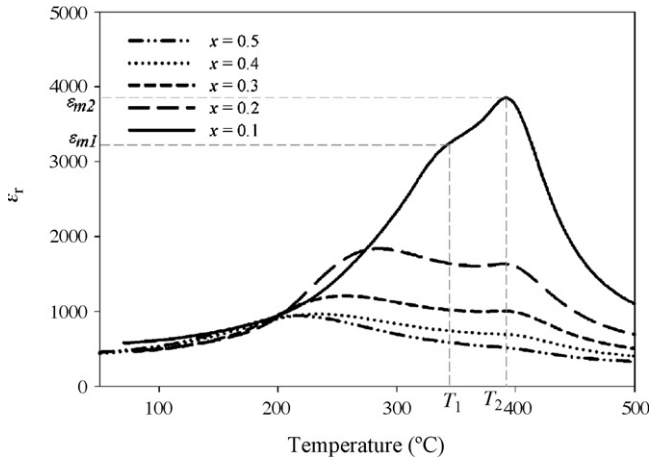

Fig. 3. Comparison of dielectric constant (ε_r) at 1 MHz for $(1-x)$PZT-xBT ceramic-nanocomposites.

Table 1
Dielectric properties of ceramic-nanocomposites in the $(1-x)$PZT–xBT system

Compositions (x)	T_1 (°C)	ε_{m1}	T_2 (°C)	ε_{m2}
0.1	340	3200	392	3800
0.2	285	1800	390	1600
0.3	257	1200	388	1000
0.4	234	960	385	700
0.5	216	940	380	530

ε_{m1} and ε_{m2} are the maximum dielectric constant at T_1 and T_2, respectively (see also Fig. 3).

the Curie temperature of BT. T_1 refers to transition temperature of BT and T_2 refers to transition temperature of PZT. There are various proposals for explaining the dielectric response of composite materials. Ausloos [13] studied effective dielectric constant theories of composite solids. Their work reported that the broad spectrum of dielectric constant is the results of clustering effects, the shape of particle (or cluster) effect and particle heterogeneity effect. In this work, it is possible that the incorporation of BT nanoparticles into a PZT matrix may hinder domain wall motion sufficiently to reduce the dielectric constant [14]. Moreover, the presence of unwanted ZrO_2 phase (confirmed by XRD) and high porosity (confirmed by SEM) are other reasons for the low dielectric constants in ceramic-nanocomposites with composition of $x > 0.2$. However, by neglect accounting for the porosity, the maximum dielectric constant (ε_{max}) of all ceramic-nanocomposites was back-calculated to 100% density for a better comparison with the solid solutions. Although the dielectric values of ceramic-nanocomposites are still lower than those of the solid solutions, the broadening is greater which infers the operating temperature with the moderate dielectric constant (∼1000–4000) of these ceramics is much wider in range, suitable for certain electronic devices.

4. Conclusions

Ceramics-nanocomposites in the system $(1 - x)$PZT-xBT were successfully processes by employing the bimodal particle concept. All PZT–BT compositions in this study were of the perovskite structure with tetragonal symmetry. The dielectric properties of all the ceramic-nanocomposites are strongly influenced by the presence of secondary phases and densification mechanism. The dielectric peak shows superimposition of the two phase transitions with no frequency dependence and the dielectric value is lower than that of solid solutions for all compositions, explained by theory of the dielectric response for composite materials. With increasing of x, the phase transition temperatures of all ceramics decrease moving toward to Curie temperature of BT.

Acknowledgement

I would like to thank the Thailand Research Fund (TRF), Commission on Higher Education (CHE) and the Faculty of Science, Chiang Mai University for all financial support.

References

[1] G.H. Haertling, Ferroelectric ceramics: history and technology, J. Am. Ceram. Soc. 82 (4) (1999) 797–818.
[2] B. Jaffe, W.R. Cook, H. Jaffe, Piezoelectric Ceramics, Academic Press, London, 1971.
[3] A.J. Moulson, J.M. Herbert, Electroceramics: Materials, Properties, Applications, John Wiley & Sons Ltd., Chichester, 2003.
[4] J. Chen, Z. Shen, F. Liu, X. Liu, J. Yun, Preparation and properties of barium titanate nanopowder by conventional and high-gravity reactive precipitation methods, Scripta Mater. 49 (2003) 509–514.
[5] W. Chaisan, S. Ananta, T. Tunkasiri, Synthesis of barium titanate-lead zirconate titanate solid solutions by a modified mixed-oxide synthetic route, Curr. Appl. Phys. 4 (2–4) (2004) 182–185.
[6] W. Chaisan, R. Yimnirun, S. Ananta, D.P. Cann, Dielectric properties of solid solutions in the lead zirconate titanate-barium titanate system prepared by a modified mixed-oxide method, Mater. Lett. 59 (2005) 3732–3737.
[7] JCPDS-ICDD card no. 37-1484, International Centre for Diffraction Data, Newtown Square, PA, 2002.
[8] S. Fushimi, T. Ikeda, Phase equilibrium in the system PbO-TiO_2-ZrO_2, J. Am. Ceram. Soc. 50 (1967) 129–132.
[9] Z. Brankovic, G. Brankovic, J.A. Varela, PZT ceramics obtained from mechanochemically synthesized powders, J. Mater. Sci. 14 (2003) 37–41.
[10] F. Xia, X. Yao, Piezoelectric and dielectric properties of PZN-BT-PZT solid solutions, J. Mater. Sci. 34 (1999) 3341–3343.
[11] N. Vittayakorn, G. Rujijanagul, T. Tunkasiri, X. Tan, D.P. Cann, Influence of processing conditions on the phase transition and ferroelectric properties of $Pb(Zn_{1/3}Nb_{2/3})O_3$-$Pb(Zr_{1/2}Ti_{1/2})O_3$ ceramics, Mater. Sci. Eng. B 108 (2004) 258–265.
[12] V.L. Balkevich, C.M. Flidlider, Hot-pressing of some piezoelectric ceramics in the PZT system, Ceramurgia Inter. 2 (1976) 81–87.
[13] M. Ausloos, Dielectric response of composite materials, J. Phys. C: Solid State Phys. 18 (1985) L1163–L1167.
[14] S.R. Panteny, C.R. Bowen, R. Stevens, Piezoelectric Particulate Reinforced Nanocomposites, The Alden Group, Oxford, 2000.

Available online at www.sciencedirect.com
ScienceDirect
Ceramics International 35 (2009) 173–176
CERAMICS INTERNATIONAL
www.elsevier.com/locate/ceramint

Effect of vibro-milling time on phase formation and particle size of barium titanate nanopowders

W. Chaisan *, R. Yimnirun, S. Ananta

Department of Physics, Faculty of Science, Chiang Mai University, Chiang Mai 50200, Thailand

Accepted 1 October 2007
Available online 26 February 2008

Abstract

Barium titanate (BT) nanopowder was synthesized by a solid state reaction via a rapid vibro-milling technique. The effect of milling time on phase formation and particle size of BT powder was investigated. Powder samples were characterized using XRD (X-ray diffraction) and SEM techniques. It was found that the resulting BT powders have a range of particle size depending on milling times. Production of a single-phase BT nanopowder can be successfully achieved by employing a combination of 30 h milling time and calcination conditions of 1200 °C for 2 h.

Keywords: A. Milling; Powders: solid state reaction; D. $BaTiO_3$

1. Introduction

Barium titanate ($BaTiO_3$ or BT), which exhibits a perovskite structure and a Curie temperature ~120 °C, is a classical ferroelectric material that has been extensively exploited both for academic and technological utilizations over the past decades [1,2]. Owing to its high dielectric constant, large mechanical-quality factor, large pyroelectric coefficient, non-toxic handling and low cost of manufacturing, compared to several lead-based perovskite ferroelectrics, BT-based ceramics have been a strong candidates for several electronic applications, including ultrasonic transducers, multilayer capacitors, pyroelectric detectors, semiconductors with positive temperature coefficient of resistance (PTCR) and electro-optic devices [3,4]. To fabricate them, a fine powder of perovskite phase with a minimal degree of particle agglomeration is needed as the starting material to achieve a dense and uniform microstructure at a given sintering temperature. In order to improve the sintering behavior of ceramics, a crucial focus of powder synthesis in recent years has been the formation of uniform-sized, single morphology particulates ranging in size from nanometer to micrometers.

The development of a method to produce nanopowders of precise stoichiometry and desired properties is complex, depending on a number of variables such as nature and purity of starting materials, processing history, temperature, etc. To obtain nanosized BT powders, many investigations have focused on several chemistry-based preparation routes, such as sol–gel [5], sol-precipitation [6], hydrothermal reaction [7], besides the more conventional solid state reaction of mixed oxides [8]. All these techniques are aimed at reducing the particle size and temperature of preparation of the compound even though they are more involved and complicated in approach than the solid state reaction. The advantage of using mechanical milling for preparation of nanosized powders lies in its ability to produce mass quantities of powders in the solid state using simple equipment and low cost starting precursors [9,10]. The ball-milling technique is a very popular solid state reaction because of easy and low cost technique, however the size of particle from this technique is still large (micrometer). Thus, the potentiality of vibro-milling technique will be then focused in order to achieve the nanosized powder. Although some research has been done in the preparation of BT nanopowders via a vibro-milling technique [11], to our knowledge a systematic study regarding the influence of milling time on the preparation of BT nanopowders has not yet been reported. Therefore, in this work, the effect of milling time on phase formation, and particle size of BT nanopowders was investigated in this connection. The potential of the vibro-

* Corresponding author. Tel.: +66 53 943376; fax: +66 53 943445.
E-mail address: wanwilai_chaisan@yahoo.com (W. Chaisan).

0272-8842/$34.00
doi:10.1016/j.ceramint.2007.10.035

milling technique as a simple and low-cost method to obtain usable quantities of single-phase BT powders at low temperature and with nanosized particles was also examined.

2. Experimental procedure

Commercially available powders of $BaCO_3$ and TiO_2 (anatase form), (Fluka, >99% purity) were used as starting materials. $BaTiO_3$ powder was synthesized by the solid state reaction of these raw materials. A vibratory laboratory mill (McCrone Micronizing Mill) powered by a 1/30 HP motor was employed for preparing the stoichiometric $BaTiO_3$ powder [9]. The mixed powder was vibro-milled for 0.5 h with corundum media in isopropyl alcohol (IPA). Drying was carried out for 2 h at 120 °C. Various calcination temperatures ranging from 700 to 1400 °C were selected to investigate the phase development of BT. Moreover, in order to investigate the effect of milling time on phase formation and particle size, the milling times were then ranged from 0.5 to 30 h. All powders were examined by room temperature X-ray diffraction (XRD; Siemens-D500 diffractometer) using Ni-filtered Cu Kα radiation, to identified the phase formed and the optimum firing temperature for the production of single-phase BT powders under various milling conditions. The crystallite size and tetragonality factor (*c*/*a*) were also estimated from these XRD patterns [12]. The morphologies of the powders observed by scanning electron microscopy (JEOL JSM-840 A SEM).

3. Results and discussion

From the TG-DTA data in previous work [13], the range of calcination temperatures between 700 and 1400 °C were designed for BT powder to investigate the phase formation. To study the phase development with increasing calcination temperature in BT powder prepared from vibro-milling technique for 0.5 h, it was calcined for 2 h in air at various temperatures, up to 1400 °C, followed by phase analysis using XRD. As shown in Fig. 1, for the uncalcined powder, only X-ray peaks of precursors, $BaCO_3$ (●) and TiO_2 (◆), which could be matched with JCPDS file numbers 5-0378 [14] and 21-1272 [15], respectively, are presented, indicating that no reaction had yet been triggered during the milling process. In this work, it is seen that the desired perovskite $BaTiO_3$ (▽) was already observed in the powder calcined at 700 °C, accompanying with unreacted $BaCO_3$ and TiO_2 precursors as

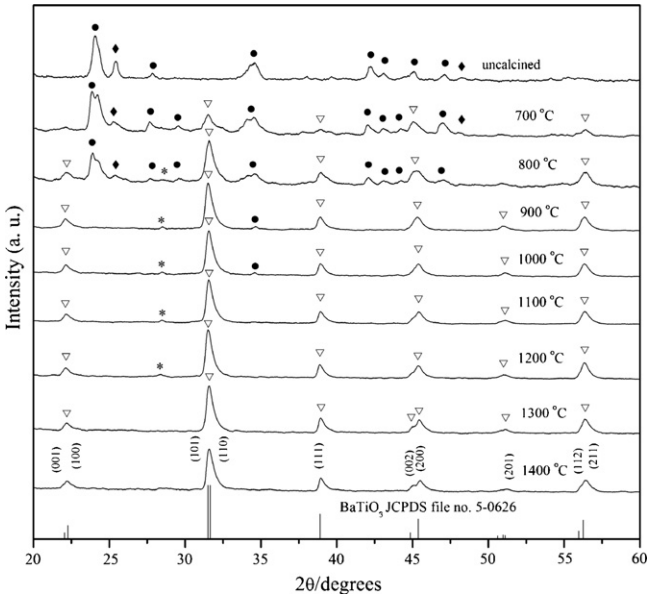

Fig. 1. XRD patterns of BT powders calcined at various temperatures for 2 h with heating/cooling rates of 10 °C/min (● = $BaCO_3$, ◆ = TiO_2, ▽ = $BaTiO_3$ and * = Ba_2TiO_4).

separated phases, in good agreement with literature [16,17]. Moreover, the unknown phase (★) started to occur at $2\theta \sim 28.5^\circ$, consistent with earlier work of Simon-Seveyrat et al. [18]. According to the literature [19,20], the reaction sequence of the phase formation in the BT mixture can be described as follow.

$$2BaCO_3 + TiO_2 \rightarrow Ba_2TiO_4 + 2CO_2 \quad (1)$$

$$Ba_2TiO_4 + TiO_2 \rightarrow 2BaTiO_3 \quad (2)$$

It was believed that this unknown phase corresponds to Ba_2TiO_4, which could be matched with JCPDS file numbers 72-0135 [21], always found in conventional mixed oxide processing [16,22]. As the temperature increased to 1000 °C, the intensity of the $BaTiO_3$ peaks was further enhanced. The starting materials completely disappeared after calcination at 1100 °C, however, the unwanted Ba_2TiO_4 phase still be detected. Upon calcination at 1300 °C, an essentially mono-phasic of $BaTiO_3$ phase was obtained. This observation agrees well with other workers [23,24]. This BT phase was indexable according to a tetragonal perovskite-type structure with lattice parameters $a = 3.994$ Å and $c = 4.038$ Å, space group *P*4*mm* (no. 99), consistent with JCPDS file number 5-0626 [25].

Table 1
Effect of milling time on the optimum calcination temperature and the variation of particle size of BT powders measured by different techniques

Milling time (h)	Perovskite phase (%)	Calcination temperature (°C)	XRD		SEM	
			A (nm)	*c*/*a*	*D* (nm)	*P* (nm)
0.5	100	1300	38.32	1.0090	610	250–1400
10	100	1250	32.09	1.0059	260	100–500
15	100	1250	32.38	1.0036	490	100–1000
20	100	1250	31.95	1.0058	590	250–700
25	100	1200	31.60	1.0065	390	250–700
30	100	1200	31.56	1.0056	250	100–400

A = crystallite size, *c*/*a* = tetragonality factor, *D* = average particle size, *P* = particle size range.

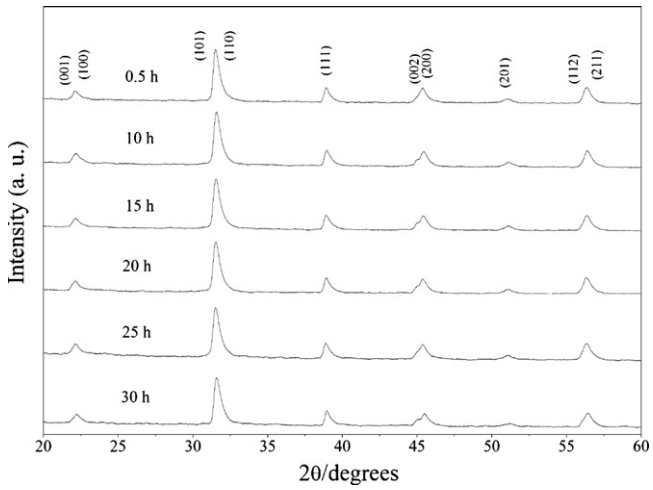

Fig. 2. XRD patterns of BT powders milled at different times.

Having established the optimum calcination temperature of BT powder vibro-milled for 0.5 h, an attempt was also made to calcine the BT powder under various milling times. The optimum calcination temperature of each powder was reported in Table 1 and the XRD patterns of all BT powders are shown in Fig. 2. It has been observed that with increasing milling time, all diffraction lines broaden, e.g., (0 0 2) and (2 0 0) peaks, an indication of a continuous decrease in particle size and of the introduction of lattice strain. These values indicate that the prolonged milling treatment affects the particle size and evolution of crystallinity of the phase formed. For BT powders, the longer the milling time, the lower the required (optimum) firing temperature. Additionally, the crystallite size and tetragonality factor (c/a) were estimated from these XRD patterns as also given in Table 1. The calculated crystalline size value was also found to decrease with increasing milling time. Though, the relative intensities of the Bragg peaks and the calculated tetragonality factor (c/a) for the powders exhibit independent of milling time, it is well documented that, as Scherer's analysis provides only a measurement of the extension of the coherently diffracting domains, the crystallite sizes determined by this method can be significantly under estimation [26]. In addition to strain, factors such as dislocations, stacking faults, heterogeneities in composition and instrumental broadening can attribute to peak broadening, making it almost impossible to extract a reliable particle size solely from XRD [27].

In this connection, SEM was also employed for particle size measurement (Table 1). The morphological evolution of the powders as a function of milling time was also revealed, as illustrated in the SEM micrographs (Fig. 3). At first sight, the morphological characteristic of BT powders with various milling times is similar for all cases. In general, the particles are agglomerated and basically irregular shape, with a substantial variation in particle sizes. The powders consist of primary particles with nanometers in size. Increasing milling time over the range 0.5–30 h, the powders exhibit spatial fluctuation in their particle sizes. The extent of the fluctuation depends on the milling time as well as on the calcination temperature applied. In this study, it is seen that the optimum milling time for the production of the smallest nanosized BT powder with low firing temperature was found to be at 30 h. The finding of this

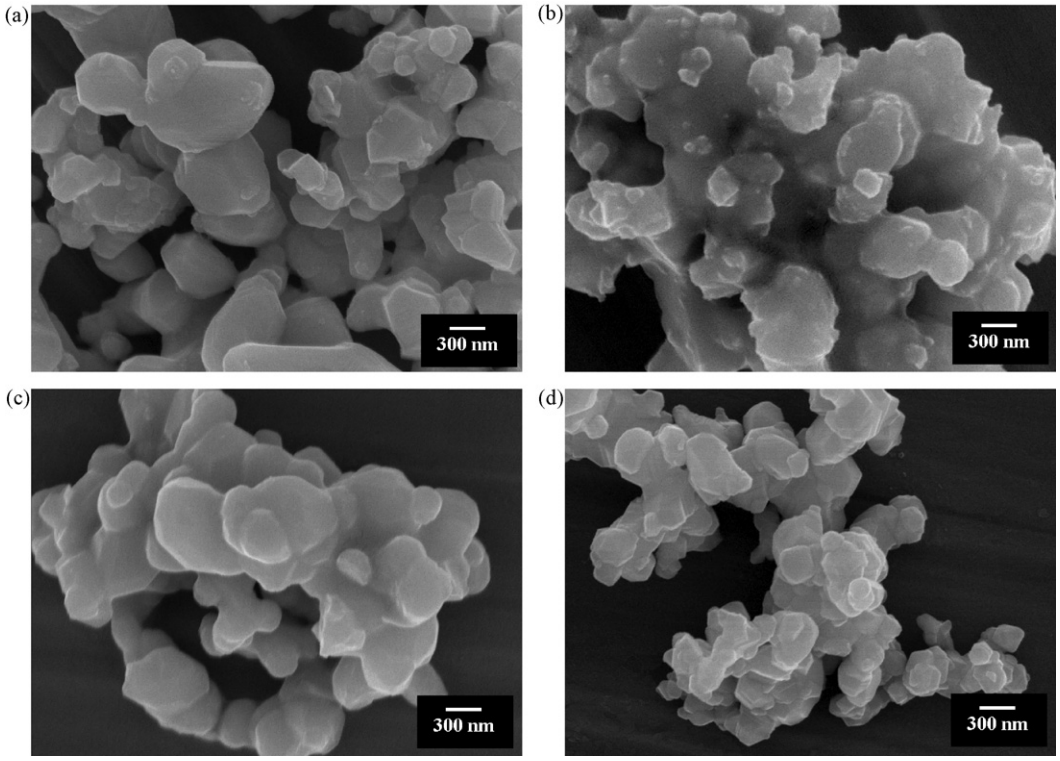

Fig. 3. SEM micrographs of BT powders after milling times of (a) 0.5, (b) 15, (c) 25 and (d) 30 h (calcined at their optimized conditions).

investigation indicates a strong relationship between the vibro-milling process and the yield of BT nanopowders.

4. Conclusions

The synthesis of perovskite BT nanopowder by a solid state reaction and the influence of milling time on its formation were studied. It was established that the milling time influences not only the development of the solid state reaction of BT phase but also particle size and morphology. It was shown that the increase of vibro-milling time significantly decreases the calcination temperature and particle size. A single phase of BT nanopowder can be successfully produced by employing a combination of 30 h milling time and calcination condition of 1200 °C for 2 h.

Acknowledgements

I would like to thank the Thailand Research Fund (TRF), Commission on Higher Education (CHE) and the Faculty of Science, Chiang Mai University for all financial support.

References

[1] A.J. Moulson, J.M. Herbert, Electroceramics: Materials, Properties, Applications, John Wiley & Sons Ltd., Chichester, 2003.
[2] G.H. Haertling, Ferroelectric ceramics: history and technology, J. Am. Ceram. Soc. 82 (4) (1999) 797–818.
[3] K. Uchino, Piezoelectrics and Ultrasonic Applications, Kluwer, Deventer, 1998.
[4] Y. Xu, Ferroelectric Materials and their Applications, Elsevier Science Publishers B.V., 1991.
[5] S. Tangwiwat, S. Milne, Barium titanate sols prepared by a diol-based sol–gel route, J. Non-Cryst. Solids 351 (12/13) (2005) 976–980.
[6] W. Luan, L. Gao, J. Guo, Study on drying stage of nanoscale powder preparation, NanoStruct. Mater. 10 (7) (1998) 1119–1125.
[7] S. Kwon, D. Yoon, Effects of heat treatment and particle size on the tetragonality of nano-sized barium titanate powder, Ceram. Int. 33 (7) (2007) 1357–1362.
[8] J. Chen, Z. Shen, F. Liu, X. Liu, J. Yun, Preparation and properties of barium titanate nanopowder by conventional and high-gravity reactive precipitation methods, Scripta Mater. 49 (2003) 509–514.
[9] R. Wongmaneerung, R. Yimnirun, S. Ananta, Effect of vibro-milling time on phase formation and particle size of lead titanate nanopowders, Mater. Lett. 60 (12) (2006) 1447–1452.
[10] R. Wongmaneerung, T. Sarakonsri, R. Yimnirun, S. Ananta, Effects of milling method and calcination condition on phase and morphology characteristics of $Mg_4Nb_2O_9$ powders, Mat. Sci. Eng. B 130 (2006) 246–253.
[11] B.D. Stojanovic, C. Jovalekic, V. Vukotic, A.Z. Simoes, J.A. Varela, Ferroelectric properties of mechanically synthesized nanosized barium titanate, Ferroelectrics 319 (2005) 65–73.
[12] C. Suryanarayana, M.G. Norton, X-Ray Diffraction: A Practical Approach, Plenum Press, New York, 1998.
[13] W. Chaisan, Preparation and Characterization of Ceramic Nanocomposite in the PZT-BT and TiO_2-SnO_2 Systems, Ph.D. Thesis, Chiang Mai University, Chiang Mai, Thailand, 2006.
[14] JCPDS-ICDD card no. 5-0378, International Centre for Diffraction Data, Newtown Square, PA, 2002.
[15] JCPDS-ICDD card no. 21-1272, International Centre for Diffraction Data, Newtown Square, PA, 2002.
[16] V. Berbenni, A. Marini, G. Bruni, Effect of mechanical milling on solid state formation of $BaTiO_3$ from $BaCO_3$–TiO_2 (rutile) mixtures, Thermochim. acta 374 (2) (2001) 151–158.
[17] E. Brzozowski, M.S. Castro, Synthesis of barium titanate improved by modifications in the kinetics of the solid state reaction, J. Eur. Ceram. Soc. 20 (2000) 2347–2351.
[18] L. Simon-Seveyrat, A. Hajjaji, Y. Emziane, B. Guiffard, D. Guyomar, Re-investigation of Synthesis of $BaTiO_3$ by conventional solid-state reaction and oxalate coprecipitation route for piezoelectric applications, Ceram. Int. 33 (1) (2007) 35–40.
[19] A. Beauger, J.C. Mutin, J.C. Niepce, Synthesis reaction of metatitanate $BaTiO_3$. Part 2: study of solid-solid reaction interfaces, J. Mat. Sci. 18 (1983) 3543–3550.
[20] L.B. Kong, J. Ma, H. Huang, R.F. Zhang, W.X. Que, Barium titanate derived from mechanochemically activated powders, J. Alloys Compd. 337 (2002) 226–230.
[21] JCPDS-ICDD card no. 72-0135, International Centre for Diffraction Data, Newtown Square, PA, 2002.
[22] J.K. Lee, K.S. Hong, J.W. Jang, Roles of Ba/Ti ratios in the dielectric properties of $BaTiO_3$ ceramics, J. Am. Ceram. Soc. 84 (9) (2001) 2001–2006.
[23] W. Chaisan, S. Ananta, T. Tunkasiri, Synthesis of barium titanate-lead zirconate titanate solid solutions by a modified mixed-oxide synthetic route, Cur. Appl. Phys. 4 (2–4) (2004) 182–185.
[24] W. Chaisan, R. Yimnirun, S. Ananta, D.P. Cann, Dielectric properties of solid solutions in the lead zirconate titanate-barium titanate system prepared by a modified mixed-oxide method, Mater. Lett. 59 (2005) 3732–3737.
[25] JCPDS-ICDD card no. 5-0626, International Centre for Diffraction Data, Newtown, PA, 2002.
[26] C. Suryanarayana, Mechanical alloying and milling, Prog. Mater. Sci. 46 (2001) 1–184.
[27] H. Klug, L.E. Alexander, X-ray Diffraction Procedures for Polycrystalline and Amorphous Materials, Wiley, New York, 1974.